OUKA
The University of Osaka
Institutional Knowledge Archive

Title	Mechanistic Study on Oxidative Stress Sensor Protein Containing Iron-sulfur Cluster
Author(s)	藤川, 麻由
Citation	大阪大学, 2015, 博士論文
Version Type	VoR
URL	https://doi.org/10.18910/52190
rights	
Note	

The University of Osaka Institutional Knowledge Archive : OUKA

https://ir.library.osaka-u.ac.jp/

The University of Osaka

Doctoral Dissertation

Mechanistic Study on Oxidative Stress Sensor Protein Containing Iron-sulfur Cluster

（鉄硫黄クラスターを持つ酸化ストレスセンサー蛋白質の応答機構に関する研究）

January 2015

Mayu Fujikawa

Department of Applied Chemistry
Graduate School of Engineering,
Osaka University

Contents

General Introduction **6**

Chapter 1

Direct Oxidation of the [2Fe-2S] Cluster in SoxR Protein by Superoxide

1.1 Introduction **12**

1.2 Experimental **13**

1.3 Results **14**

1.4 Discussion **16**

1.5 Conclusion **18**

References **18**

Chapter 2

Mechanistic Studies on Formation of the Dinitrosyl Iron Complex of the [2Fe-2S] Cluster of SoxR Protein

2.1 Introduction **21**

2.2 Experimental **22**

2.3 Results **23**

2.4 Discussion **29**

2.5 Conclusion **32**

References **32**

Chapter 3

Redox-Dependent DNA Distortion in a SoxR Protein-Promoter Complex Studied using Fluorescent Probes

3.1 Introduction **35**

3.2 Experimental **36**

3.3 Results **37**

3.4 Discussion **44**

3.5 Conclusion **46**

References **46**

Chapter 4

SoxR Conformational Changes upon Redox Changes of the [2Fe-2S] Cluster Probed with Ultraviolet Resonance Spectroscopy

4.1 Introduction **48**

4.2 Experimental **49**
4.3 Results **50**
4.4 Discussion **55**
4.5 Conclusion **58**
References **58**

Chapter 5
Binding of Promoter DNA to SoxR Protein Decreases the Reduction Potential of the [2Fe-2S] Cluster
5.1 Introduction **61**
5.2 Experimental **61**
5.3 Results **62**
5.4 Discussion **67**
5.4 Conclusion **69**
References **69**

Conclusion **71**
List of Publications **73**
Acknowledgments **75**

Abbreviations: ROS, reactive oxygen species; MerR, mercury resistance operator regulators; SoxR, superoxide response regulon; $SoxR_{red}$ reduced SoxR; $SoxR_{ox}$, oxidized SoxR; $[2Fe\text{-}2S]^{+}$, reduced [2Fe-2S]; $[2Fe\text{-}2S]^{2+}$, oxidized [2Fe-2S]; SOD, superoxide dismutase; e_{aq}^{-}, hydrated electron; Fd, ferredoxin; Ad, adrenodoxin; DNIC, dinitrosyl iron complex; NOC7, 3-[2-hydroxy-2-nitrosohydrazino]-N-methyl-1-propanamine; Mb, myoglobin; sGC, soluble guanylate cyclase; A, Adenine; 2Ap, 2-aminopurine; C, cytosine; T, thymine; G, guanine; UVRR, UV resonance raman; CRP, cytochrome P-450

General Introduction

When life began on Earth about 3.5 billion years ago, molecular oxygen was not present. The primitive atmosphere contained carbon dioxide, ammonia, methane, and water vapor. The origin and evolution of life processes are anaerobic, as is the metabolism of most primitive prokaryotic organisms. About 1 billion years ago, photosynthetic prokaryotes of cyanobacteria appeared. Once photosynthesis began, oxygen molecule was evolved into the atmosphere of Earth. Some molecular oxygen was converted into the more reactive forms, atomic oxygen (O), and ozone (O_3). Formation of an ozone layer, which blocks radial rays from the space, prompted life to go to land. Under low concentration of oxygen, the creatures got energy by anaerobic respiration like denitrification and desulfurization. With increase in oxygen atmosphere, some of them got more efficient aerobic breathing, at the same time, were exposed to oxidative stress.

Oxygen molecule is essential for aerobes, simultaneously causes oxidative stress. The retinopathy of prematurity is a typical example showing the oxygen toxicity. Several reactive oxygen species ($^1O_2$, O_2^-, H_2O_2, $OH^\cdot$, ROS) are chronically produced as byproducts of aerobic metabolism. ROSs may cause oxidative damage to proteins, DNA and lipids, and rapidly detoxified by various cellular enzymatic and nonenzymatic mechanisms. There are various response mechanisms for ROS, for example, OxyR transcriptional factor, responsible for H_2O_2, is activated through the formation of disulfide bond[(1)]. The protective response systems are widely distributed throughout current living organisms, both aerobic and anaerobic. This suggests that organisms have evolved defense systems from the start of the rise of molecular oxygen on Earth.

Microorganisms are constantly exposed to variations of many environmental factors, including temperature, oxygen, nutrient, toxic compounds, and interactions with other organisms. Expression of genes in bacteria is a main adaptive response to the environment and is controlled by a variety of

Table i-1. Examples of members of the MerR family.

Protein	Inducer	Regulated genes
	Heavy metals	
MerR[(2)]	Hg (II)	mercury resistance (*mer*) genes
ZntR[(3)]	Zn (II), Cd (II), Pb (II)	*zntA* transport
CueR[(4)]	Cu (I), Ag (I), Au (I)	*copA, cueO* genes
	Drug, Antibiotics	
BmrR[(5)]	various dyes	*bmr* multidrug resistance
Mta[(6)]	various dyes	*blt* and *bmr* multidrug resistance
	Oxidative stress	
SoxR[(7)]	oxidative stress	*soxs*

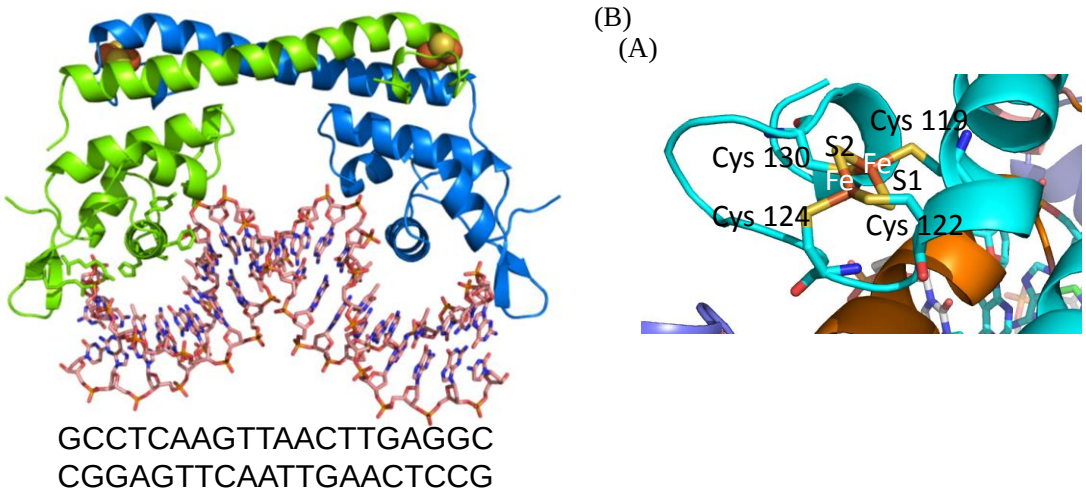

Figure i-1. (A) An X-ray structure of the SoxR-*soxs* promoter complex. (B) crystallographic structure of SoxR. A close-up view of the [2Fe-2S] cluster is shown. These structures were produced with PyMOL using a structure from the Protein Data Bank (code 2ZHG)[8].

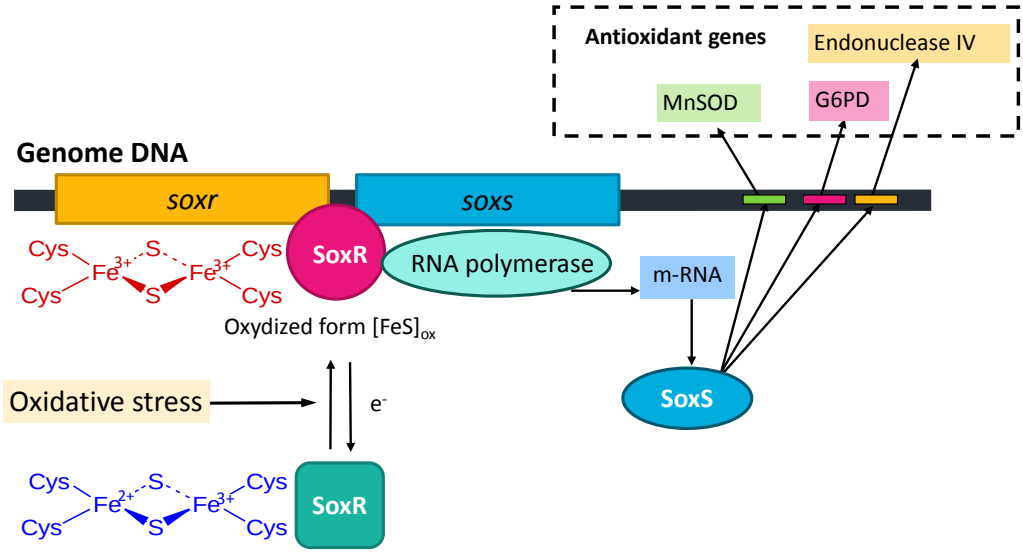

Figure i-2. Regulation of transcriptional activation by SoxR

mechanisms. In the vast majority cases, the gene regulation is mediated by the specific regulatory proteins that receive a signal and trigger the specific response. One typical example is the mercury resistance operon regulator (MerR) family. Members of the MerR family function as transcriptional activators responsible for various stresses in environment, including heavy metals, ROS and antimicrobial agents (Table i-1). The archetype of the MerR family was reported as the regulator of Gram-negative mercury resistance (*mer*) operons, and activates the *mer* genes in the presence of Hg (II)[2]. MerR promoter responds to nanomolar concentrations of Hg(II), and enhances the production of products metabolize inorganic and organic mercury compounds to less toxic forms. By advent of

bacterial genome study, MerR-like transcription factor have been found in various bacteria[3, 4, 5, 6, 7]. MerR family has a similar structure, N-terminal helix-turn-helix DNA binding domain, coiled-coli dimerization region and C-terminal sensor domain**.** The MerR family acts by a very similar mechanism. Upon activation, in response to the appropriate stimulus, these proteins undergo conformational changes which activate gene expression by distorting the promoter DNA and cause RNA polymerase to initiate transcription.

In *E. coli* cells, the [2Fe-2S] transcription factor SoxR, a member of the MerR family, functions as a sensor of oxidative stress such as O_2^- and nitric oxide (NO) (Figure i-1)[7, 8]. The activation of SoxR is controlled by reversible one-electron redox change of the [2Fe-2S] cluster. In the absence of oxidative stress, SoxR is kept in reduced, inactive form ($SoxR_{red}$)[9]. Upon oxidative stress, the [2Fe-2S] cluster is oxidized, changes to oxidized form ($SoxR_{ox}$)[10], and induces the transcription of the *soxS* gene[11]. The increased level of the SoxS protein enhances the various antioxidant proteins and repair proteins including superoxide dismutase (SOD) (Figure i-2). In vivo, the $SoxR_{ox}$ is reduced rapidly and maintained in its reduced state by specific enzymes[12].

Iron-sulfur proteins are ubiquitous in nature and play critical roles in a wide range of biological processes. In most iron-sulfur proteins, the clusters function as redox centers in electron transfer reaction, such as ferredoxin (Fd) and adrenodoxin (Ad). Alternatively, some have other functions including enzymatic reactions and metabolic regulation. For example, the activation of IRP, responsible to the iron concentrations, is regulated by controlled by the assembly/disassembly of the [4Fe-4S] cluster[13]. Within this group of redox-sensing transcription factors, SoxR is unique in that which is regulated by reversible one-electron oxidation-reduction of the [2Fe-2S] cluster.

X-ray crystallographic structures have been obtained for the *E. coli* $SoxR_{ox}$ and its complex with a 20-bp DNA of the target promoter (Figure i-1)[8]. The structure reveals N-terminal winged helix DNA-binding, dimerization helix, and [2Fe-2S] cluster-binding domains. The [2Fe-2S] cluster of SoxR is coordinated to four cysteine residues (Cys-119, Cys-122, Cys-124, and Cys-130). One of the sulfur atoms (S_2) and two iron atoms are fully exposed to solvent (Fig. i-1 (B)). The structural alterations of SoxR induced by redox changes of [2Fe-2S] clusters are communicated to the DNA-binding domain, leading to target promoter DNA distortion.

SoxR is also activated by nitric oxide (NO). *In vivo* study of phagocytosed bacteria within murine macrophages, the gene expression of *soxS*, the effect of a *soxRS* mutant and the inhibitor of NO synthase suggested that induction of the SoxRS by NO counteracts most of the cytotoxic effects of NO produced by macrophages[14]. The SoxS-induced enzymes such as endonuclease IV and glucose 6-phosphate dehydrogenase were shown to be required for resistance to macrophage killing[14, 15]. SoxR activation by NO occurs through direct modification of the [2Fe-2S] centre to form protein-bound DNICs observed by ESR signals both in intact bacterial cells and in purified SoxR[16]. However, little is known about the actual mechanism of cluster nitosylation.

SoxR homologs have been identified in 176 α-, β-, δ-, γ-Proteobacteria and Atinobacteria[17].. All of these homologs contain the SoxR-specific cysteine motif CI[G/Q]CGC[L/M][S/L]XXC required for binding of the [2Fe-2S] cluster. Unlike *E. coli* and related enteric bacteria, however, the majority of SoxR regulons in *Pseudomonas aeruginosa* (*P. aeruginosa*) and *Streptomyces coelicolor* lack the genes typically involved in O_2^- resistance and detoxification[18]. Many of these bacteria produce redox-active pigments independent of oxidative stress[19]. *P. aeruginosa* SoxR was shown to be activated by the endogenous, redox-cycling antibiotic compound pyocyanin[19], which is the physiological signal for the upregulation of quorum-sensing controlled genes. *P. aeruginosa* SoxR, a homolog with 62 % sequence identity and 77 % sequence similarity to *E. coli* SoxR[20], exhibited physic-chemical properties similar to that of *E. coli* protein, including the redox potential of the [2Fe-2S] cluster and visible absorption spectra[21].

Because of the instability of the signal molecules of SoxR such as O_2^- and NO, it is difficult to observe their reactions directly by other chemical methods. In contrast, it becomes possible to measure for determining the spectral and kinetic behavior of NO and O_2^- with pulse radiolysis method by LINAC of ISIR Osaka University.

This thesis deals with the mechanisms of SoxR proteins, which respond to oxidative stress. The contents of each chapters are briefly described below.

CHAPTER 1 and 2 deals with the reaction mechanisms by the use of pulse radiolysis. In CHAPTER 1, to elucidate the activation mechanism with O_2^-, the reaction of O_2^- with SoxR was investigated. In addition, a similar experiment was performed with *P. aeruginosa* SoxR, where the functional difference of SoxR between *E. coli* and *P. aeruginosa* SoxR was described. In CHAPTER 2, the reaction of NO with SoxR was described, of which results are compared with those obtained spinach Fd, a typical [2Fe-2S] cluster of protein. While the structure of transcriptionally activated SoxR has been solved, the molecular mechanisms through which redox changes of the [2Fe–2S] cluster induce protein conformational alteration and regulate transcription of the target promoter remain to be established. However, the lack of a SoxR structure in the reduced state limits our understanding of the structural transitions required for DNA binding and transcriptional activation.

In CHAPTER 3 and 4, the structural changes of SoxR between oxidized and reduced form were described. In CHAPTER 3, the redox-dependent structural changes in the promoter DNA bound to SoxR by fluorescence probes were described. CHAPTER 4 deals with UV resonance Raman (UVRR) spectroscopic analysis of SoxR, in which was shown conformational changes upon reduction of SoxR.

In CHAPTER 5 deals with the reduction potential for SoxR in the absence and presence of DNA from equilibrium data coupled with NADPH and NADPH-cytochrome P-450 (CRP).

Reference

(1) M. Zheng, F. Åslund, G. Storz, *Science*, **1998,** *279*, 1718-1722.

(2) (a) P. A. Lund, S. J. Ford, N. L. Brown, *J. Gen. Microbiol.*, **1986,** *132*, 465-480. (b) P. A. Lund, N. L. Brown, *J. Mol. Biol.*, **1989,** *205*, 343-353.

(3) K. R. Brocklehurst, J. L. Hobman, B. Lawley, L. Blank, S. J. Marshall, N. L. Brown, A. P. Morby, *Mol. Microbiol.*, **1999,** *31*, 893-902.

(4) F. W. Outten, C. E. Outten, J. Hale, T. V. O'Halloran, *J. Biol. Chem.*, **2000,** *275*, 31024-31029.

(5) M. Ahmed, L. Lyass, P. N. Markham, S. S. Taylor, N. Vazquezlaslop, A. A. Neyfakh, *J. Bacteriol.*, **1995,** *177*, 3904-3910.

(6) M. H. Godsey, N. N. Baranova, A. A. Neyfakh, R. G. Brennan, *J. Biol. Chem.*, **2001,** *276*, 47178-47184.

(7) (a) C. F. Amábile-Cuevas, B. Demple, *Nucleic Acids Res.*, **1991,** *19*, 4479-4484. (b) J. Wu, B. Weiss, J. Bacteriol, 1991, 173, 2864-2871.

(8) S. Watanabe, A. Kita, K. Kobayashi, K. Miki, *Proc. Natl. Acad. Sci. USA.*, **2008**, *105*, 4121-4126.

(9) (a) H. Ding, E. Hidalgo, B. Demple, *J. Biol. Chem.*, **1996**, *271*, 33173-33175. (b) H. Ding, B. Demple, *Proc. Natl. Acad. Sci. U.S.A.*, **1997**, *94*, 8445-8449.

(10) P. Gaudu, N. Moon, B. Weiss, *J. Biol. Chem.*, **1997**, *272*, 5082-5086.

(11) P. J. Pomposiello, M. H. Bennik, B. Demple, *J. Bateriol.*, **2001**, *183*, 3890-3902.

(12) (a) K. Kobayashi, S. Tagawa, *FEBS Lett.*, **1999,** *451*, 227-230. (b) M. Koo, J. Lee, S. Rah, W. Yeo, J. Lee, K. Lee, Y. Koh, S. Kang. J. Roe, *EMBO J.*, **2003,** *22*, 2614-2622.

(13) A. Picciocchi, C. Saguez, A. Boussac, C. Cassier-Chauvat, F. Chauvat, *Biochemistry*, **2007**, *46*, 15018-15026.

(14) T. Nunoshiba, T. deRojas-Walker, J. S. Wishnok, S. R. Tannenbaum, *Infect. Immun.*, **1995,** *63*, 794-798.

(15) T. Nunoshiba, T. deRojas-Walker, J. S. Wishnok, S. R. Tannenbaum, P*roc. Natl. Acad. Sci. USA.*, **1993,** *90*, 9993-9997.

(16) (a) H. Ding, B. Demple, *Proc. Natl. Acad. Sci. USA.*, **2000**, *97*, 5146-515-. (b) F. C. Lo, C. L. Chen, C. M. Lee, M. C. Tsai, T. T Lu, W. F. Liaw, S. S. F. Yu, *J. Biol. Inorg. Chem.*, **2008,** *13*, 961-972. (c) F. C. Lu, J. F. Lee, W. F. Liaw I. J. Hsu, Y. F. Tsai, S. C. Chan, S. S. F. Yu, *Chem. Eur. J.*, **2012,** *18*, 2565-2577.

(17) I. E. P. Dietrich, T. K. Teal, A. Price-Whelan, A., D. K. Newman, *Science*, **2008**, *321*, 1203-1206.

(18) W. Park, S. Peña-Llopis, Y. Lee, B. Demple, B. *Biochem. Biophys. Res. Commun*., **200**6, *341*. 51-56.

(19) M. Palma, J. Zurita, J. A. Ferreras, S. Worgall, D. H. Larone, L. Shi, F. Campagne, L. E. N. Quadri, *Infect. Immune.*, **2005**, *73* 2958-2966.

(20) K. Kobayashi, S. Tagawa, *J. Biochem.*, **2004**, *136*, 607-615.

CHAPTER 1
Direct Oxidation of the [2Fe-2S] Cluster in SoxR Protein by Superoxide

1.1 Introduction

ROS, byproducts of cellular aerobic metabolism, produce cellular and genetic damage in aerobic organisms. Cells have thus evolved defense systems against reactive oxygen species and respond to sublethal levels of oxidative stress through coordinated activation of a battery of antioxidant genes[(1)]. The molecular signals that activate these multifunctional defense systems have been the object of considerable interest. The protective responses initiated in response to ROS exposure have been most thoroughly investigated in *E. coli*, where the induction of antioxidant genes is mediated by activation of the *soxRS* regulon.

A crucial unanswered question concerns the nature of the cellular signal sensed by SoxR. O_2^- was the first candidate suggested as the SoxR-activating signal, reflecting the early observation that SoxR responded to agents that generate O_2^- [(2)]. Experiments in intact cells showed that expression of the *soxRS* regulon member fumarase C was increased by an elevation of O_2^- caused by the deletion of SOD[(3)]. The induction of fumarase C in the parental strain was eliminated by mutational deletion of the *soxRS* response[(4)]. Similarly, the expression of *soxRS*-dependent glucose-6-phosphate dehydrogenase was higher in a control strain compared with *E. coli* cells overexpressing Mn-SOD[(5)]. However, there is no evidence that the direct oxidant of the [2Fe-2S] cluster of SoxR is O_2^- itself [(6), (7), (8)]. On the other hand, Gu and Imlay[(7)] recently demonstrated that the *soxRS* response of *E. coli* is directly activated by redox-cycling drugs rather than by O_2^-. $SoxR_{red}$ was reported to be oxidized directly by redox-cycling drugs such as paraquat in the absence of SOD. However, there were arguments against this proposal[(8)]. As an alternative, it was suggested that the *soxRS* regulon does not respond to a change in O_2^- concentration, but rather responds to the redox state ($NADPH/NADP^+$ ratio) [(9)]. Accordingly, NADPH could maintain $SoxR_{red}$ by reactions linked by NADPH[(10), (11)], whereas depletion of available reducing equivalents would produce a shift in the redox balance toward oxidized $SoxR_{ox}$.

SoxR homologs have been identified in many bacterial species. All of these homologs contains the SoxR-specific cysteine motif CI(G/Q)CGC(L/M)(S/L)*XXX*C, required for binding of the [2Fe-2S] cluster[(12)]. *P. aeruginosa* SoxR, a homolog with 62% sequence identity and 77% sequence similarity to *E. coli* SoxR[(13)], exhibits similar physicochemical properties as the *E. coli* protein, such as redox potential of the [2Fe-2S] cluster and visible absorption spectra[(14)]. However, the *P. aeruginosa* SoxR function differs dramatically from that of *E. coli* (Figure 1-1). The SoxR regulon in *P. aeruginosa*, in which there is no obvious *SoxS* homolog, is composed of genes encoding an efflux pump, a transporter, and a putative monooxygenase[(13), (14), (15)] and does not control any of the genes typically involved in O_2^- resistance and detoxification [(16)]. It was shown that *P. aeruginosa* SoxR is activated

by the endogenous redox-cycling antibiotic compound pyocyanin[12, 15], which is the physiological signal for the up-regulation of quorum sensing-controlled genes. This reaction can occur anaerobically in intact cells, suggesting O_2^--independent activation.

This CHAPTER was designed to investigate the hypothesis that O_2^- has a direct role as a signal for the *soxRS* regulon. Using the pulse radiolysis method, It has been confirmed that O_2^- reacts rapidly and directly with $SoxR_{red}$, but not with $SoxR_{ox}$. In addition, I present evidence that the sensitivity of SoxR to O_2^- is much higher in *E. coli* than in *P. aeruginosa*.

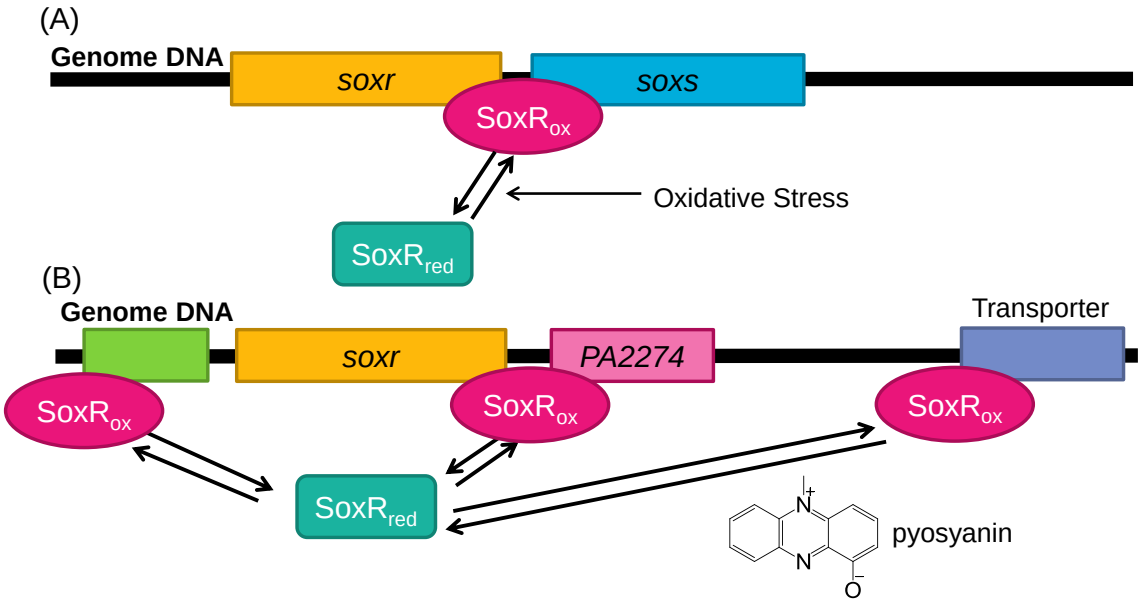

Figure 1-1. Regulation of transcriptional activation by SoxR in (A) *E. coli* and (B) *P. auruginosa.*

1.2 Experimental

Materials

Human Cu/Zn-SOD, overproduced by *E. coli*, was kindly provided by Nippon Kayaku. All other reagents were commercially obtained and analytical grade.

Expression and Purification

The expression plasmids for *E. coli* [10] and *P. aeruginosa* [14] SoxR were transformed into *E. coli* C41(DE3) and coexpressed with the *isc* operon[17] as described previously[18]. SoxR was purified essentially as described previously[18]. SoxR protein samples were purified as the oxidized form and confirmed as >95% homogeneous by SDS-polyacrylamide gel electrophoresis. The concentration of SoxR was determined using an extinction coefficient of 12.7 mM^{-1} cm^{-1} at 417 nm[19].

SoxR-DNA complexes were prepared according to the crystallization method described previously [18]. The palindromic DNA GCCTCAAGTTAACTTGAGGC (Sigma-Aldrich) was formed into a double-stranded DNA structure by dissolving in an aqueous solution containing 20 mM potassium phosphate (pH 7.0), 50 mM KCl, and 10 mM potassium/sodium tartrate; heating to 94 °C; and

gradually cooling to room temperature. SoxR-DNA complexes were prepared by mixing 40–70 μM SoxR (20 mM potassium phosphate (pH 7.0), 250 mM KCl, and 10 mM potassium/sodium tartrate) and DNA solutions at molar ratios of 2 : 1.05–1.1 and incubating for at least 4 h at 4 °C [18]. Fd from spinach was purified by a combination of DEAE-cellulose and Sephadex G-75 column chromatographies essentially as described[20].

Pulse Radiolysis

Samples of SoxR for pulse radiolysis were prepared by bubbling a solution containing 20 mM potassium phosphate (pH 7.0), 10 mM potassium/sodium tartrate, 0.5 M KCl, and 0.1 M sodium formate (for scavenging $OH^{\cdot}$) with O_2 gas for 2 min and then adding a concentrated solution of SoxR (1–2 mM) (Scheme 1-1). Pulse radiolysis experiments were performed with a linear accelerator at the Institute of Scientific and Industrial Research of Osaka University[21]. The pulse width and energy were 8 ns and 27 MeV, respectively. A 1-kilowatt xenon lamp was used as a light source. After passing through an optical path, the transmitted light intensities were analyzed and monitored by a fast spectrophotometric system composed of a Nikon monochromator, an R-928 photomultiplier, and a Unisoku data analysis system. For the time-resolved transient absorption spectral measurement, the monitor light was focused into a quartz optical fiber, which transported the electron pulse-induced transmittance changes to a gated multichannel spectrometer (Unisoku TSP-601-02). The initial concentration of superoxide radical generated by pulse radiolysis was 20–30 μM, which was estimated using the relationship $\epsilon_{260} = 1925\ M^{-1}\ cm^{-1}$ [22].

$H_2O \rightsquigarrow e_{aq}^-, OH^{\cdot}$

O_2 saturated

$O_2 + e_{aq}^- \longrightarrow O_2^-$

$HCOO^- + OH^{\cdot} \longrightarrow H_2O + CO_2^-$

$CO_2^- + O_2 \longrightarrow CO_2 + O_2^-$

$[2Fe\text{-}2S]^{2+} + e_{aq}^- \longrightarrow [2Fe\text{-}2S]^{+}$

Scheme 1-1. Reaction scheme after pulse radiolysis in O_2 saturated aqueous solution containing formate ion.

Spectrophotometric Measurements

Optical absorption spectra were measured with a Hitachi U-3000 spectrometer.

1.3 Results

To follow the reaction of O_2^- with SoxR, the absorption changes after pulse radiolysis of oxygen-saturated phosphate buffer in the presence of 50 μM $SoxR_{ox}$ were studied. Under these conditions, although most hydrated electrons (e_{aq}^-) generated reacted with O_2 to form O_2^-, a portion of the e_{aq}^- were found to react very rapidly with $SoxR_{ox}$, resulting in reduction of the [2Fe-2S] cluster of the protein. This reduction was reflected in a decrease in absorbance at 420 nm. The initial transient spike in absorbance indicated the formation and decay of hydrated electrons (Figure 1-2 (A)). Subsequently, these initial changes in absorption partially reversed (~38%) on a time scale of milliseconds (Figure 1-2 (B)). Figure 1-2 (C) shows difference spectra obtained at 2 μs and 20 ms

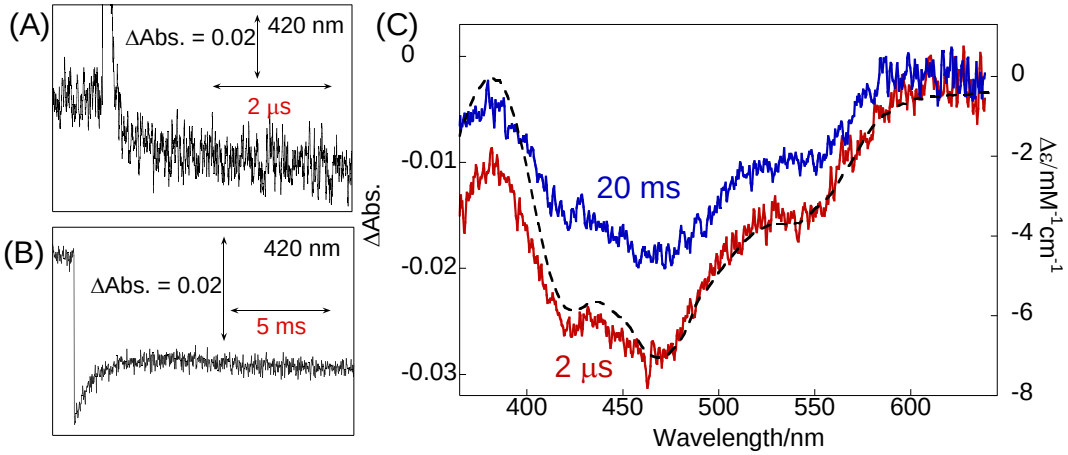

Figure 1-2. (A), (B) Absorbance changes at 420 nm after pulse radiolysis of SoxR under O_2 saturated conditions. (C) Comparison of the kinetic difference spectra of SoxR obtained at 2 μs (red line) and 20 ms (blue line) after pulse radiolysis with the reduced-oxidized difference spectrum (dashed line). Samples contained 50 μM SoxR, 10 mM phosphate buffer (pH 7.0), 10 mM sodium tartrate and 0.1 M sodium formate.

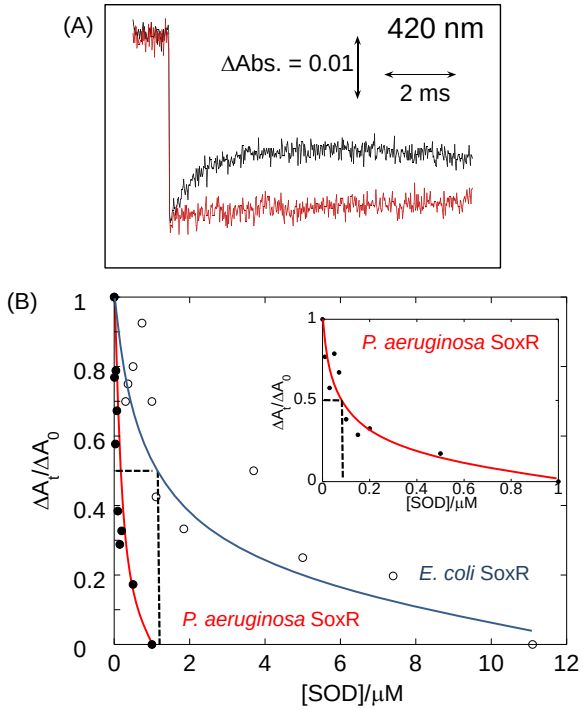

Figure 1-3. (A) Absorbance changes after pulse radiolysis of SoxR in the absence (black line) or presence (red line) of 11 μM SOD. (B) Effect of SOD on the oxidation of *E. coli* (○, blue line) and *P. aeruginosa* (●, red line) SoxR.

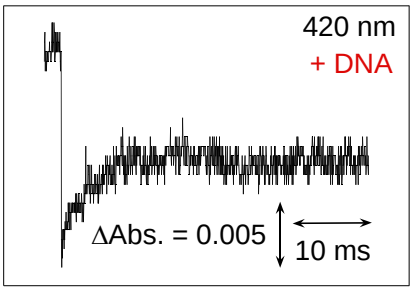

Figure 1-4. Absorbance change after pulse radiolysis of *E. coli* SoxR in the absence of promoter DNA under O_2-saturated conditions.

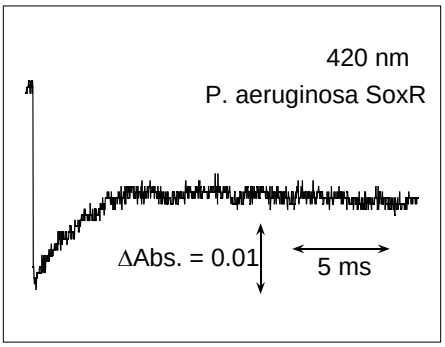

Figure 1-5. Absorbance change after pulse radiolysis of *P. aeruginosa* SoxR under O_2-saturated conditions.

after pulse radiolysis. Both spectra are similar to the $SoxR_{red}$-minus-$SoxR_{ox}$ spectrum. From these findings, it can be concluded that $SoxR_{ox}$ was initially reduced, and subsequently, the [2Fe-2S] cluster became partially reoxidized. As shown in Figure 1-3 (A), this millisecond time scale recovery of oxidation was inhibited by addition of Cu/Zn-SOD (11 μM), which completely eliminated the delayed change in absorption without affecting the initial rapid decrease. From this, it's concluded that the recovery process reflects the oxidation of $SoxR_{red}$ by O_2^-.

Following the spectral changes, the absorbance very slowly returned to the initial $SoxR_{ox}$ state and was almost recovered after ~20 s. Under the deaerated condition, the spectrum was persistent for at least 30 s. Therefore, the spectroscopic changes at 20 s account for the direct oxidation of the [2Fe-2S] cluster of $SoxR_{red}$ with O_2. This suggests that the spectral changes after pulse radiolysis corresponds to reversible reduction of the protein, not by irreversible destruction of the iron-sulfur cluster.

Electrochemical studies have shown that the reduction potential of SoxR bound to promoter DNA is positively and dramatically shifted from −285 mV[23] to 200 mV[24]. Thus, it was particularly interested in investigating the spectroscopic changes and rate constant after pulse radiolysis in the presence of the promoter DNA. As was the case without the promoter DNA, $SoxR_{ox}$ was initially reduced and subsequently oxidized. Although the spectra and kinetics obtained after pulse radiolysis were not affected by the presence of DNA (Figure 1-4), the absorbance recovery 10 ms after pulse radiolysis was ~50% (Figure 1-4), which is larger than that in the absence of DNA (~38%) (Figure 1-2 (B)). It is important to note that a reduction in $[2Fe\text{-}2S]^{2+}$ of the DNA-bound form of SoxR by O_2^- was not obsereved, although this reaction is expected to be energetically favorable on the basis of the redox potential between O_2/ O_2^- (E_0 = −160 mV)[25] and $[2Fe\text{-}2S]^{2+}$/$[2Fe\text{-}2S]^{+}$ (E_0 = 200 mV)[24].

To extend the analysis, the effect of Cu/Zn-SOD on the oxidation of $SoxR_{red}$ was examined. The dependence of the absorption changes at 420 nm on Cu/Zn-SOD is presented in Figure 1-3 (B), which shows that SOD dose-dependently inhibited the recovery of oxidation. Half-maximal inhibition was observed at 1 μM SOD. Inhibition of the oxidation of $SoxR_{red}$ by SOD can be expressed as inhibition (%) = k_1[SOD]/k_2[$SoxR_{red}$], where k_1 and k_2 are the rate constants of O_2^- with SOD and $SoxR_{red}$, respectively. Under these conditions, the concentrations of O_2^- and $SoxR_{red}$ formed after pulse radiolysis were ~20–30 and 6 μM, respectively. It can be estimated that a rate constant of 5×10^8 M^{-1} s^{-1} for the reaction of O_2^- with $SoxR_{red}$, given the concentration of SOD needed to half-maximally inhibit the oxidation of $SoxR_{red}$, and a rate (k_1) for the reaction of O_2^- with SOD of 2×10^9 M^{-1} s^{-1} [26].

A similar result was also obtained with *P. aeruginosa* SoxR, as shown in Figure 1-5. However, subsequent millisecond scale oxidations were different between *E. coli* and *P. aeruginosa*. The recovery of oxidation for *P. aeruginosa* (~50%) was larger than that for *E. coli*. Notably, the

oxidation of *P. aeruginosa* was nearly completed inhibited by 0.5 μM SOD, whereas this same concentration resulted in only ~20% inhibition in *E. coli*. Half-maximal inhibition of oxidation of *P. aeruginosa* was observed at 80 nM SOD, from which it can be estimated a rate constant of 4×10^7 M^{-1} s^{-1} for the reaction of O_2^- with *P. aeruginosa* $SoxR_{red}$.

1.4 Discussion

In this thesis, it was demonstrated that the direct reaction of O_2^- with $SoxR_{red}$ to form $SoxR_{ox}$. The reaction schemes after pulse radiolysis can be summarized as follows (Reactions 1-1 and 1-2),

$$e_{aq}^- + [2Fe\text{-}2S]^{2+} \rightarrow [2Fe\text{-}2S]^{+} \qquad (1\text{-}1)$$

$$O_2^- + [2Fe\text{-}2S]^{+} + 2H^{+} \rightarrow H_2O_2 + [2Fe\text{-}2S]^{2+} \qquad (1\text{-}2)$$

The reaction sequence is reversible; thus, iron-sulfur clusters are not irreversibly destroyed. The second-order rate constant of *E. coli* SoxR (5×10^8 M^{-1} s^{-1}) is in the same range as that of Mn-SOD ($15–1.6 \times 10^8$ M^{-1} s^{-1}) [27] and Fe-SOD (3.3×10^8 M^{-1} s^{-1}) [28]. In fact, Reaction 1-2 was not inhibited completely, even in the presence of 5 μM Cu/Zn-SOD (Figure 1-3 (B)). This suggests that O_2^- formed intracellularly reacts with $SoxR_{red}$. However, it is not clear that O_2^- is available to interact with SoxR because high levels of SOD are present, and the SoxR protein is produced constitutively at a low level of ~100 molecules/cell. It has been calculated that the level of SOD found in aerobic cells (~10^{-5} M) would efficiently reduce O_2^- at steady-state concentrations of 10^{-10}–10^{-11} M[29]. Thus, the basal amount of SOD is sufficient to maintain O_2^- steady-state concentrations at a nontoxic level[29]. However, high levels of SOD are often required to protect enzymes against O_2^-, which is frequently used as a killing agent in mammalian immune systems. Changes in O_2^- concentration may trigger pathways involved in host-pathogen interactions. The response to O_2^- is partially organized around the reversible oxidation of the sensor, SoxR, which enhances the expression of the regulator, SoxS.

The results obtained here using pulse radiolysis techniques are in conflict with those obtained using a competition assay with the reduction of cytochrome *c* in the absence and presence of $SoxR_{red}$, in which xanthine oxidase and xanthine under aerated conditions are used to produce O_2^- [7]. It was reported that the rate constant of $SoxR_{red}$ with O_2^- must be <1000 M^{-1} s^{-1}. However, cytochrome *c* could be reduced by $SoxR_{red}$ directly[10]. In addition, under aerated conditions, $SoxR_{red}$ is readily autoxidized in the absence of sodium dithionite, and O_2^- would be formed during the process. A complication arises with the previously used assay conditions. In contrast, the pulse radiolysis method does not require any chemical reagents; thus, complications arising from kinetic constraints imposed by chemical events will not occur.

An important finding is that the sensitivity of the *E. coli soxRS* response to O_2^- with a rate constant of $5 \times 10^8\ M^{-1}\ s^{-1}$, is 10-fold higher compared that that of *P. aeruginosa* ($4 \times 10^7\ M^{-1}\ s^{-1}$). This difference reflects the physiological function of SoxR-mediated gene regulation. For *E. coli*, direct oxidation of SoxR by O_2^- leads to induction of SoxS. In turn, SoxS activates genes involved in O_2^- stress protection and repair [30]. The *SoxR* regulon responds to metabolically generated O_2^- adjusting SOD synthesis to control intracellular O_2^- levels. In contrast, *P. aeruginosa* SoxR is activated by the endogenous redox-cycling antibiotic compound pyocyanin [13, 15], which is the physiological signal for up-regulating quorum sensing-controlled gene expression and serves as an electron acceptor to balance the intracellular redox state[31]. These present data also support the view that the major function of the SoxR regulon in *P. aeruginosa*, unlike that in *E. coli*, is not O_2^- responsiveness.

Importantly, this study is the first to provide a direct observation of the reaction between an iron-sulfur protein and O_2^-, revealing an interesting effect of O_2^- on iron-sulfur clusters. O_2^- has been reported to inactivate several iron-sulfur proteins with second-order rate constants in the range of 10^6–$10^7\ M^{-1}\ s^{-1}$[32]. In each of these cases, the process was irreversible and was associated with concomitant cluster degradation. The reactions of O_2^- with spinach Fd and Ad was also examined using the pulse radiolysis method. However, unlike the case with SoxR (Figure 1-2), after reduction of the [2Fe-2S] cluster of these proteins, there was no recovery of absorbance due to oxidation on a time scale of milliseconds. A slower recovery of direct O_2 oxidation of the reduced form of ferredoxin was observed, as in the case of SoxR. Therefore, it can be said that Reaction 1-2 observed here is a specific characteristic of the SoxR protein. The SoxR-dependent conversion of O_2^- to H_2O_2 (Reaction 1-2) requires one electron and two protons. Although O_2^- (E_0 (O_2^-/H_2O_2) = 0.83 V) [33] can act as an oxidant for $[2Fe\text{-}2S]^+$ of SoxR ($E_0 = -280$ mV for DNA-free; $E_0 = 200$ mV for DNA-bound), O_2^- reduction is favored in the presence of a proton source, as is observed in the reaction of superoxide reductase [34]. Both proton and solvent may play important roles in the SoxR mechanism. An analysis of the crystal structure revealed that the [2Fe-2S] clusters of oxidized SoxR are solvent-exposed, creating an asymmetrically charged environment and a possible conformational change in SoxR. The unusual positioning of the metal ion on the surface of SoxR provides an active site with a readily available source of protons.

1.5 Conclusion

In conclusion, SoxR-mediated transcription is activated by oxidation of the $[2Fe\text{-}2S]^+$ cluster in SoxR. I found that the SoxR $[2Fe\text{-}2S]^+$ cluster of *E. coli* was more readily oxidized by O_2^- compared with that of *P. aeruginosa*. Although *soxR* regulons can be induced through multiple pathways, direct oxidation by O_2^- is an important mechanism for activating *E. coli* SoxR signaling. For *P. aeruginosa*, O_2^- is not responsible for the activation of the SoxR $[2Fe\text{-}2S]^+$ cluster.

Reference

(1) (a) G. Storz, J. A. Imlay, *Curr. Opin. Microbiol.,* **1999**, *2*, 188-194. (b) P. J. Pomposiello, B. Demple, *Trends Biotechnol.,* **2001,** *19,* 109-114. (c) J. Green, M. S. Paget, *Nat. Rev. Microbiol.,* **2004,** *2*, 954-966. (d) J. A. Imlay, *Annu. Rev. Biochem.,* **2008,** *77*, 755-776. (e) T. Nguyen, P. Nioi, C. B. Pickett, *J. Biol. Chem.,* **2009,** *284,* 13291-13295. (f) G. M. DeNicola, F. A. Karreth, T. J. Humpton, A. Gopinathan, C. Wei, K. Frese, D. Mangal, K. H. Yu, C. J. Yeo, E. S. Calhoun, F. Scrimieri, J. M. Winter, R. H. Hruban, C. Iacobuzio-Donahue, S. E. Kern, I. A. Blair, D. A. Tuveson, *Nature,* **2011**, *475*, 106-109.

(2) P. Gaudu, N. Moon, B. Weiss, *J. Biol. Chem.,* **1997,** *272,* 5082-5086.

(3) S. I. Liochev, I. Fridovich, *Arch. Biochem. Biophys.,* **1993,** *301,* 379-384.

(4) S. I. Liochev, I. Fridovich, *Proc. Natl. Acad. Sci. USA.,* **1992,** *89,* 5892-5896.

(5) S. I. Liochev, I. Fridovich, *J. Biol. Chem.* **1991,** *266,* 8747-8750.

(6) I. R. Tsaneva, B. Weiss, *J. Bacteriol.,* **1990,** *172*, 4197-4205.

(7) M. Gu, J. A. Imlay, *Mol. Microbiol.,* **2011,** *79,* 1136-1150.

(8) S. I. Liochev, *Free Radic. Biol. Med.,* **2011,** *50,* 1813.

(9) A. R. Krapp, M. V. Humbert, N. Carrillo, *Microbiology,* **2011,** *157,* 957-965.

(10) K. Kobayashi, S. Tagawa, *FEBS Lett.,* **1999**, *451*, 227-230.

(11) M. S. Koo, J. H. Lee, S. Y. Rah, W. S. Yeo, J. W. Lee, K. L. Lee, Y. S. Koh, S. O. Kang, J. H. Roe, *EMBO J.,* **2003,** *22,* 2614-2622.

(12) L. E. Dietrich, T. K. Teal, A. Price-Whelan, D. K. Newman, *Science,* **2008,** *321,* 1203-1206.

(13) M. Palma, J. Zurita, J. A. Ferreras, S. Worgall, D. H. Larone, L. Shi, F. Campagne, L. E. Quadri, *Infect. Immun*., **2005**, *73*, 2958-2966.

(14) K. Kobayashi, S. Tagawa, *J. Biochem*., **2004,** *136,* 607-615.

(15) L. E. Dietrich, A. Price-Whelan, A. Petersen, M. Whiteley, D. K. Newman, *Mol. Microbiol.,* **2006,** *61,* 1308-1321.

(16) W. Park, S. Peña-Llopis, Y. Lee, B. Demple, *Biochem. Biophys. Res. Commun.,* **2006,** *341,* 51-56.

(17) M. Nakamura, K. Saeki, Y. Takahashi, *J. Biochem.,* **1999**, *126,* 10-18.

(18) S. Watanabe, A. Kita, K. Kobayashi, Y. Takahashi, K. Miki, *Acta Crystallogr. Sect. F Struct. Biol. Cryst. Commun.,* **2006,** *62,* 1275-1277.

(19) J. Wu, W. R. Dunham, B. Weiss, *J. Biol. Chem.,* **1995,** *270,* 10323-10327.

(20) T. Hase, K. Wada, H. Matsubara, *J. Biochem.,* **1977,** *82,* 267-276.

(21) (a) K. Kobayashi, K. Hayashi, M. Sono, *J. Biol. Chem,* **1989,** *264,* 15280-15283. (b) K. Kobayashi, M. Miki, S. Tagawa, *J. Chem. Soc. Dalton Trans.*, **1995,** 2885-2889. (c) G. Mustafa, Y. Ishikawa, K. Kobayashi, C. T. Migita, M. D. Elias, S. Nakamura, S. Tagawa, M. Yamada, *J. Biol. Chem.,* **2008,** *283,* 22215-22221.

(22) B. H. Bielski, *Photochem. Photobiol.*, **1978,** *28*, 645-649.

(23) (a) H. Ding, E. Hidalgo, B. Demple, *J. Biol. Chem.*, **1996**, *271*, 33173-33175. (b) P. Gaudu, B. Weiss, *Proc. Natl. Acad. Sci. USA.*, **1996**, *93*, 10094-10098.

(24) A. A. Gorodetsky, L. E. Dietrich, P. E. Lee, B. Demple, D. K. Newman, J. K. Barton, *Proc. Natl. Acad. Sci. USA.*, **2008,** *105*, 3684-4689.

(25) (a) P. Muir Wood, *FEBS Lett.*, **1974,** *44*, 22-24. (b) Y. Sawada, T. Iyanagi, *Biochemistry*, **1974,** *14*, 3761-3764.

(26) D. Klug, J. Rabani, I. Fridovich, *J. Biol. Chem.*, **1972,** *247*, 4839-4842.

(27) M. Pick, J. Rabani, F. Yost, I. Fridovich, *J. Am. Chem. Soc.*, **1974,** *96*, 7329-7333.

(28) C. Bull, J. A. Fee, *J. Am. Chem. Soc.*, **1985,** *107*, 3295-3304.

(29) J. Imlay, I. Fridovich, *J. Biol. Chem.*, **1991**, *266*, 6957-6965.

(30) (a) T. Nunoshiba, E. Hidalgo, C. F. Amábile Cuevas, B. Demple, *J. Bacteriol.*, **1992,** *174*, 6054-6060. (b) J. Wu, B. Weiss, *J. Bacteriol.* **1992,** *174*, 3915-3920.

(31) A. Price-Whelan, L. E. Dietrich, D. K. Newman, *J. Bacteriol*, **2007**, *189*, 6372-6381.

(32) (a) C. F. Kuo, T. Mashino, I. Fridovich, *J. Biol. Chem.*, **1987**, *262*, 4724-4727. (b) P. R. Gardner, I. Fridovich, *J. Biol. Chem.*, **1991,** *266*, 1478-1483. (c) V. R. Sutton, A. Stubna, T. Patschkowski, E. Münck, H. Beinert, P. J. Kiley, *Biochemistry*, **2004,** *43*, 791-798.

(33) J. A. Kovacs, L. M. Brines, *Acc. Chem. Res.*, **2007**, *40*, 501-509.

(34) (a) E. D. Coulter, J. P. Emerson, D. M. Jr. Kurtz, D. E. Cabelli, *J. Am. Chem. Soc.*, **2000,** *122*, 11555-11556. (b) C. Mathé, V. Nivière, T. A. Mattioli, *J. Am. Chem. Soc.*, **2005,** *127*, 16436-16441. (c) F. Bonnot, T. Molle, S. Ménage, Y. Moreau, S. Duval, V. Favaudon, C. Houée-Levin, V. Nivière, *J. Am. Chem. Soc.*, **2012,** *134*, 5120-5130.

Chapter 2
Mechanistic Studies on Formation of the Dinitrosyl Iron Complex of the [2Fe-2S] Cluster of SoxR Protein

2.1 Introduction

NO is a key signalling molecule in a diverse array of cellular processes, ranging from signal transduction in the nervous system to blood pressure regulation [(1)] and involvement in the immune response [(2)]. On the other hand, NO is a highly reactive and toxic-free radical gas that can freely diffuse into cells and attack cellular components [(3)]. In activated macrophages, NO can be a powerful toxic agent that kills pathogenic bacteria and tumour cells[(2)]. To survive the deleterious effects of NO, most bacteria have evolved specific NO-sensor proteins that regulate the expression of enzymes required for rapid detoxification of NO [(4), (5)]. It has become apparent that there are multiple regulatory systems in prokaryotes that mediate responses to NO [(4), (6)]. The bacterial transcriptional regulators NsrR[(7)], SoxR [(8)] and FNR[(9)]—all of which contain an iron–sulfur cluster—are involved in coordinating physiological responses to NO. In addition, the biological activity of iron–sulfur proteins, such as mitochondrial aconitase[(10)], IRP [(11)], ferrochelatase[(12)] and AirSR[(13)] are controlled by NO binding. Therefore, iron–sulfur clusters are potential sites for both NO-derived physiological signal transduction and toxicity.

Reactions of NO with cysteine-ligated iron–sulfur cluster proteins typically result in disassembly of the iron–sulfur core and formation of a dinitrosyl iron complex (DNIC)(Scheme 2-1)[(14), (15), (16)]. The identity and assignment of the DNIC are based on its observed g = 2.03 ESR signals[(17)], which have been used to follow DNIC formation from iron–sulfur clusters[(18), (19)]. However, other types of reaction products, such as an ESR-silent, thiolate-bridged $[Fe_2(\mu\text{-}SR)_2(NO)_4]$ species with a Roussin's red ester (RRE) formula have also been observed[(20), (21)]. More convincing evidence for the mechanism of DNIC formation and the intermediates along the reaction pathway is provided by data obtained using the synthetic model compounds [2Fe-2S] and [4Fe-4S] clusters [(22), (23)].

e_{aq}^- react with NO_2^- to form NO[(24)]. With the pulse radiolysis technique, it is possible to produce NO within nanoseconds, allowing the reaction of NO to be followed spectrophotometrically through pulse radiolysis of aqueous solutions in the presence of nitrite under anaerobic conditions[(25), (26)]. Spectral identification of products has been reported for the reactions of NO with O_2^- [(25)] and the iron complex of *N*-(dithiocarboxy)sarcosine [(26)]. This method has also recently been used to characterize thionitrous acid (HSNO), by investigating the reaction of NO with SH·[(27)].

The disassembly of an iron-cluster by NO is exceedingly rapid, and intermediate nitrosylation products are too unstable to observe[(22), (28), (29), (30), (31)]. In this CHAPTER, it is described the application of pulse radiolysis to follow the reaction of NO with the [2Fe-2S] cluster of SoxR with nanosecond time resolution. The method aids in the identification of intermediate species and

mechanistic pathways for nitrosylation of iron–sulfur clusters. Using this approach, it was confirmed that NO reacts rapidly with the [2Fe-2S] cluster of SoxR. In addition, it is evident that the sensitivity of iron–sulfur proteins to NO is much higher in SoxR than in spinach Fd, an observation with possible wider implications for understanding the reaction of NO with iron–sulfur cluster-containing proteins.

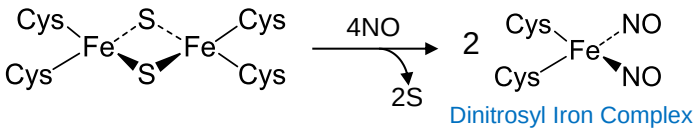

Scheme 2-1. Nitrosylation of [2Fe-2S] cluster.

2.2 Experimental

Materials

All chemicals were the highest purity available and were used without further purification. NOC7 (3-[2-hydroxy-2-nitrosohydrazino]-N-methyl-1-propanamine) was purchased from Dojin (Kumamoto, Japan). Bovine Ad, prepared from bovine adrenal glands[32], was kindly provided by Prof. Satoshi Miura (Tokyo University of Science). SoxR was prepared in the same manner as described in CHAPTER 1.

Pulse radiolysis

Pulse radiolysis experiments were performed using a linear accelerator at the Institute of Scientific and Industrial Research, Osaka University as described in CHAPTER 1. All experiments were performed at room temperature.

SoxR samples for pulse radiolysis were prepared by deoxygenating a solution containing 20–150 μM SoxR, 10 mM sodium phosphate (pH 7.0), 20 mM sodium tartrate, 0.5 M KCl, 0.1 M tert-butyl alcohol (for scavenging OH·) and 1–100 mM $NaNO_2$ by repeated evacuation and flushing with argon. The initial concentration of NO generated after the pulse was estimated from the concentration of e_{aq}^-, with the assumption that e_{aq}^- reacts quantitatively with NO_2^-. The e_{aq}^- concentration generated by pulse radiolysis was determined based on the absorbance change at 650 nm using an extinction coefficient of 14.1 mM^{-1} cm^{-1} [33]. The maximum concentration of NO was ~110 μM and could be adjusted by varying the dose of the electron beams.

Nitrosylation of SoxR and Fd. SoxR and Fd were nitrosylated by treatment with NOC7[28] or NO gas injection

A 1 mM stock solution of the NO donor NOC7 was prepared by dissolving in anaerobic 10 mM NaOH. Aliquots of solutions were rapidly mixed with SoxR or Fd at a molar ratio of 1:2 and incubated for 10–30 min. NO gas was injected into a sample cuvette containing SoxR or Fd after evacuation.

Sulfur determination

Elemental sulfur (S^0) was determined by Sörbo's method [30], [34], [35] using the addition of cyanide ion to generate SCN^-, which yields an absorption band at 460 nm upon addition of Fe^{3+} ions. Fe^{3+}-SCN^- concentrations were determined by reference to a calibration curve generated from a solution of sodium thiocyanate. For determination of S^0 following NO additions, nitrosylated SoxR and Fd were prepared by injection of NO gas under anaerobic conditions and used immediately.

Spectrophotometric measurements

Optical absorption spectra were measured with a Hitachi U-2900 spectrometer.

ESR measurements

ESR spectra were measured using a JES-RE2X spectrometer (X-band) with 100 kHz field modulation. Nitrosylated SoxR and Fd in ESR tubes were prepared by treatment with NOC7 or NO gas injection under anaerobic conditions, and were frozen at 77 K.

Samples for ESR measurements after pulse radiolysis were performed as follows: solutions of SoxR (40–100 μM) containing 10 mM potassium phosphate (pH 7.0), 20 mM potassium tartrate, 0.5 M KCl, 0.1 M tert-butyl alcohol and 50 mM $NaNO_2$ were deoxygenated in ESR tubes by repeated evacuation and flushing with argon. The samples in ESR tubes received one irradiation pulse from the electron linear accelerator, and then the reaction mixture was frozen immediately in liquid N_2. ESR spectra were measured at 77 K. Spin concentrations were measured by double integration of the first-derivative ESR spectra and comparison with the corresponding intensities of known standards.

2.3 Results

Nitrosylation of $SoxR_{ox}$ proteins was accomplished by treating with the NO donor NOC7. Addition of the NO-releasing reagent NOC7 to an anaerobic sample of $SoxR_{ox}$ was followed by measurement of UV-visible absorption. Progressive decreases in absorption were observed at 325 nm and in the region ~450–560 nm, with a smaller increase observed at ~400 nm. Time-course experiments indicated that formation of the DNIC of SoxR was completed within 20 min. Figure 2-1 (A) shows the absorption spectra of $SoxR_{ox}$ and the DNIC form of SoxR. The spectrum of the DNIC of SoxR is essentially identical to that reported previously[36]. Verification of the formation of DNICs was provided by the presence of an ESR spectrum with a signal at g = 2.03 (Figure 2-2). A similar ESR spectrum was obtained on NO gas injection to $SoxR_{ox}$ under anaerobic conditions.

It has been reported that Fd gives no indication of NO-induced cluster degradation, unlike mammalian ferrochelatase[12]. In contrast, upon the anaerobic addition of NOC7 to anaerobic sample of Fd, we observed a small change in the absorption of Fd over 30 min (Figure 2-1 (B)). A similar

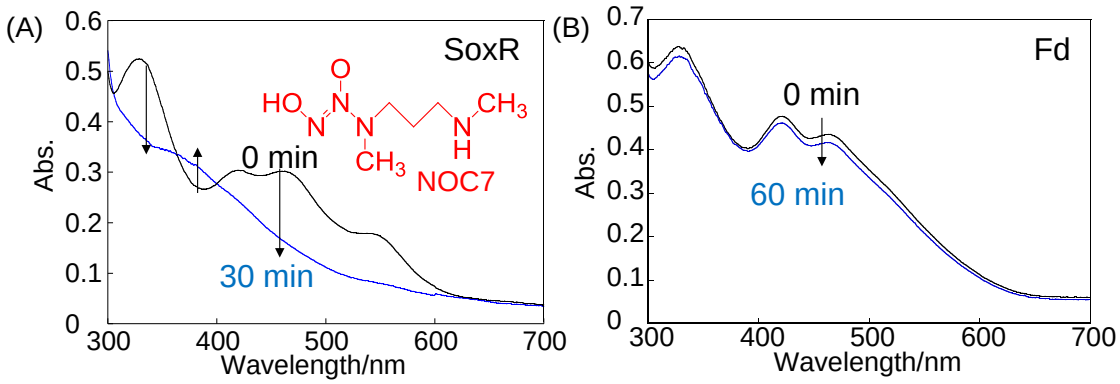

Figure 2-1. Absorbance changes upon the mixing of (A) 30 μM SoxR with 85 μM NOC7 and (B) 42 μM Fd with 105 μM NOC7.

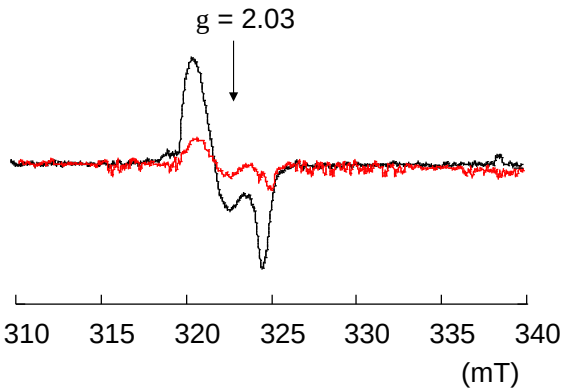

Figure 2-2. ESR spectra (77 K) of SoxR (black line) and spinach Fd (red line) at 30 min after addition of 2 equivalents of NOC7.

Table 2-1. Sulfur (S^0) content after treatment of SoxR and Fd with NO (~1 mM).

Sample	[2Fe-2S]/μM	S^0/μM	S^0/[2Fe-2S]
SoxR1	30	54.8	1.82
SoxR2	40	88.5	2.21
SoxR3	50	86.0	1.72
Fd	80	25.2	0.32

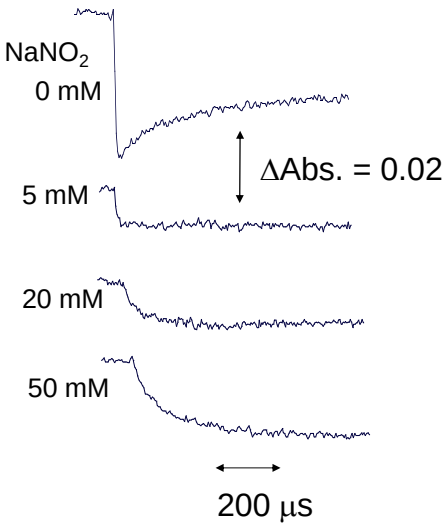

Figure 2-3. NO_2^- concentration dependence of absorption changes after pulse radiolysis of SoxR in the presence of NO_2^- measured at 420 nm. The samples contained 40 μM SoxR and 68 μM NO.

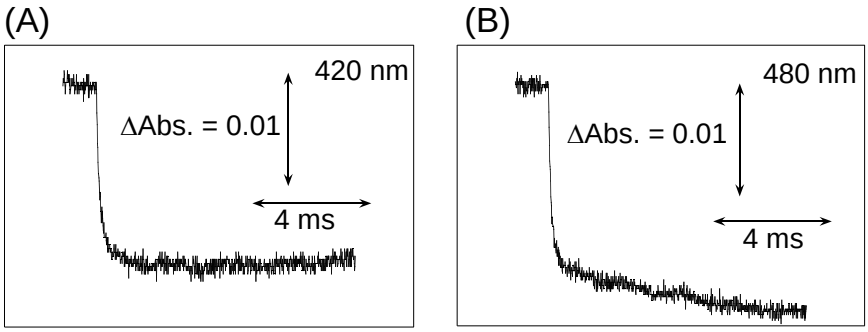

Figure 2-4. Absorbance changes after pulse radiolysis of $SoxR_{ox}$, measured at (A) 420 nm and (B) 480 nm in the presence of 50 mM $NaNO_2$. Samples contained 40 μM $SoxR_{ox}$ and 68 μM NO.

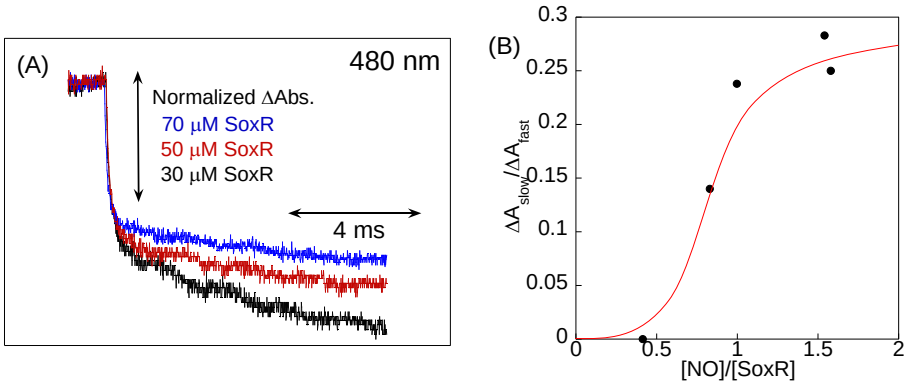

Figure 2-5. (A) SoxR-concentration dependence of absorption changes monitored at 480nm after pulse radiolysis in the presence of 50 mM NaNO2. Samplese contained 52 mM NO. Absorbance changes of slower phase were normalized to the respective faster phase for each SoxRox concentration. (B) The SoxR-concentration dependence of the slow phase fraction. The rations ([B]/[A]) are plotted against the concentration of SoxR, where A and B are the absorbance changes of faster and slower absorbance changes respectively.

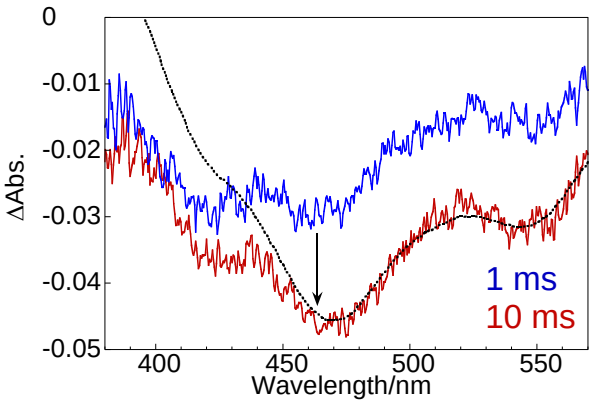

Figure 2-6. Comparison of the kinetic difference spectra obtained 1 ms (blue line) and 10 ms (red line) after pulse radiolysis with DNICs minus the oxidized difference spectrum (dashed line). Samples contained 70 μM $SoxR_{ox}$ and 75 μM NO.

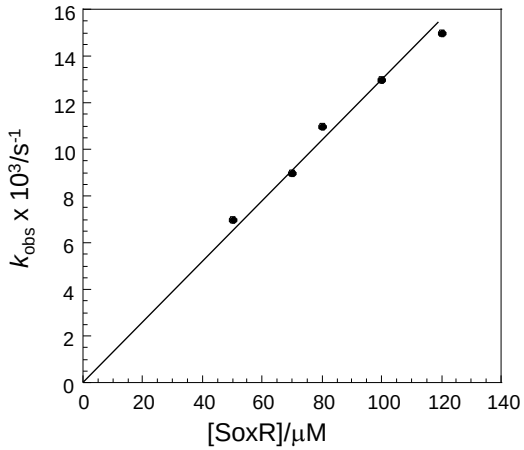

Figure 2-7. SoxR-concentration dependence of apparent rate constants of the absorption decrease at 420nm.

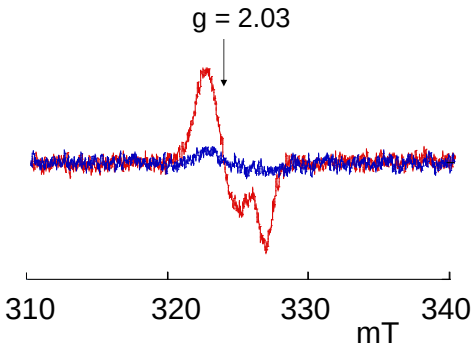

Figure 2-8. ESR spectra of $SoxR_{ox}$ treated with a saturated solution of NO (red line) and $SoxR_{ox}$ after pulse radiolysis in the presence of $NaNO_2$ (blue line) at 77K

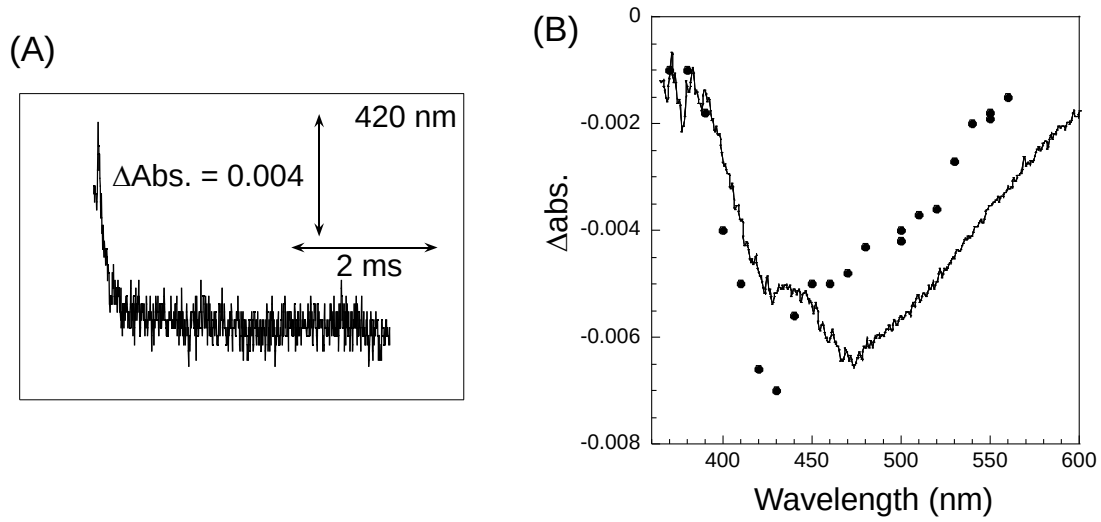

Figure 2-9. (A) Absorbance change at 420 nm after pulse radiolysis of spinach Fd, measured in the presence of 50 mM NaNO2. Samples contained 80 μM Fd, 10 mM sodium phosphate buffer (pH7.0), 0.1 M tert-butyl alcohol. 39 μM NO was generated. (B) Comparison of the kinetic difference spectrum obtained 1 ms (●) with that of NOC7-treated Fd minus oxidized Fd (solid line).

spectral change of Fd was seen on injection of NO gas. The formation of DNICs of Fd was confirmed based on ESR spectra (Figure 2-2). Integration of the g = 2.03 signal yielded only 5–8% of the ESR spectrum of the [2Fe-2S] cluster, and correlated with the absorption change accompanying the nitrosylation of Fd (Figure 2-1 (B)). From these results, it is concluded that [2Fe-2S] cluster of SoxR is so readily nitrosylated by low concentration of NO, as compared with that of Fd.

The amount of elemental sulfur was quantified after reactions of SoxR and Fd with excess NO. Approximately two S^0 atoms were detected on completion of the nitrosylation reaction of SoxR (Table 2-1). In contrast, 0.3 equivalents of S^0 were detected after reaction of NO with Fd, reflecting the incomplete nitrosylation of Fd.

Using pulse radiolysis, it has been shown that NO is produced by the reaction of e_{aq}^- with NO_2^- under deaerated conditions [(36), (24)]. This was confirmed spectrophotometrically by formation of the NO complex of Fe^{2+} myoglobin (Mb). In this study, it was reported that the application of this method to the reaction of NO with the [2Fe-2S] cluster of SoxR. In the absence of NO_2^-, e_{aq}^- rapidly reacted with $SoxR_{ox}$ to form the reduced form of SoxR ($SoxR_{red}$) in a microsecond time scale. These initial changes in absorption subsequently partially reversed on a time scale of milliseconds (Figure 2-3). The recovery process corresponds to reoxidation of [2Fe-2S] cluster of $SoxR_{red}$ by O_2^-, since the recovery was inhibited by addition of superoxide dismutase (CHAPTER 1). In the presence of NO_2^-, e_{aq}^- reacted with both $SoxR_{ox}$ and NO_2^-. The initial rapid decrease in absorption, caused by the reaction of e_{aq}^-, decreased with increases in the concentration of NO_2^-. At an NO_2^- concentration of

20 mM, the rapid decrease in absorption was completely lost, indicating that all the e_{aq}^- generated by pulse radiolysis reacted with NO_2^- to give NO. Instead, the slower decrease was seen on a time scale of hundreds of microseconds and increased up to an NO_2^- concentration of 50 mM. Therefore, we conclude that the change in absorption observed in the presence of 50 mM $NaNO_2$ in Figure 2-3 is due to the reaction of NO with $SoxR_{ox}$. Under these conditions studied (50 mM $NaNO_2$), e_{aq}^- reacts with NO_2^- nearly quantitatively.

When 68 μM NO was generated in a solution of 40 μM $SoxR_{ox}$, the time profile observed at 480 nm was composed of two phases—a fast phase and a slow phase. In contrast, only the faster decrease was observed at 420 nm (Figure 2-4). This indicates that at least two distinct reactions are involved under the experimental condition. The effect of $SoxR_{ox}$ concentration on the biphasic behavior at 480 nm was investigated at a fixed radiation dose ([NO] = 52 μM). As shown in Figure 2-5 (A), which depicts absorbance changes normalized to the respective faster phase for each $SoxR_{ox}$ concentration, the fraction of the slower phase with respect to the faster phase increased with decreasing $SoxR_{ox}$ concentration. In contrast, no second phase was observed at 420 nm. The ratios of the slower phase to the faster absorbance change were plotted against the ratio, [NO]:[$SoxR_{ox}$] (Figure 2-5 (B)). The absorbance changes displayed single-phase at less than ~0.5 equivalents of NO to SoxR. The fraction of the slower phase increased with increases in the molar ratio [NO]/[SoxR] and reached a plateau at ~2 equivalents of NO. Accordingly, it is concluded that the faster phase corresponds to the reaction of 1 NO equivalent with the [2Fe-2S] cluster of SoxR, followed by the reaction of 2 NO equivalents.

The kinetic difference spectra corresponding the faster and slower phases are shown in Figure 2-6. The spectrum at the end of the faster phase (1 ms) exhibited absorption minima at 420, 460 and ~550 nm. In contrast, the spectrum of the slower phase at 10 ms had an absorption minimum at 460 nm. A comparison of the species appearing at 10 ms with the DNIC of SoxR revealed that both spectra are similar from 440 nm to 600 nm, although they are quite distinct in the range of 350–440 nm. The spectrum of DNIC has a broad absorption band at ~390 nm [15].

The rate constant of the reaction of NO with $SoxR_{ox}$ was determined by generating 5–9 μM NO in a solution containing 50–100 μM $SoxR_{ox}$. Under these conditions, the slower absorbance changes at 480 nm were not seen, and the absorption change at 420 nm obeyed pseudo-first-order kinetics, with a rate constant that increased with the concentration of $SoxR_{ox}$ (Figure 2-7). This indicates that the faster absorbance change is a consequence of a bimolecular reaction of NO with $SoxR_{ox}$. The second-order rate constant of the reaction was calculated to be $1.3 \times 10^8\ M^{-1}\ s^{-1}$.

To examine the formation of DNICs after pulse radiolysis of $SoxR_{ox}$ in the presence of 50 mM $NaNO_2$, the ESR spectrum of a one-shot irradiated sample was measured. The appearance of the ESR signal at g = 2.03, characteristic of the DNIC of SoxR, was identical to that obtained upon anaerobic introduction of NO gas into a $SoxR_{ox}$ solution (Figure 2-8). However, quantification of the

signal recorded in Figure 2-7 yielded a concentration corresponding to only 3–5% of the original cluster. This result reflects the fact that the amount of NO generated by the pulse is not sufficient for the formation of a DNIC. In addition, only a small cross section of a sample was analysed in the present experiment and diffusion would occur before the sample was frozen.

Figure 2-9 shows results obtained in similar experiments using Fd. A decrease in absorption at 420 nm was observed in a millisecond time scale (Figure 2-9 (A)). However, the absorbance changes were ~5-times smaller than those of $SoxR_{ox}$. Also in contrast to the results obtained with SoxR, the absorbance changes were not seen at a low dose of irradiation (NO concentrations < 20 μM). This can be explained by the low affinity of NO for the [2Fe-2S] cluster of Fd. In addition, it is noteworthy that further absorption changes were not observed at least 30 s after pulse radiolysis. Figure 2-9 (B) shows the kinetic difference spectrum at 1 ms after pulse radiolysis of Fd. The spectrum exhibited absorption minima at 420 nm, as was the case for SoxR, whereas the difference spectrum between Fd and the DNIC showed an absorption minimum at 460 nm. In contrast, bovine Ad, which contains a [2Fe-2S] cluster, showed no indication of a reaction with NO after pulse radiolysis.

When cells under non-stressed conditions are exposed to NO, NO would predominantly interact with $SoxR_{red}$ because SoxR is maintained in its reduced, inactive form, $SoxR_{red}$ [28]. However little is known about the kinetics of the reaction of $SoxR_{red}$ with NO. Here, to follow the reaction of NO with $SoxR_{red}$, it was monitored absorption changes after pulse radiolysis of a solution of $SoxR_{ox}$ in the presence of 1 mM NO_2^-. Under these conditions, e_{aq}^- reacts with both NO_2^- and $SoxR_{ox}$. The concentration of NO generated was ~10 μM. The initial absorption decrease at 420 nm was observed. However, further absorbance changes were not observed at least 10 s after pulse radiolysis. This may reflect the low affinity of NO for the [2Fe-2S] cluster of $SoxR_{red}$. It has been reported that treatment of $SoxR_{red}$ with a saturated solution of NO leads to degradation of the iron-cluster to give several species, including reduced Roussin's red ester (rRRE) and RRE[28]. These reactions seem to be complex and occurred more slowly.

2.4 Discussion

The spectrophotometric data presented here suggest the transient formation of 1 and 2 equivalent nitrosylations of the [2Fe-2S] cluster in $SoxR_{ox}$ through two successive NO binding steps. This proposal is supported by the dependence of the molar ratio ([NO]/[SoxR]) on biphasic absorbance changes (Figure 2-5). The observed biphasic character disappeared at less than ~0.5 equivalents of NO to SoxR. Under these conditions, a mononitrosyl iron complex would be formed by binding of the first NO equivalent. Binding of the second NO equivalent corresponds to the slower process in Figure 2-5. The fraction of the slower phase was increased with increases in the concentration of NO and reached a plateau at ~2 equivalents of NO. On the other hand, the reaction of $SoxR_{ox}$ with

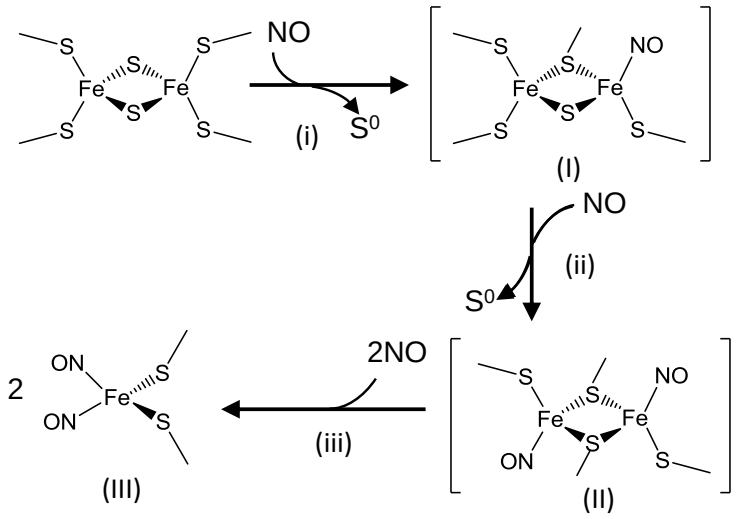

Scheme 2-2. Possible reaction pathway for [2Fe-2S] clusters with NO, based on the proposed synthetic model inorganic [2Fe-2S] cluster.

NO is complete at 4 NO molecules per [2Fe-2S] cluster, yielding two DNICs. In the present method, formation of the DNIC, characterized by an increase in absorption at ~390 nm [(14), (16), (20)] was not detected, even following generation of 110 μM NO in a solution of 20–40 μM $SoxR_{ox}$. In fact, only a portion of [2Fe-2S] clusters formed DNICs, as confirmed by the ESR spectrum of DNICs. The reaction of an additional 2 equivalents of NO may be a slow process.

Based on the proposed synthetic model inorganic [2Fe-2S] cluster[(22), (23)], a possible pathway for the formation of DNIC of SoxR is shown in Scheme 2-2. The reaction of the first NO equivalent with the [2Fe-2S] clusters to form a mononitrosyl iron complex (intermediate I), followed by the reaction of the second NO equivalent to form a dinitrosyl complex (intermediate II). These NO additions in each step result in reductive elimination of 1 mol equivalent of elemental sulfur, respectively. Reactions of another 2 equivalents of NO result in the disassembly of the iron complex to form the corresponding DNIC. In this reaction scheme, Harrop*et al.* [(22)] proposed that the breakdown of iron–sulfur cluster occurs in tandem with the sequestration of inorganic sulfur. The cysteine residues of SoxR may stabilize the DNIC formed during nitrosylation. When approximately equimolar NO was generated in a solution of $SoxR_{ox}$, two intermediates—a faster and a slower fraction considered to correspond to the mononitrosyl (intermediate I) and the dinitrosyl complexes (intermediate II), respectively—were formed. The most characteristic feature of intermediates I and II are their decreased absorption minima at 420 nm and 460 nm, respectively. These changes suggest that iron–sulfide and/or iron–cysteine interactions are significantly disrupted during these steps, but they also indicate the reduction of iron and oxidation of S^{2-} to S^0. The data in the present thesis provide

experimental support for the formation of two S^0 atoms on completion of the nitrosylation reaction of SoxR.

The first identified physiological target of NO was soluble guanylate cyclase (sGC). The binding of NO to the ferrous heme in sGC is only limited by the diffusion rate of NO to the heme pocket, with $k_{on} \approx 10^6$–$10^7\ M^{-1}\ s^{-1}$ and $k_{off} < 10^{-3}\ s^{-1}$ [37]. Such fast and tight binding to heme would guarantee NO signalling even in the presence of O_2 in the medium. Similarly, the reaction of NO with $SoxR_{ox}$ is very fast, leading to efficient formation of the DNIC. The rate constant (k_i) between NO and $SoxR_{ox}$ in the first step of Scheme 2-2 is $1.3 \times 10^8\ M^{-1}\ s^{-1}$. This rate is at least three orders of magnitude greater than that for the reaction of the [4Fe-4 S] cluster of WhiB protein with FNR (~ $10^5\ M^{-1}\ s^{-1}$)[29, 30]. This difference is a reflection of the protein environment of SoxR, in which the [2Fe-2S] cluster is located on the molecular surface. The upper sulfur atom (S2) and two Fe atoms are fully exposed to solvent[38]. The location of the [2Fe-2S] cluster in a solvent-exposed environment likely enables fast NO binding. SoxR responds not only directly to superoxide but also to multiple signals indicative of possible oxidative stress [39]. In Fd and Ad, on the other hand, the [2Fe-2S] cluster is shielded from the solvent by surrounding residues [40].

The results presented here provide the following important implications for the NO response in [2Fe-2S] clusters of proteins. The iron–sulfur cluster of Fd was insensitive to NO-induced disassembly, unlike that of SoxR. Moreover, the absorbance changes after pulse radiolysis of Fd were not detected at a low dose of irradiation (NO concentrations < 20 μM). This result suggests that NO binds the [2Fe-2S] cluster of Fd with low affinity. In addition, no slower phase was observed for Fd. The Fd reaction-product spectrum, which exhibited an absorption minimum at 420 nm (Figure 2-9), may indicate the reaction of 1 NO equivalent with the Fd cluster, which is analogous to intermediate I of SoxR. NO binding and S^{2-}oxidation occur concomitantly to yield S^0 in the model inorganic [2Fe-2S] clusters[22] and SoxR. In Fd and Ad, both sulfur atoms of the [2Fe-2S] cluster form similar hydrogen bonds with the main chain. In contrast, the S2 atom of the [2Fe-2S] cluster is fully exposed to the solvent. This may result in an inefficient and slow 2 equivalent NO reaction in Fd. In addition, an unusual CX_2CXCX_5C motif for the binding of the [2Fe-2S] cluster of SoxR, which has only a single residue (Gly123) between the two internal Cys residues, is different from those of other [2Fe-2 S] proteins. Disassembly of the iron–sulfur cluster in $SoxR_{ox}$ to form the DNIC is rapid, presumably owing to the high affinity of diferric iron for NO.

The mechanisms of NO- and O_2^--meditated activation differ markedly. The redox regulation with SoxR is mediated by a shift in the redox equilibrium of SoxR[41], with transcription reversibly inhibited by reactions linked to NAD(P)H[42]. In contrast, the reaction between NO and $SoxR_{ox}$ is irreversible, with the concomitant formation of a protein-bound DNIC. Enzymatic pathways, however, may eliminate the DNIC[19]. For example, cysteine desulfurase, together with L-cysteine, has been shown to efficiently repair the NO-modified form of the [2Fe-2S] cluster of ferredoxin [43].

2.5 Conclusion

Spectrophotometric analyses revealed the transient formation of 1 and 2 equivalents of nitrosylation products in the [2Fe-2S] cluster of SoxR. The second process was not observed with Fd under the same experimental conditions. These results suggest that the reaction of the second equivalent of NO may be important for the disassembly of a variety of iron–sulfur proteins.

References

(1) (a) L. J. Ignarro, G. M. Buga, K. S. Wood, R. E. Byrns, G. Chaudhuri, *Proc. Natl. Acad. Sci. USA.*, **1987,** *84*, 9265-9269. (b) R. M. Rapoport, M. B. Draznin,, F. Murad, *Nature,* **1983,** *306*, 174-176. (c) R. F. Furchgott, P. M. Vanhoutte, *FASEB J.,* **1989,** *3*, 2007-2018. (d) H. Prast, A. Philippu, *Prog. Neurobiol.,* **2001,** *64*, 51-68.

(2) (a) C. Bogdan, *Nat. Immunol.*, **2001,** *2,* 907-916. (b) J. MacMicking, Q. W. Xie, C. Nathan, *Annu. Rev. Immunol.*, **1997**, *15*, 323-350.

(3) (a) M. C. Broillet, *Cell. Mol. Life Sci.,* **1999,** *55*, 1036-1042. (b) Y. M. Kwon, B. Weiss, *J. Bactriol.*, **2009,** *191*, 5369-5376. (c) B. Weiss, *J. Bactriol.* **2006,** *188*, 829-833. (d) C. Nathan, J. Clin. *Invest.* **2003,** *111*, 769-778.

(4) S. Spiro, *FEMS Microbiol. Rev.*, **2007,** *31*, 193-211.

(5) (a) B. D. Autréaux, N. P. Tucker, R. Dixon, S. Spiro, *Nature*, **2005,** *437*, 769-772. (b) D. M. Bodenmiller, S. Spiro, *J. Bacteriol.,* **2006,** *188*, 874-881.

(6) (a) H. Corker, R. K. Poole, *J. Biol. Chem.*, **2003**, *278*, 31584-31592. (b) A. M. Gardner, C. R. Gessner, P. R. Gardner, *J. Biol. Chem.,* **2003**, *278*, 10081-10086. (c) M. M. Nakano, H. Geng, S. Nakano, K. Kobayashi, *J. Bactriol.*, **2006,** *188*, 5878-5887. (d) P. Mukhopadhyay, M. Zheng, L. A. Bedzyk, R. A. LaRossa, G. Storz, *Proc. Natl. Acad. Sci. USA.,* **2004,** *101*, 745-750.

(7) (a)N. P Tucker, M. P. Hicks, T. A. Clarke, J. C. Crack, G. Chandra, N. E. LeBrun, R. Dixon, M. J. Hutchings, *PLoS ONE*, **2008**, *3*, e3623.(b) E. T. Yuki, M. A. Elbaz, M. M. Nakano, P. MoënneLoccoz, *Biochemistry*, **2008,** *47*, 13084-13092.

(8) T. Nunoshiba, T. DeRojas-Walker, J. S. Wishnok, S. R. Tannenbaum, *Proc. natl. Acad. Sci. USA.*, **1993,** *90*, 9993-9997.

(9) H. Cruz-Ramos, J. Crack, G. Wu, M. H. Hughes, C. Scott, A. J. Thomson, J. Green, R. K. Poole, *EMBO J.,* **2002,** *21*, 3235-3244.

(10) L.Castro, M. Rodriguez, R. Radi, *J. Biol. Chem.,* **1994,** *269*, 29409-29415.

(11) J. C. Drapier, H. Hirling, J. Wietzerbin, P. Kaldz, L. C. Kühn, *EMBO J.*, **1993,** *12*, 3643-3649.

(12) V. M. Sellers, M. K. Johnson, H. A. Dailey, *Biochemistry*, **1996,** *35*, 2669-2704.

(13) F. Sun, Q. Ji, M. B. Jones, X. Deng, H. Ling, B. Frank, J. Telser, S. N. Perterson, T. Bae, C. He, *J. Am. Chem. Soc.,* **2012,** *134*, 305-314.

(14) A. R. Butler, I. L. Megson, *Chem. Rev*., **2002,** *102*, 1155-1166.

(15) H. Lewandowska, M. Kalinowska, K. Brzòska, K. Wòjciuk, g. Wòjciuk, M. Kruszewski, *Dalton Trans.*, **2011**, *40*, 8273-8289.

(16) A. F. Vanin, *Nitric Oxide*, **2009,** *21*, 1-13.

(17) S. Costanzo, S. Menage, R. Purrelo, R. P. Bonomo, M. Fontecave, *Inorg. Chem. Acta*, **2001**, *318*, 1-7.

(18) (a) G. M. Pieper, N. L. Halligan, G. Hilton, E. A. Konorev, C. C. Felix, A. M. Rosa, M. B. Adams, O. W. Griffith, *Proc. Natl. Acad. Sci. USA.*, **2003,** *100*, 3125-3130. (b) M. C. Kenedy, W. E. Antholine, H. Beinert, *J. Biol. Chem.*, **1997,** *272*, 3125-3130.

(19) H. Ding, B. Demple, *Proc. Natl. Acad. Sci. USA.*, **2000**, *97*, 5146-5150.

(20) Z. J. Tonzetich, H. Wang, D. Mitra, C. E. Tinberg, L. H. Do, F. E. Jr. Jenney, M. W. W. Adams, S. P. Cramer, S. J. Lippard, *J. Am. Chem. Soc.*, **2010,** *132*, 6914-6916.

(21) C. E. Tinberg, Z. J. Tonzetich, H. Wang, L. H. Do, Y. yoda, S. P. Cramer, S. J. Lippard, *J. Am. Chem. Soc.*, **2010,** *132*, 18168-18176.

(22) T. C. Harrop, Z. J. Tonzetich, E. Reisner, S. J. Lippard, *J. Am. Chem. Soc.*, **2008,** *130*, 15602-15610.

(23) A. G. Tennyson, S. Dhar, S. J. Lippard, *J. Am. Chem. Soc.*, **2008,** *130*, 15087-15098.

(24) M. Grätzel, H. Henglein, J. Lilie, G. Beck, *Ber. Busenges. Phys. Chem.*, **1969**, *73*, 646-653.

(25) K. Kobayashi, M. Miki, S. Tagawa, *J. Chem. Soc. Dalton Trans.*, **1995**, *17*, 2885-2889.

(26) S. Fujii, K. Kobayashi, S. Tagawa, *J. Chem. Soc. Dalton Trans.*, **2000,** *19*, 3310-3315.

(27) M. R. Filipovic, J. L. Miljkovic, T. Nauser, M. Royzen, K. Klos, T. Shubina, W. H. Koppenol, S. J. Lippard, Ivanovic-Burmazovic, *J. Am. Chem. Soc*., **2012**, *134*, 12016-12027.

(28) F. C. Lo, C. L. Chen, C. M. Lee, M. C. Tsai, T. T. Lu, W. F. Liaw, S. S. F. Yu, *J. Biol. Inorg. Chem.*, **2008**, *13*, 961-972.

(29) Z. J. Tonzetich, L. E. McQuade, S. J. Lippard, *Inorg. Chem.*, **2010**, *49*, 6338-6348.

(30) J. C. Crack, L. J. Smith, M. R. Stapleton, J. Peck, J. Watmough, M. J. Buttner, R. S. Buxton, J. Green, V. S. Oganesyan, A. J. Thomson, N. E. L. LeBrun, *J. Am. Chem. Soc*., **2010,** *133*, 1112-1121.

(31) J. C. Crack, M. R. Stapleton, J. Green, A. J. Thomson, N. E. Lebrun, *J. Miol. Chem.*, **2013**, *288*, 11492-11502.

(32) A. Hiwatashi, Y. Ichikawa, N. Maruya, T. Yamano, K. Aki, *Biochemistry*, **1976**, *15*, 3082-3090.

(33) S. Gordon, E. J. Hart, *J. Am. Chem. Soc*., **1964**, *86*, 5343-5344.

(34) B. Sörbo, *Biochim. Ciophys. Acta*, **1957,** *23*, 412-416.

(35) D. Petering, J. A. Fee, G. Palmer, *J. Biol. Chem*., **1971**, *246*, 643-653.

(36) F. C. Lo, J. F. Lee, W. F. Liaw, I. J. Hsu, Y. F. Tsai, S. C. Chan, S. S. F. Yu, *Chem. Eur. J.*, **2012**, *18*, 2565-2577.

(37) (a)J. R. Stone, M. A. Marletta, *Biochemistry*, **1996,** *35*, 1093-1099. (b) V. G. Kharitonov, V. S. Sharma, D. Magde, D. Koesling, *Biochemistry*, **1999**, *38*, 10699-10706.

(38) S. Watanabe, A. Kita, K. Kobayashi, K. Miki, *Proc. Natl. Acad. Sci. USA.*, **2008,** *105*, 4121-4126.

(39) L. E. Dietrich A. Price-Whelan, A. Petersen, M. Whiteley, D. K. Newman, *Mol. Microbiol.*, **2006**, *61*, 1308-1321.

(40) (a) W. R. Rypniewski, D. R. Breiter, M. M. Benning, G. Wesenber, B. H. Oh, J. L. Markley, I. Rayment, H. M. Holden, *Biochemistry*, **1991**, *30*, 4126-4131. (b) A. Müller, J. J. Müller, Y. A. Muller, H. Uhlmann, R. Mernhardt, U. Heinemann, *Structure*, **1998**, *6*, 269-280.

(41) (a) E. Hidalgo, B. Demple, *EMBO J*., **1994**, *13*, 138-146. (b) H. Ding, B. Demple, *Proc. Natl. Acad. Sci. USA.*, **1997**, *94*, 8445-8449.

(42) K. Kobayashi, S. Tagawa, *FEBS Lett.*, **1999**, *45*, 227-230.

(43) (a) P. A. Roger, H. Ding, *J. Biol. Chem.*, **2001,** *277*, 30980-30986. (b) W. Yang. P. A. Roger, H. Ding, *J. Biol. Chem*., **2002**, *277*, 12868-12873.

Chapter 3
Redox-Dependent DNA Distortion in a SoxR Protein-Promoter Complex Studied using Fluorescent Probes

3.1 Introduction

The critical steps involved in the regulation of prokaryotic gene expression typically occur at transcription initiation [(1)]. Interactions between activators or repressors and RNA polymerase are integral to the regulation of transcriptional initiation. Some transcriptional activators bind to specific sites upstream of the transcription start point and cause DNA bending at the site to which such activators bind[(2)]. Activator-induced DNA bending is typically associated with binding site recognition[(3)], alterations in DNA loop structures[(4)], or optimal positioning of the activator for promoting interactions with RNA polymerase[(5)]. MerR family is a unique example of these DNA-binding activators. Members of the MerR family activate transcription in response to a variety of environmental stresses in bacteria, including exposure to heavy metals [(6), (7)], oxidative stress[(8), (9)], and the presence of antimicrobials[(10), (11)], and regulate transcription via a DNA distortion mechanism [(7), (10), (12), (13), (14)].

MerR proteins invariably bind tightly to specific sites in dyad-symmetric DNA sequences within a promoter. In response to specific signals, these proteins undergo conformational changes that unwind the promoter region and allow RNA polymerase to initiate transcription. Promoters with 19-base-pair (bp) or 20-bp spacers are bent sharply in their center regions, locally untwisting base pairs and remodeling -35 and -10 promoter elements on the same face of the DNA helix[(10), (13), (14)]. Inducer-free structures in the inactive forms of MerR family proteins have not yet been reported.

The [2Fe–2S] cluster-containing SoxR protein, a member of the MerR family, is a transcription factor that regulates the soxRS response to oxidative stress [(8), (9)] and nitric oxide[(15)] in bacteria. X-ray crystallographic structures of the active state of *E. coli* SoxR and its complex with a 20-bp oligonucleotide of the target promoter have been reported[(14)]. The overall structure of the SoxR-DNA complex is similar to the structures reported for other MerR proteins[(10), (13), (16)]. Redox-induced structural changes in the [2Fe-2S] cluster of SoxR are communicated to the DNA-binding domain, which then distorts the target promoter structure[(14), (17)]. How the redox change of the [2Fe-2S] cluster is coupled to DNA distortion and transcription in the SoxR-DNA complex is not yet understood. In particular, it is not known whether DNA bound to the reduced form of SoxR is distorted.

In this CHAPTER, I addressed these questions by performing fluorescence measurements on the oxidized and reduced forms of SoxR in the presence of fluorescent probes introduced site-specifically into the promoter DNA. Localized changes in the structure and dynamics of promoter DNA incorporating these probes were then characterized using spectroscopic methods [(18),

[19]. The probes used, the adenine (A) analog of 2-aminopurine (2Ap) (Figure 3-1 (A)) and the cytosine (C) analog pyrrolo-dC (Figure 3-1 (B)), are highly fluorescent and pair well with thymine (T) and guanine (G), respectively[20], [21], [22], [23]. Both fluorescent analogs display diminished fluorescence quantum yields in the context of duplex DNA compared to the corresponding quantum yields in singlestranded DNA[22], [23]. Fluorescence quenching can be used to monitor local DNA melting. In the current study, we investigated the conformational changes in SoxR-bound promoter DNA upon reduction of the SoxR [2Fe-2S] cluster.

3.2 Experimental

Materials.

Oligonucleotides were synthesized and purified by HPLC at Sigma Genosis Co., Ltd., Japan. The pyrrolo-dC- and 2Ap-containing oligonucleotides were synthesized using the phosphoramidite method, and were purified by HPLC. All chemicals were of the highest purity available and were used without further purification.

Expression and Purification.

SoxR was prepared in the same manner as described in CHAPTER 1. The concentration of Δ37 SoxR protein was determined by the Coomerssie Blue method using bovine serum albumin as a standard. The Δ37 SoxR mutant was cloned from the *E. coli* chromosome using the primers (5'-GGTAAAGCGACATATGGAAAAGAAATTACC-3') and (5'-ACATCCCTCGAGTTCGTCACGCAGCGCCAT-3'). The PCR fragment was digested with NdeI and XhoI and inserted into pET21b (Novagen) digested with the same enzymes. The resulting expression plasmid was transformed into BL21(DE3) cells (Novagen). The mutant proteins were purified using a Ni-NTA-agarose column (Qiagen, Tokyo, Japan) that had been pre-equilibrated with buffer consisting 20 mM Tris-HCl (pH 7.4), 0.5 M NaCl, 1 mM EDTA, and 20 mM imidazole. The column was washed with the same buffer, and the protein was eluted with the same buffer containing 100 mM imidazole. Fractions containing the Δ37SoxR mutant protein were collected and applied to a gel-filtration column (HiLoad 16/60 Superdex 75 pg, GE Healthcare) equilibrated with 20 mM Tris-HCl (pH 7.6), 0.5 M NaCl. The molecular mass of Δ37SoxR was determined to be 14,113.4 Da (calculated: 14112.3 Da) by matrixassisted laser desorption/injection-time of flight (MALDI-TOF Bruker UltrafleXtreme™) using a sinapinic acid matrix with cytochrome C as the calibration standard.

Fluorescence Measurements

Fluorescence measurements were performed at 15°C using a Perkin-Elmer LS-50B spectrophotometer. Fluorescence emission from pyrrolo-dC and 2Ap were measured with excitation at 350 and 315 nm, respectively. Fluorescence measurements were conducted by adjusting the protein concentration to ~1 μM (in a buffer consisting of 10 mM Tris-HCl, (pH 7.3), 0.2 M KCl, and

10 mM potassium/sodium tartrate), and mixing with ~0.5 μM oligonucleotide solutions. Reduced SoxR was prepared by deoxygenating a sample of SoxR by repeated evacuation and flushing with argon in a sealed cell, followed by addition of sodium dithionite using a gastight Hamilton microsyringe under deaerated conditions (final sodium dithionite concentration: 0.5-1 mM).

Gel Filtration Chromatography

The molecular weight of Δ37SoxR was determined by gel filtration on a HiLoad 16/60 Superdex 200 pg (GE Healthcare) equilibrated with 20 mM Tris-HCl (pH 7.6), 0.5 M NaCl. The buffer flow rate was 1 ml/min, and protein was monitored at 280 nm.

Fluorescence Polarization Assay

Solution polarization was monitored using a Pan Vera Beacon 2000 Fluorescence Polarization System (Pan Vera Corp), with excitation at 485-490 nm, and emission collected at 525-535 nm, as described previously [13], [24]. Oligonucleotides (5`-fluorescene-labeled 5'-GCCTCAAGTTAACTTGAGGC-3') were synthesized and purified by HPLC (Sigma Genosys Biotech Co., Ltd.). Oligonucleotide solutions were heated to 90°C for 5 min and then cooled slowly back to room temperature over a period of 1 h to allow strands to anneal. The annealed, labeled oligonucleotides in 75 mM KCl, 10 mM Tris-HCl buffer (pH 7.3) were mixed with 0-1.3 mM Δ37 SoxR protein at 20°C (final volume of 100 μL). Each set of experiments was conducted by titrating protein into the DNA solution. After each addition of protein, the samples were incubated for 30 s to allow equilibrium to be reached before measurements were taken. The increase in fluorescence polarization of the fluorophore upon protein binding was measured.

3.3 Results

Five distinct 20-mer duplex oligonucleotides constructs incorporating 2Ap or pyrrolo-dC bases in the SoxR binding sequence at specific positions were synthesized (Table 3-1). The nucleotide numbering, by convention, is relative to the central base in the palindromic sequence of the 20-bp oligonucleotide. In the absence of SoxR, the fluorescence spectrum of 2Ap within the B-form duplex DNA was characterized by a peak at 356 nm, and was typically small (Fig. 3-2), owing to quenching by base stacking and hydrogen bonds[22], [23]. Under these conditions, the fluorescence peaks and their intensities were largely unaffected by the incorporated positions of probes in the oligonucleotides. In contrast, the addition of $SoxR_{ox}$ to the DNA constructs resulted in an increase in the fluorescence intensity and a shift in the fluorescence peak positions. The positions of peaks in SoxRox-DNA were 352 nm (Ap5), 356 nm (Ap7), 362 nm (Ap1), and 368 nm (Ap2) (Figure 3-2. 3-4). These results suggest a difference in the environment around 2Ap in the DNA-$SoxR_{ox}$ complex. We noted that the fluorescence intensity of 2Ap incorporated into the central bases (Ap1 and Ap2) was 2-3 times higher than that at different positions (Ap5 and Ap7). This can be interpreted to reflect

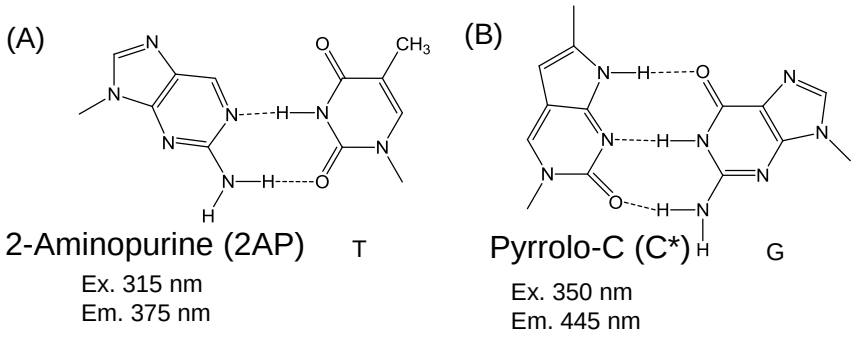

Figure 3-1. Structures of (A) 2AP base-paired with T and (B) pyrrolo-dC base-paired with G.

Table 3-1. Oligonucleotide sequences. The nucleotides the positions with colored back replaced with fluorescent analogs.

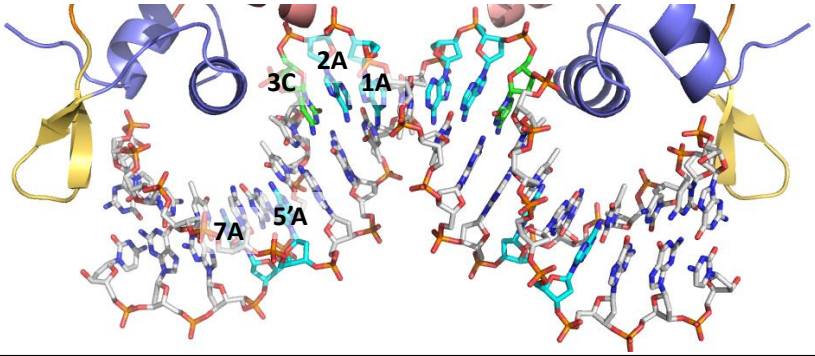

Name	Sequence																			
	10'	9'	8'	7'	6'	5'	4'	3'	2'	1'	1	2	3	4	5	6	7	8	9	10
Ap1	G	C	C	T	C	A	A	G	T	T	A	A	C	T	T	G	A	G	G	C
	C	G	G	A	G	T	T	C	A	A	T	T	G	A	A	C	T	C	C	G
Ap2	G	C	C	T	C	A	A	G	T	T	A	A	C	T	T	G	A	G	G	C
	C	G	G	A	G	T	T	C	A	A	T	T	G	A	A	C	T	C	C	G
Ap5	G	C	C	T	C	A	A	G	T	T	A	A	C	T	T	G	A	G	G	C
	C	G	G	A	G	T	T	C	A	A	T	T	G	A	A	C	T	C	C	G
Ap7	G	C	C	T	C	A	A	G	T	T	A	A	C	T	T	G	A	G	G	C
	C	G	G	A	G	T	T	C	A	A	T	T	G	A	A	C	T	C	C	G
Pc3	G	C	C	T	C	A	A	G	T	T	A	A	C	T	T	G	A	G	G	C
	C	G	G	A	G	T	T	C	A	A	T	T	G	A	A	C	T	C	C	G

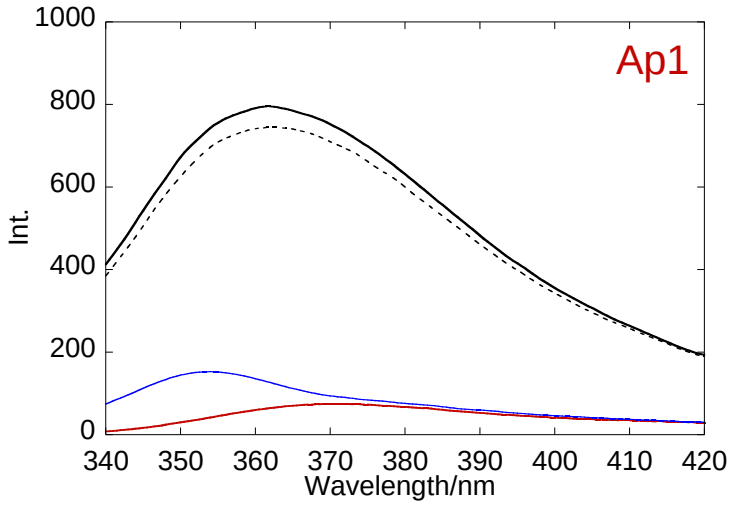

Figure 3-2. Fluorescence spectra of the SoxR-free Ap1 and SoxR-DNA (Ap1) complex. Shown are spectra of the SoxR-free Ap1 (blue line), the oxidized form (black solid line), the reduced form (red line) and the re-oxidized form (black dashed line) recorded after exposure to air for 20 min. The SoxR-free Ap1 sample contained 2μM Ap1, 10 mM Tris-HCl (pH 7.3), and 0.2 M KCl buffer. Each sample of SoxR contained 4μM SoxR, 2 μM Ap1, 10 mM Tris-Hcl, 10 mM sodium tartrate and 0.2 M KCl.

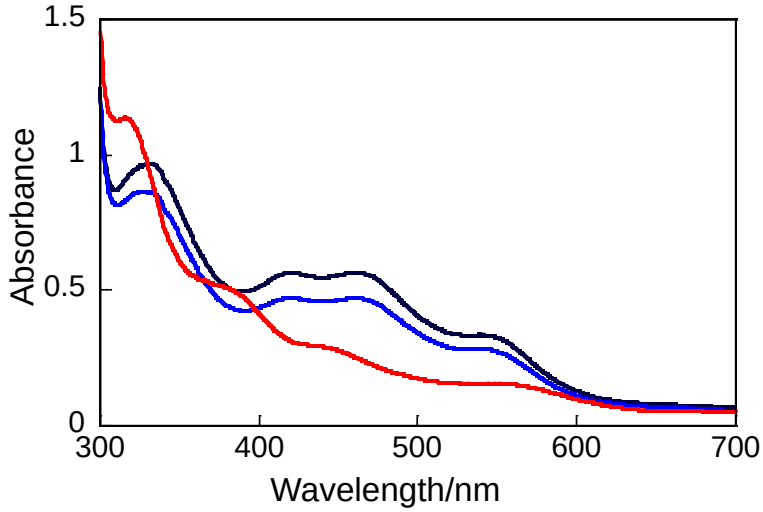

Figure 3-3. UV-visible absorbance spectra of DNA-SoxR complexes. Spectra of the oxidized (black line), reduced (red line) and reoxidized (blue line) forms recorded after re-exposure to air for 20 min are shown. Samples contained 63 μM SoxR, 60 μM Ap1, 10 mM Tris-HCl (pH7.3), 10 mM sodium tartrate and 0.2 MKCl.

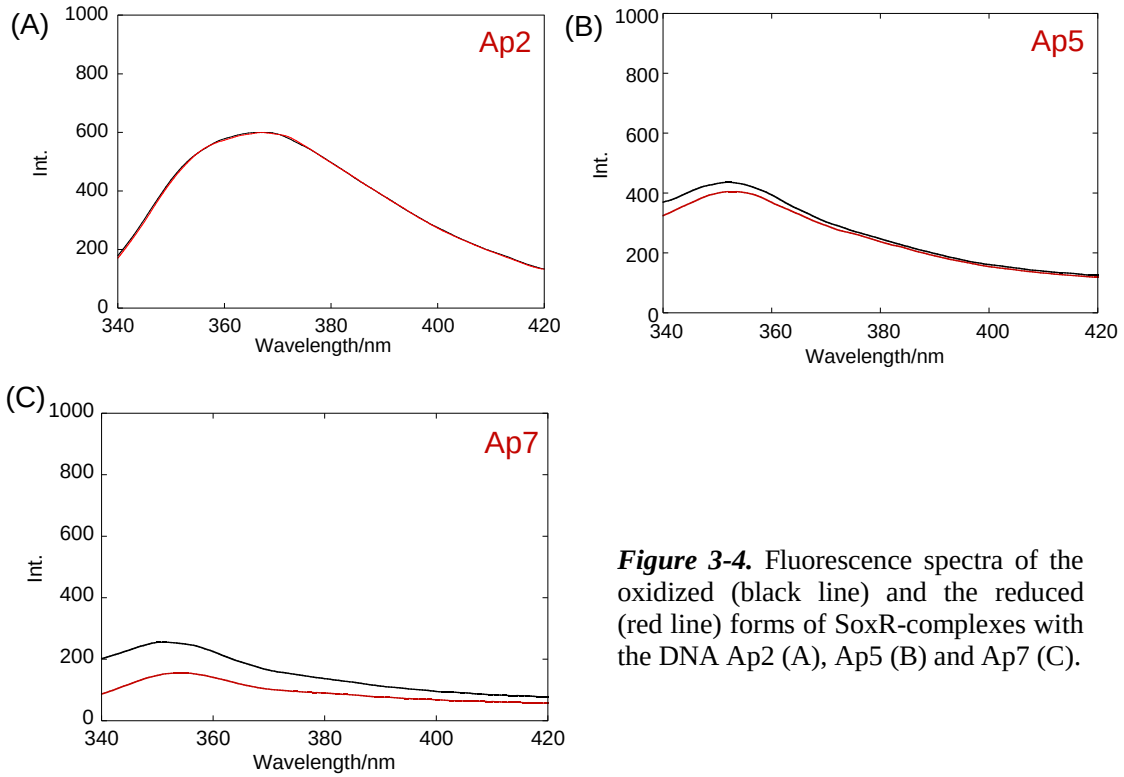

Figure 3-4. Fluorescence spectra of the oxidized (black line) and the reduced (red line) forms of SoxR-complexes with the DNA Ap2 (A), Ap5 (B) and Ap7 (C).

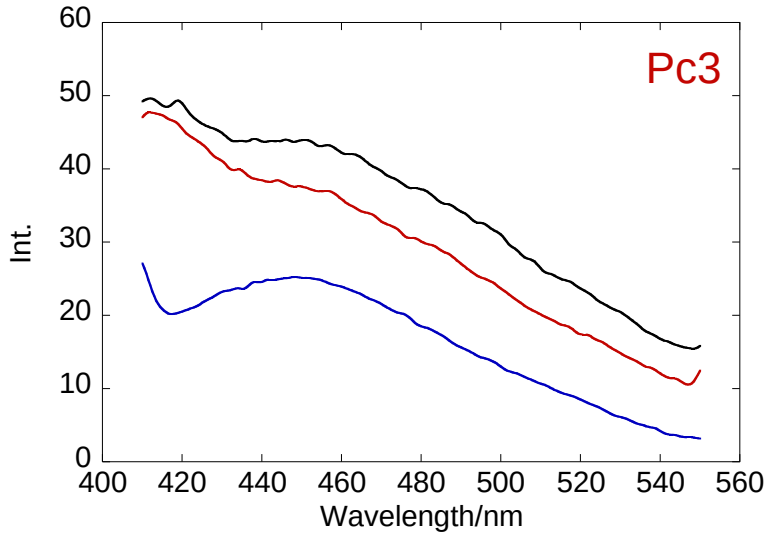

Figure 3-5. Fluorescence spectra of oxidized (black line) and reduced (red line) forms of SoxR-Pc3 complexes and the SoxR-free Pc3 (blue line).

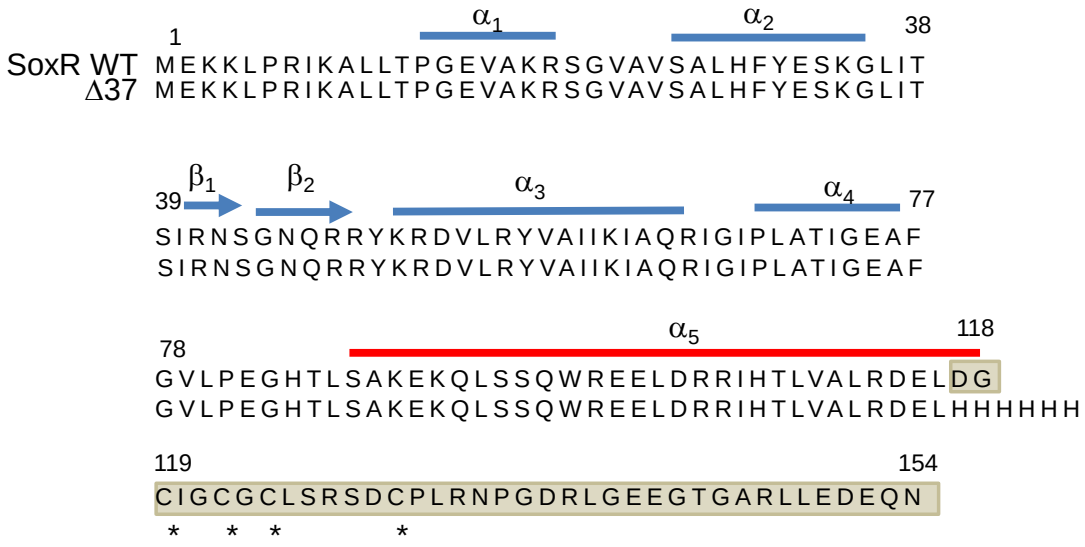

Figure 3-6. The amino acid sequence (single-letter format) of the SoxR wild-type and deletion mutant. The [2Fe-2S] cluster-bind cysteines are marked with asterisks.

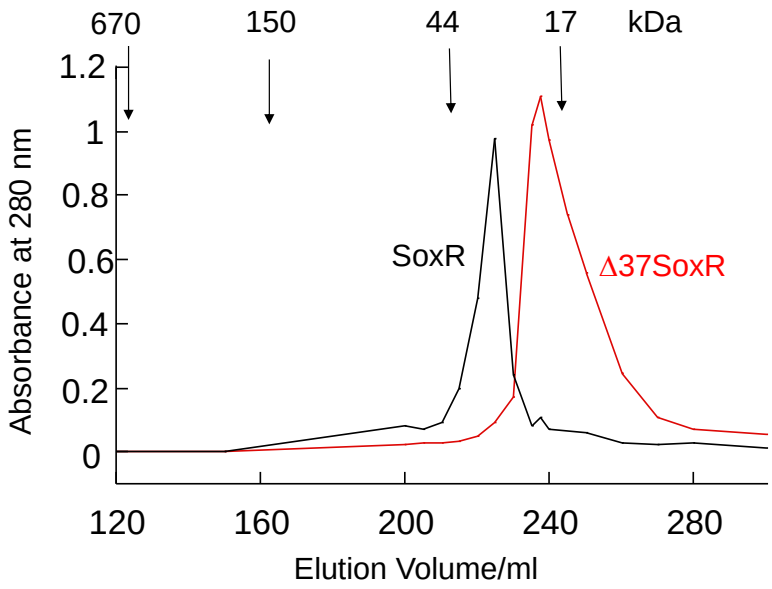

Figure 3-7. Gel filtration chromatography of SoxR and Δ37SoxR proteins. Arrows mark elution positions of protein molecular weight standards.

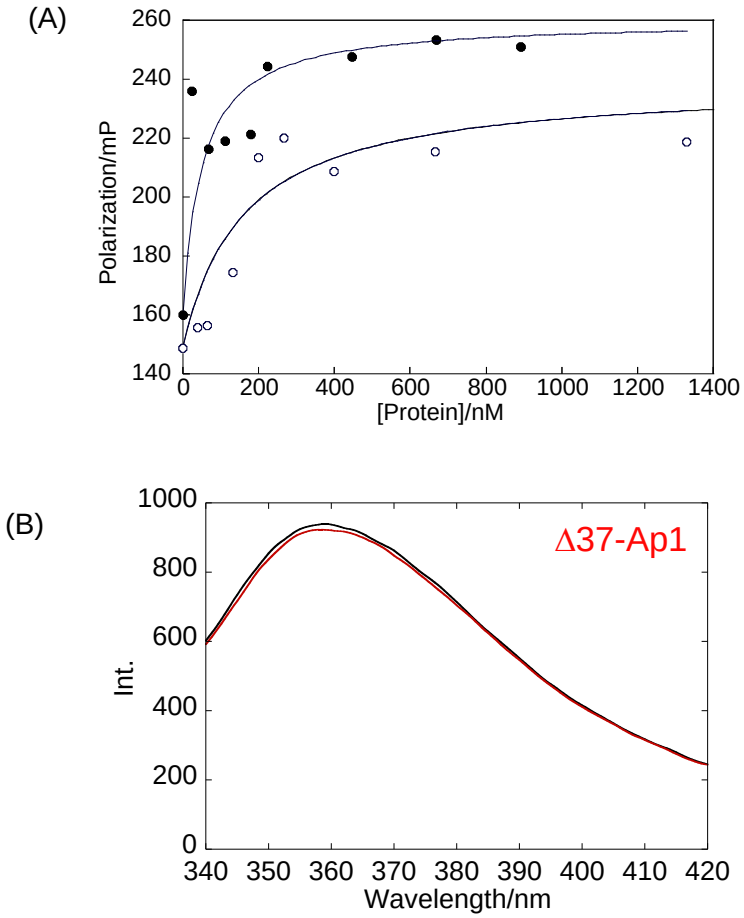

Figure 3-8. (A) DNA binding to wild-type SoxR (●) and the Δ37SoxR mutant (○), monitored by measuring fluorescence polarization. (B) Fluorescence spectra of Δ37SoxR-Ap1 complexes in the presence or absence of sodium dithionite.

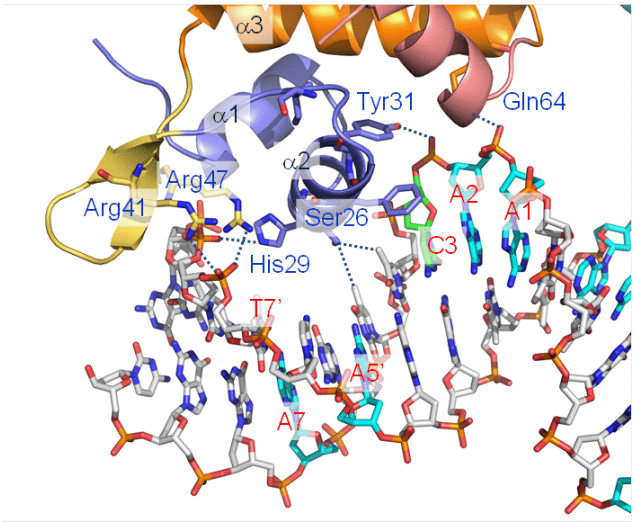

Figure 3-9. SoxR- DNA interaction. SoxR-DNA half-site interface. The structure was reproduced using PyMol, based on a structure obtained from the Protein Data Bank (code 2ZHF).

the poor stacking among conformers and the weakness of base pairing between 2Ap and T, which is consistent with the crystal structure of the SoxRox-DNA complex[14]. The two central A1/T1' and T1'/A1 base pairs form a distorted Watson-Crick base pairs, where the rise, roll, and twist values of the central base step between A1/T1' and T1'/A1 are 3.1, 12.5, and 43.9 Å, respectively. Distortion of the base stacking between the adjacent A2 and A1 bases is observed, and this reflected on the fluorescence intensity of Ap2. Beyond this localized distortion, the remaining base pairs of the promoter, 3/3' to 10/10', return to duplex B-form DNA.

This is consistent with the fluorescence spectra of Ap5 and Ap7, which were highly similar to that of 2Ap within the B-form duplex DNA. Addition of the reducing agent sodium dithionite to the [2Fe-2S] cluster of the SoxRox-DNA (Ap1) complex dramatically decreased the fluorescence intensity while shifting the fluorescence peak from 362 nm to 370 nm (Figure 3-2). In a control experiment, the fluorescence spectra of SoxR-free Ap1 were completely unaffected by the addition of sodium dithionite. Aeration of the reduced protein completely restored the original fluorescence (Figure 3-2). The corresponding changes in UV-visible absorption spectra in the DNA complex of SoxR (Figure 3-3) reflect the direct oxidation of the [2Fe-2S] clusters of SoxR by O_2. These findings indicate that the fluorescence change shown in Figure 3-2 was caused by the reversible reduction of the protein, not by irreversible destruction of the iron-sulfur cluster. The fluorescence changes associated with DNA complexes in which 2Ap was introduced at different positions provided additional insight into the structural transitions that accompany the redox process. Figure 3-4 shows a comparison of changes in fluorescence spectra caused by reduction of the SoxR-DNA (Ap2, Ap5, and Ap7) complexes. Upon reduction, the fluorescence intensity of Ap7 decreased by approximately 40%, whereas that of Ap2 and Ap5 did not change significantly. The redox states of the SoxR protein had little effect on the fluorescence of Ap2 and Ap5, implying that the redox change does not affect the environment of A2 and A5 in DNA- bound SoxR.

Pyrrolo-dC, which emits fluorescence at 445 nm upon excitation at 350 nm, was incorporated into the central region (C3 and C3') of the promoter sequence. In the absence of SoxR, Pc3 exhibited weak fluorescence. The addition of SoxRox slightly increased the fluorescence intensity of Pc3, and the subsequent reduction of the SoxR [2Fe-2S] cluster resulted in a small change (~16%) in the fluorescence intensity (Figure 3-5). These observations suggest that the redox change does not affect the environment of Pc3.

The role of the [2Fe-2S] cluster in fluorescence changes was further examined by characterizing the properties of a deletion mutant (Δ37SoxR) lacking a CX_2CXCX_5C motif in the C-terminus of the SoxR [2Fe-2S] cluster. The Δ37SoxR mutant (Figure 3-6), which consists of an N-terminal winged helix (α1-4) DNA-binding domain and a dimerization helix (α-5) domain, was designed based on an X-ray structure analysis[14]. Although the molecular mass of Δ37SoxR was 14112.3, the protein had an elution volume between that of native SoxR (34 kDa) and myoglobin (17 kDa), determined by gel

filtration chromatography (Figure 3-7). Thus, Δ37SoxR forms a stable dimer. The binding affinity of the Δ37SoxR mutant for DNA was compared with that of wild-type SoxR by performing fluorescence polarization assays using a fluorescence-labeled 20-bp oligonucleotide containing the promoter DNA sequence. The degree of polarization increased upon addition of Δ37SoxR and SoxR in a dose dependent manner, reaching saturation at protein concentrations greater than 500 nM (Figure 3-8 (A)). Under the conditions used, K_d values of 160 and 60 nM were calculated for Δ37SoxR and SoxR, respectively. Although the binding affinity of Δ37SoxR was approximately threefold lower than that of SoxR, Δ37SoxR retained its ability to bind the promoter region. Specifically, the Kd value indicates that 90% of the DNA was present as a Δ37SoxR protein-promoter complex under the experimental conditions used. Similar experiments with SoxRred could not be performed using this method owing to interference from added sodium dithionite.

The fluorescence spectrum for the DNA (Ap1)-Δ37SoxR complex, shown in Figure 3-8 (B), reveals a fluorescence at 358 nm. Interestingly, the fluorescence intensity was higher than that measured for native SoxR, suggesting that the fluorescence in native SoxR is quenched by interaction with the [2Fe-2S] cluster. The distance between the 2Ap and [2Fe-2S] cluster is approximately 30 Å in this complex, based on the crystal structure of SoxRox-DNA[14]. Recently, it was reported that fluorescein-labeled DNA is quenched by the [2Fe-2S] cluster of DNA-bound SoxR[25]. Unlike the case with native SoxR, the addition of sodium dithionite to the deletion mutant did not alter the fluorescence spectrum (Figure 3-8 (B)). These findings confirm that the observed fluorescence changes correspond to redox-induced changes in SoxR protein-bound promoter.

3.4 Doscussion

The crystal structure of SoxR bound to its promoter in the oxidized (active) state reveals that initiation of transcription by RNA polymerase is activated by distortion of the target promoter region [14], in a manner similar to that of MerR family proteins[10, 13]. The DNA structure is a bent conformation with local untwisting, and is unwound by~ 3-bp compared with B-form DNA [14]. However, there is no information on the DNA structure of the inactive form of $SoxR_{red}$. Here, it was employed a fluorescence-based approach to monitor changes in the environment in the promoter DNA using site-specifically introduced fluorescent probes. Our data showed that reduction of the [2Fe-2S] cluster in the SoxR-DNA complex induced an anomalous decrease in the fluorescence of Ap1 by more than a factor of 10, concomitant with a shift in the fluorescence peak from 362 nm to 370 nm (Figure 3-2). By contrast, reduction did not significantly alter the fluorescence of constructs in which fluorescent probes had been introduced at other positions. However, in our systems, the fluorescence of the probes employed was quenched by the [2Fe-2S] clusters, as evidenced by the fluorescence spectrum of Δ37SoxR (Figure 3-8 (B)) and supported by fluorescence resonance energy

transfer (FRET) experiments reported previously by Liu et al.[25]. Thus, it is conceivable that the decrease in the fluorescence observed here is attributable to a change in FRET between the [2Fe-2S] cluster and the Ap moiety, caused by changes in distance or in the electron spin states of the [2Fe-2S] cluster. However, this possibility can be excluded by the experimental results obtained for Ap1 and Ap2. The electrostatic interaction between 2Ap and the [2Fe-2S] cluster in Ap1 and Ap2, with the closest distances of 30 Å and 28 Å, respectively, could contribute to the change in the fluorescence intensity upon reduction. However, the results presented here show that reduction differentially impacted the fluorescence of Ap1 and Ap2, affecting Ap1 but not Ap2. This suggests that a change in FRET by the reduction can be excluded. Therefore, it can be concluded that redox changes in the [2Fe-2S] cluster of SoxR caused a large conformational change within the region confined to the central A-T base pairs in Ap1. The bases of the T1'-A1 base pair slid and twisted away from one another at this point, forming poor Watson-Crick hydrogen bonds in the oxidized state[14]. The fluorescence changes arose from fluorescence quenching of 2Ap owing to the formation of hydrogen bonds and stacking interactions. However, the 10-nm red shift in the fluorescence peak could not be interpreted simply as the effects of hydrogen bonds and base-pairing. Modeling studies[21, 22] and theoretical calculations[23] have shown that hydrogen bond formation shifts florescence peaks to the red by 3 nm. These results suggest that the environment around 2Ap changed upon reduction, with the distinct electronic properties of the probe reflecting a new set of interactions with the nearest neighboring bases and amino acid residues of SoxR.

The incorporation of pyrrolo-dC into the central region of the CueR promoter sequence provides a means to optically probe local and global DNA conformation [19]. The fluorescence of pyrrolo-C in the CueR complex with duplex DNA was quenched in the absence of Cu^{1+}, whereas binding of Cu^{1+} to CueR increased fluorescence intensity, indicating distortion of the DNA structure. This finding suggests that G-C formed base pairs through hydrogen bonds within DNA bound to MerR proteins in the absence of an inducer.

An important issue is whether DNA bound to $SoxR_{red}$ in the inactive form is distorted. The weak fluorescence of Ap1 in $SoxR_{red}$ suggests that base stacking and base-pair hydrogen bonds are formed in the central A-T base pairs. It seems likely that DNA bound to $SoxR_{red}$ is in the B- form structure, and its duplex structure is not distorted. However, FRET analyses of apo-SoxR, which activates transcription poorly in vitro [26], indicate that apo-SoxR-bound DNA is distorted [25]. In our experiments, the fluorescence spectrum of Ap1-Δ37SoxR, which exhibited a peak at 360 nm, was distinct from that of B-form DNA. Therefore, it is reasonable to assume that Δ37SoxR protein can bind and bend the promoter DNA.

X-ray crystal structure of SoxRox-DNA [14] show that the distorted DNA conformation is stabilized by interactions between the bent phosphate backbone near the center of the DNA element and the SoxR residues Ser26 and Tyr31, located in the helix-turn-helix motif, and Gln64 in the α3 helix

(Figure 3-9). An ultraviolet resonance Raman analysis of the SoxR-DNA complex has further shown that the hydrogen bond interaction between Tyr31 and the phosphate backbone of DNA remains unaltered in the reduced form (CHAPTER 4). In the present experiments, the fluorescence changes displayed by Ap2, Ap5, and Pc3 revealed that the A2-T2', C3-G3', and A5-T5' base pairs did not change significantly upon reduction. These results indicate that the conformation of DNA at positions between 2 and 6 bound to SoxR remains unaltered by reduction.

Beyond localized distortion at the central base position, the base pairs between 3/3' and 10/10' formed a duplex B-like conformation (Figure 3-9), supporting the Ap5 and Ap7 fluorescence data. Bases 6-10 are bent~15° toward the α2-helix[14]. The bent conformation is stabilized by interactions between the C8 phosphate and residues Arg47 and His29 in the helix-turn-helix motif and Arg41 in α1. The fluorescence spectrum of Ap7 reported here exhibited significant changes upon reduction. This finding is consistent with DNA footprint results obtained for MerR [6], ZntR [7], and SoxR [27]. These latter studies indicated that positions in symmetrical promoter regions similar to those of Ap7 (base 7 or 8) are hypersensitive to DNase I. They further showed that the DNase I hypersensitive bands were lost in response to activation of MerR proteins, indicating that a similar conformation is formed in the target promoter.

3.4 Conclusion

The transcriptional control through DNA underwinding, mediated by SoxR, is unique among regulatory proteins. This CHPATER clearly demonstrates that the redox changes experienced by SoxR modulate the confined region of the DNA structure. Although both $SoxR_{ox}$ and $SoxR_{red}$ bend the promoter DNA, the modes of distortion are different between $SoxR_{ox}$ and $SoxR_{red,}$ and the degree of distortion by $SoxR_{red}$ is less. Recent single-molecule FRET measurements have revealed the dynamic interactions between CueR and DNA associated with a novel mechanism for turning off transcription [28]. Ongoing efforts are expected to lend additional insight into the dynamics underlying the mechanisms by which MerR regulates transcription.

References

(1) A. Hochschild, S. L. Dove, *Cell*, **1998**, *92*, 597-600.

(2) (a) J. S. Fassler, G. N. Gussin, *Methods Enzymol.*, **1997,** *273*, 3-29. (b) N. Ptashne, *Nature*, **1988**, *335*, 683-689.

(3) T. A. Steitz, *Rev. Biophys.*, **1990**, *23*, 205-280.

(4) (a) R. B. Lobell, R. F. Schleif, *Science*, **1990**, *250*, 528-532. (b) S. S. Zinkel, D. M. Crothers, *J. Mol. Biol.*, **1991**, *219*, 201-215.

(5) S. C. Schultz, G. C. Shields, T. A. Steitz, *Science*, **1991**, *253*, 1001-1007.

(6) A. Z. Ansari, M. L. Chael, T. V. O'Halloran, *Science*, **1992,** *261*, 715-725.

(7) C. E. Outten, F. W. Outten, T. V. O'Halloran, *J. Biol. Chem.* **1999**, *274*, 37517-37524.

(8) I. R. Tsaneve, B. Weiss, *J. Bacteriol*., **1990**, *172*, 4197-4205.

(9) J. T. Geenberg, P. Monach, J. H. Chou, P. D. Josephy, B. Demple, *Proc. Natl. Acad. Sci. USA.*, **1990,** *87*, 6181-6185.

(10) E. E. Heldwein, R. G. Brennan, *Nature*, **2001,** *409*, 378-382.

(11) J. D. Kahmann, H. J. Sass, M. G. Allan, S. Haruo, C. J. Thompson, S. Crzesiek, *EMBO J.*, **2003**, *22*, 1824-1834.

(12) (a) N. L. Brown, J. V. Stoyanov, S. P. Kidd, J. L. Hobman, *FEBS Microbiol. Rev*., **2003**, *27*, 145-163. (b) T. V. O'Halloran, B. Frantz, M. K. Shin, D. M. Ralston, J. G. Wright, *Cell*, **1989**, *29*, 4747-4751. (c) B. Frantz, T. V. O'Halloran, *Biochemistry*, **1990**, *29*, 4747-4751.

(13) K. J. Newberry, R. G. Brennan, *J. Biol. Chem.*, **2004,** *279*, 20356-20362.

(14) S. Watanabe, A. Kita, K. Kobayashi, K. Miki, *Proc. Natl. Acad. Sci. USA.*, **2008,** *105*, 4121-4126.

(15) (a) T. Nunoshiba, T. DeRojas-Walker, J. S. Wishnok, S. R. Tannenbaum, B. Demple, *Proc. Natl. Acad. Sci. USA.*, **1993**, *90*, 9993-9997.

(16) A. Changela, K. Chen, Y. Xue, J. Holschen, C. E. Outten, T. V. O'Halloran, A. Mondragón, *Science*, **2003**, *301*, 1383-1387.

(17) K. Kobayashi, M. Fujikawa, T. Kozawa, *J. Inorg. Biochem*., **2014,** *133*, 87-91.

(18) (a) C. A. Dunlap, M. D. Tsai, *Biochemistry*, **2002**, *133*, 87-91. (b) C. Liu, C. T. Martin, *J. Mol. Biol.*, **2001**, *308*, 465-475.

(19) P. Chen, C. A. He, *J. Am. Chem. Soc*., **2004,** *126*, 728-729.

(20) (a) K. C. Thompson, N. Miyake, *J. Phys. Chem. B*, **2005**, *109*, 6012-6019. (b) D. Xu, K. O. Evans, T. M. Nordlund, *Biochemistry*, **1994**, *33*, 9592-9599.

(21) E. L. Rachofsky, R. Osman, J. B. A. Ross, *Biochemistry*, **2001**, *40*, 946-956.

(22) S. J. Hardman, K. C. Thompson, *Biochemistry*, **2006**, *45*, 9145-9155.

(23) J. X. Liang, S. Matsika, *J. Am. Chem. Soc*., **2011**, *133*, 6799-6808.

(24) K. Kobayashi, S. Tagawa, *J. Biochem*., **2004**, *136*, 607-615.

(25) C. Liu, E. Kim, B. Demple, N. C. Seeman, *Biochemistry*, **2012**, *51*, 937-943.

(26) E. Hidalgo, B. Demple, *J. Biol. Chem.*, **1996,** *271*, 7269-7272.

(27) E. Hidalgo, B. Demple, *EMBO J.*, **1994,** *13*, 138-146.

(28) C. P. Joshi, D. Panda, D. J. Martell, N. M. Andoy, T. Y. Chen, A. Gaballa, J. D. Helmann, P. Chen, *Proc. Natl. Acad. Sci. USA.*, **2012**, *109*, 15121-15126.

Chapter 4

SoxR Conformational Changes upon Redox Changes of the [2Fe-2S] Cluster Probed with Ultraviolet Resonance Spectroscopy

4.1 Introduction

Signal transduction in sensor proteins is increasingly important in different research fields, and elucidation of the structural mechanism is a current focus of interest[1]. Sensor proteins are generally composed of a sensor domain and functional domain with a catalytic or DNA binding site for transcriptional activity. Binding of an external signal to the sensor domain induces slight alterations in structure, and subsequent conformational changes in the protein are propagated to the functional domain, leading to regulation of activity. Elucidation of these structural changes is thus essential to understand the mechanism of action of these proteins. One typical example is the MerR family[2].

SoxR, belonging to the MerR family, regulates the oxidative stress response to superoxide and nitric oxide in enteric *E. coli* and *Salmonella enterica*. The overall architecture of the SoxR–DNA complex is similar to those of other MerR proteins [3], [4], [5]. The DNA structure in the complex is in a bent conformation with local untwisting. SoxR in *E. coli* contains two Trp and three Tyr residues. Trp91 is located near the [2Fe–2S] cluster of other subunit, whereas Trp98 in the α5 helix is stabilized via van der Waals contacts with conserved residues in the α3, α4, and α5 helices. Tyr31, Tyr49, and Tyr56 are located within the DNA-binding domain and thus used as probes to monitor protein conformational changes close to and distant from the [2Fe–2S] cluster. While the structure of transcriptionally activated SoxR has been solved, the molecular mechanisms through which redox changes of the [2Fe–2S] cluster induce protein conformational alteration and regulate transcription of the target promoter remain to be established. However, the lack of a SoxR structure in the reduced state limits our understanding of the structural transitions required for DNA binding and transcriptional activation.

To address this CHAPTER, it was performed UV resonance Raman (UVRR) measurements of the oxidized and reduced forms of SoxR, in both the absence and presence of promoter oligonucleotide. UVRR spectroscopy is a powerful tool for monitoring protein structures and conformational changes[6], [7]. Upon excitation at around 220–250 nm, side-chain vibrations of Tyr and Trp residues are selectively enhanced. UVRR bands of Trp and Tyr residues provide information on the hydrophobic/hydrophilic surroundings as well as hydrogen bonding[6]. In the current study, conformational changes in SoxR upon reduction of the [2Fe–2S] cluster was investigated.

4.2 Experimental

Sample Preparation

Cloning of *E. coli* SoxR, construction of expression plasmids, and purification of wild-type (WT) protein were performed essentially as described in CHAPTER 1. Site-directed mutagenesis was performed using a PCR-based approach following the instructions of the Quik Change kit (Stratagene). The palindromic oligonucleotide (GCCTCAAGTTAACTTGAGGC) purchased from Sigma Genosis Biotech Co., Ltd. (Japan) formed double-stranded DNA. Oligonucleotide was dissolved in aqueous solution containing 20 mM Tris-HCl (pH 7.6), 50 mM KCl, and 10 mM potassium/sodium tartrate, heated to 94 °C and gradually cooled to room temperature. For preparation of the SoxR-DNA complex, 40–50 μM SoxR (20 mM Mops, pH 7.6, 250 mM KCl, and 10 mM potassium/sodium tartrate) and oligonucleotide solutions were mixed at molar ratios of 2:1.05–1.1 and incubated for more than 4 h at 4 °C[8].

For Raman measurements, the protein concentration was adjusted to 40–50 μM in 20 mM MOPS, pH 7.6, 0.25–0.5 M KCl, and 10 mM potassium/sodium tartrate. Reduced SoxR was prepared using the following method: a sample of SoxR was deoxygenated by repeated evacuation and flushing with nitrogen in a sealed cell. Sodium dithionite solution was added to the protein solution with a gastight Hamilton microsyringe under nitrogen atmosphere (final concentration, 0.5–1 mM). SoxR reduction was confirmed using visible absorption spectrophotometer.

UV Resonance Raman Measurements

UV probe pulses (20 ns, 1 kHz) at 230 nm were obtained by frequency quadrupling of the output of a Nd:YLF-pumped Ti:sapphire laser (Photonics Industries, TU-L). The probe power was kept as low as possible (0.5 μJ/pulse) to avoid photodamage of the protein sample. The probe beam was focused onto the sample cell with spherical and cylindrical lenses. Sodium sulfate (Na_2SO_4) (200 mM) was used as an internal intensity standard in all samples.

The sample solution was contained in a quartz 10 mm diameter NMR tube and spun with a spinning cell device designed to minimize off-center deviation during rotation. Raman scattering light was collected in the 135° backscattering geometry mode and focused onto the entrance slit of a custom-made Littrow prism prefilter (Bumko Keiki) coupled to a 55 cm single spectrograph (iHR550, Horiba Jobin-Yvon) equipped with holographic grating (2400 grooves mm^{-1}) using two achromatic doublet lenses. The prefilter effectively rejected stray background due to Rayleigh scattering and visible fluorescence. Dispersed light was detected with a liquid nitrogen-cooled CCD camera (SPEC-10:400B/LN, Roper Scientific) using the second diffraction order of the monochromator. Spectra were calibrated using the standard Raman spectra of cyclohexane.

Protein was replaced with a fresh sample every 5–10 min. The total exposure time to obtain a single

spectrum was about 1 h. The integrity of the sample after exposure to UV laser light was carefully confirmed by comparing visible absorption spectra obtained before and after UVRR measurements.

4.3 Results

Changes in the UVRR Spectra of SoxR Excited at 230 nm upon Reduction of the [2Fe–2S] Clusters

Raman bands arising from Trp and Tyr residues are selectively enhanced upon excitation around 220–250 nm and can be used as structural probes for their surroundings[(6)]. Figure 4-1 depicts raw UVRR spectra of the oxidized and reduced forms of WT SoxR. Trp and Tyr bands in UVRR spectra were identified by comparison with spectra of aqueous amino acid solutions[(6)]. The raw spectrum was dominated by bands arising from two Trp (Trp91, 98) and three Tyr (Tyr31, 49, 56) residues (labeled W and Y, respectively, followed by the mode number)[(6)]. Since the protein concentrations were the same in all measurements performed at a given excitation wavelength, the intensities of the Raman features were comparable in all raw spectra.

Reduction of the [2Fe–2S] cluster of SoxR caused intensity changes and frequency shifts in Trp vibrational modes (Figures 4-1(a), (b)). To further clarify the spectral changes, difference spectra were calculated so that the band for SO_4^{2-} (981 cm^{-1}), present at the same concentration as the internal intensity standard, was taken as zero. The difference spectrum yielded the following data: 757(+)/767(−) cm^{-1} (W18), 1004(−)/1012(+) cm^{-1} (W16), 1558(−)/1569(+) cm^{-1} (W3) (Figure 4-1 (d)).

The WT spectrum arises from contributions of both Trp91 and Trp98. To identify the specific Trp residue responsible for spectral changes in WT, we performed UVRR measurements on SoxR proteins in which one of the two Trp residues was substituted with Phe. The W98F mutant (Trp91) contained low levels of [2Fe–2S] centers. The mutation of Trp98 may have compromised their structural integrity such that handling during purification. Therefore, we could not perform Raman measurement of Trp91. The spectrum for Trp91 was obtained by subtracting that of W91F mutant (Trp98) from that of WT under the assumption that the environment of Trp98 in W91F is not affected by the mutation.

The difference spectra of the reduced minus oxidized forms were compared for Trp91 and Trp98 (Figure 4-1 (e), (f)). Interestingly, spectral changes of Trp91 were distinct from those of the Trp98, except for a frequency shift of the W18 band, which is commonly observed for the two Trp residues. The difference spectrum of Trp91 yielded positive peaks at 1010 (W16) and 1343 cm^{-1} (W7), indicating an increase in the intensity of Trp bands in the reduced form, compared with the oxidized form. In contrast, the difference spectrum of Trp98 yielded negative peaks at 1009 (W16) and 1558 cm^{-1} (W3). Peaks at around 1010 and 1560 cm^{-1} were thus derived from the intensity differences in

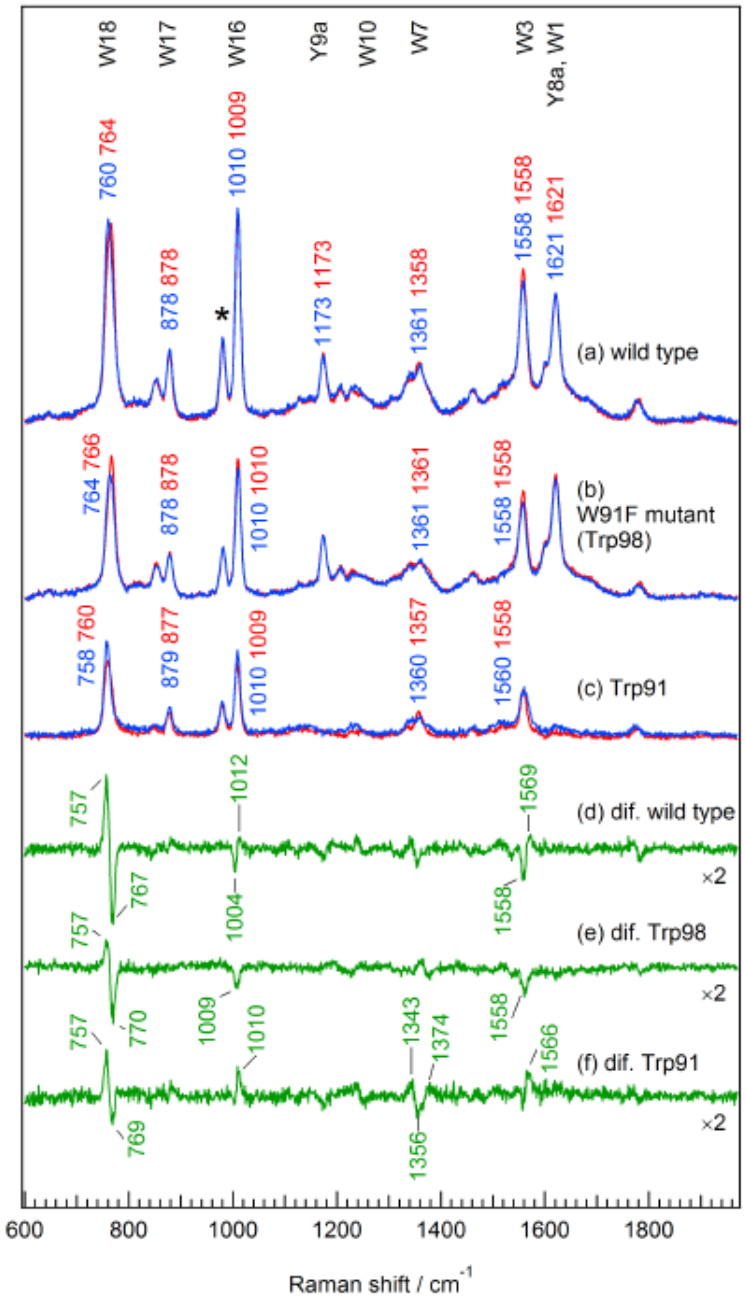

Figure 4-1. The 230 nm excited UVRR spectra of (a) WT and (b)W91F mutant (Trp98) of SoxR. Spectra of the oxidized (red line) and reduced forms (blue line) are shown. The spectrum of Trp91 (c) was calsulated from that of WT minus that of W91F. The reduced minus oxidized spectra for (d) WT, (e) Trp98 and (f) Trp91 are shown.

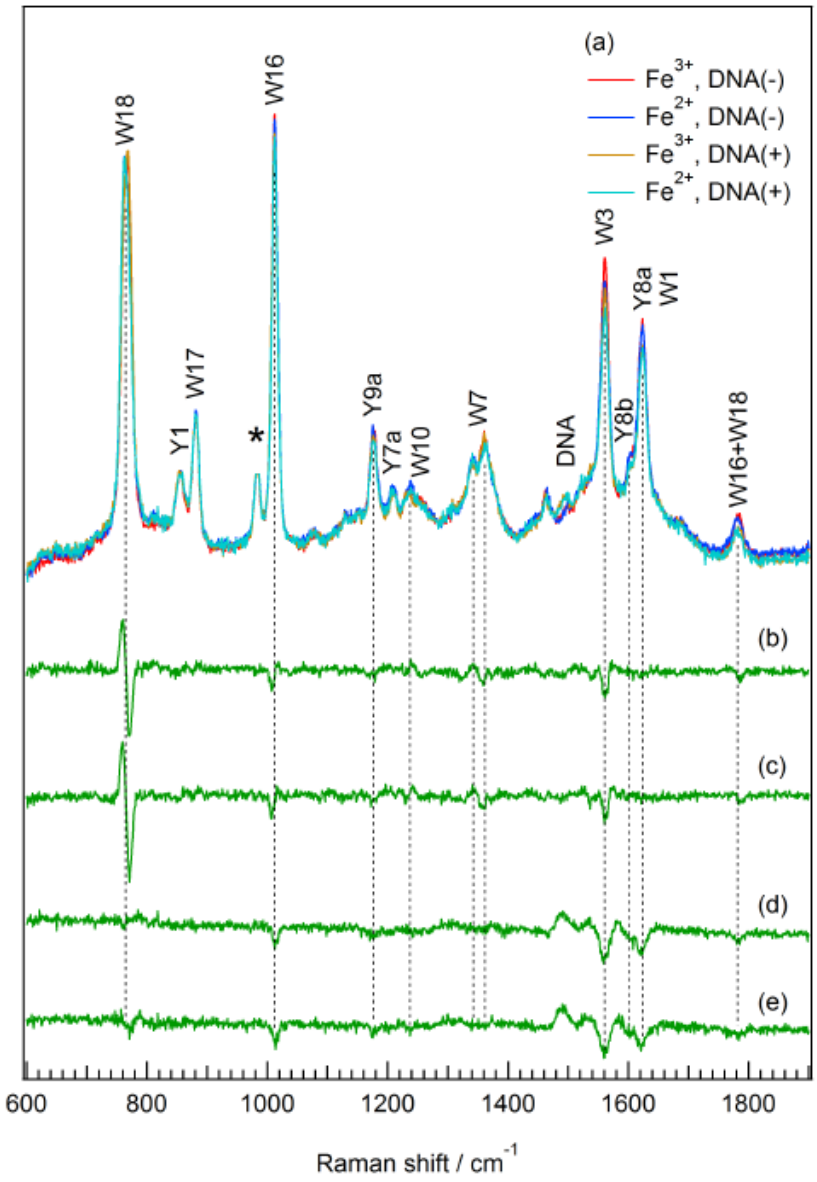

Figure 4-2. The 230 nm excited UVRR spectra of (a) DNA-free forms of the oxidized and reduced and DNA-bound forms of the oxidized and the reduced SoxR. The difference spectra: (b) reduced minus oxidized in the DNA-free forms, (c) reduced minus oxidized in the DNA-bound forms, (d) DNA-bound minus DNA-free in the oxidized forms and (e) DNA-bound minus DNA-free in the reduced forms.

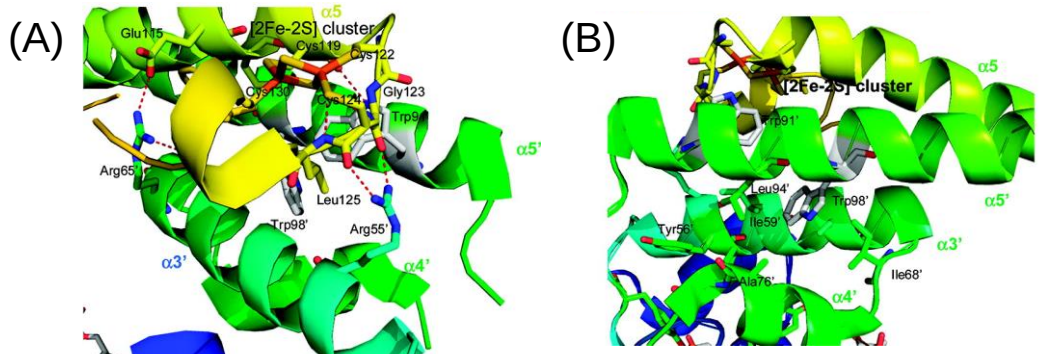

Figure 4-3. Crystallographic structure of SoxR. Close-up of the region near (A) Trp91 and (B) Trp98 residues. These structures were produced with PyMol using a structure from the Protein Data Bank (PDB, 2ZHG).

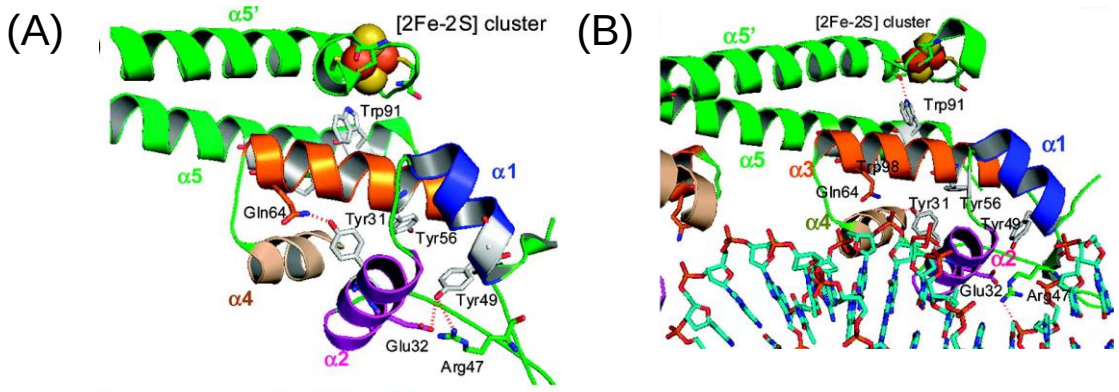

Figure 4-4. Crystallographic structure of SoxR. Close-up the region near the Tyr residues (A) DNA-free form of SoxR and (B) SoxR-soxs promoter complexes. These structures were produced with PyMol using a structure from the Protein Data Bank (PDB, 2ZHG and 2ZHH).

the two Trp residues. In addition, the difference spectrum of Trp91 exhibited a positive band at 1374 cm^{-1}, suggesting the appearance of a high-frequency component of the W7 band. This type of frequency perturbation is likely to arise from steric repulsion between the indole ring and its environment[9]. A similar frequency shift observed for the Trp W7 band in bacteriorhodopsin has been attributed to repulsion between the indole ring and methyl groups of retinal chromophore[10].

The positive/negative peaks at 1340/1360 cm^{-1}, arising due to the intensity of the low- and high-frequency components, were increased and decreased, respectively, for Trp91. The W7 band of Trp usually splits into a doublet at 1360/1340 cm^{-1} owing to Fermi resonance between a fundamental mode and a combination of two out-of-plane modes involving benzene and pyrrole rings comprising the Trp side chain[9, 11, 12]. The intensity ratio, $R(I_{1360}/I_{1340})$, is sensitive to the polarity of the environment around Trp residues[12]. The R value for solvent-exposed Trp is the

lowest value measured at ≤1.1, while the *R* values for least polar environments similar to ethanol and dioxane are >1.5[9]. The *R* values for Trp91 and Trp98 in the oxidized state were 2.0 and 1.0, respectively. This finding suggests that Trp91 is buried in a more hydrophobic environment than Trp98. Upon SoxR reduction, the *R* value for Trp91 was remarkably decreased to 1.2, whereas that for Trp98 exhibited a relatively limited increase to 1.2. These results suggest that upon reduction the environment around Trp91 changes significantly to become more hydrophilic while that around Trp98 undergoes a small change to become more hydrophobic.

The W3 frequencies of Trp are sensitive to the absolute value of torsion angle ($\chi^{2,1}$) about the C_β–C_3 bond connecting the indole ring to the peptide main chain[13], [14], [15]. The W3 frequency of Trp98 at 1558 cm^{-1} corresponded to a $\chi^{2,1}$ angle of 120° [13], [16]. This value is close to the X-ray-determined torsion angle of 111°[17]. On the other hand, the W3 frequency of 1560 cm^{-1} for Trp91 was higher than that predicted, based on crystallographic data. The difference spectrum exhibited a positive band at 1566 cm^{-1}. Conversely, the difference spectrum of Trp98 W3 showed a negative band at 1558 cm^{-1}.

In contrast to the data obtained with Trp, we observed no changes in Tyr Raman bands, including Y1, Y9a, Y7a, Y8b, and Y8a, upon reduction of WT, suggestive of no alterations in the Tyr (Tyr31, Tyr49, Tyr56) environment of WT protein upon reduction.

UVRR Spectra of SoxR Excited at 230 nm upon Binding of Promoter DNA

Figure 4-2 presents the UVRR spectra of oxidized, reduced, DNA-bound oxidized, and DNA-bound reduced forms of the protein (a) excited at 230 nm and the difference spectra (reduced minus oxidized) of the DNA-free forms (b), DNA-bound forms (c), DNA-bound minus DNA-free oxidized forms (d), and DNA-bound minus DNA-free reduced forms (e). DNA binding to the SoxR protein induced changes in several negative peaks. The negative bands at 1174, 1602, and 1617 cm^{-1} resulted from reduction in the intensities of Y9a, Y8b, and Y8a. This finding is indicative of alterations in the environment around Tyr residues upon DNA binding. To identify the specific Tyr residue(s) contributing to spectral changes in WT protein, each of the three Tyr residues was mutated to Phe. However, these mutants contained only low levels of [2Fe–2S] centers, and therefore, we could not perform Raman measurements. In contrast, Trp Raman bands exhibited small spectral changes (except intensity reduction of 1010 cm^{-1} (W16) and 1560 cm^{-1} (W3)), suggesting that Trp residues undergo minor environmental changes. The positive peak at 1485 cm^{-1} observed in the presence of DNA was attributed to the Raman band of oligonucleotide[18].

Notably, the difference spectrum between the reduced and oxidized DNA-bound forms resembled that of the DNA-free form (Figure 4-2 (b), (c)). Thus, it appears that the conformational changes induced upon reduction of DNA-bound SoxR are not significantly different from those in the

DNA-free form.

4.4 Discussion

Conformational Changes in Trp and Tyr Residues upon Reduction of [2Fe–2S] Clusters of SoxR

The SoxR protein contains two Trp residues at positions 91 and 98. Both Trp residues are involved in long dimerization of the α5 helix and play structurally and functionally important roles. Magnified images of the region near the Trp residues are presented in Figure 4-3 (a), (b). Trp91, a conserved residue among SoxR proteins, is located in close proximity to the [2Fe–2S] cluster of other subunit, and the $N_{\varepsilon 1}$ atom of indole forms a hydrogen bond with the backbone carbonyl of Cys119 coordinated to the [2Fe–2S] cluster in the α5′ (where the prime indicates the other subunit) helix. On the other hand, Trp98 (also highly conserved but replaced with Leu in *S.pomeroyi* SoxR) is located so that the α5 helix is stabilized by hydrophobic interactions with conserved residues in the α3 and α4 helices. In the present study, the two Trp residues were employed to probe tertiary structure changes in the protein conformation upon reduction of the [2Fe–2S] cluster. Our UVRR data showed that both Trp91 and Trp98 undergo intensity changes and frequency shifts upon reduction, supporting significant environmental changes. The decreased I_{1360}/I_{1340} ratio for Trp91 clearly suggests that the surrounding environment becomes more hydrophilic in the reduced state, implying partial exposure of this residue to solvent. On the other hand, hydrophobicity in the Trp98 environment is increased to a small extent. Reduction of the [2Fe–2S] cluster may accompany the relative orientations of α3, α5 and α4 helices, and cause tightness of the nonbonded contacts of Trp98. Since no frequency shift was observed for the hydrogen bond marker band (W17 at 878 cm^{-1}[11] and W10 at 1237 cm^{-1} [19]), it is suggested that the hydrogen bond between Trp91 and the backbone carbonyl of Cys119 is barely affected.

W16 (benzene ring-breathing mode) and W18 (indole ring-breathing mode) are sensitive to an electronic state of the aromatic ring. Model studies have shown that increases in solvent dielectric constant and hydrogen-bonding strength lower the frequencies of these bands[20]. Since no frequency shift was observed for the hydrogen bond marker band (W17 and W10) in the present data, the frequency change of the W18 band can be ascribed to changes in the hydrophobicity of Trp. In addition, the intensity changes in the W16 band have been characterized for not only hydrophobicity but also cation–Trp π interactions in both proteins and small molecule model systems [9], [21], [22], [23], where the cations involve metal ions[21] and protonated imidazole of His[22], [23]. In This experiments, frequency changes in the W18 bands were commonly observed for Trp91 and Trp98, whereas spectral changes in the W16 band in Trp91 were distinct from that of Trp98 (Figure 4-1 (e), (f)). These results suggest that electrostatic interactions between the [2Fe–2S] cluster and π orbital of the indole side chain, with the closest distance of about 4.5 Å, contribute to the W16 band intensity of Trp91. The observed increase in Trp91 W16 intensity can be interpreted as a decrease in cation−π

interactions upon reduction.

The W3 frequency of Trp residue is correlated with the Trp $\chi^{2,1}$ dihedral angle[13), (14), (15)]. The dihedral angle, predicted based on the W3 frequencies of Trp98, was similar to that determined using X-ray crystallography[17]. However, the W3 band frequency of Trp91 was high. The frequency of the W3 vibration of Trp91 was further upshifted upon reduction. Juszczak and Desamero proposed that weak electrostatic interactions, such as anion–quadrupole, cation−π, and aromatic face–edge interactions, influence the W3 frequency of Trp[15]. Similarly, electrostatic interactions between the [2Fe–2S] cluster and π orbital of indole side chain may contribute to the W3 band frequency of Trp91. The further upshift in the reduced state of the protein may be attributed to changes in interactions between the [2Fe–2S] cluster and Trp residue.

This UVRR results showed that Tyr residues experience no alterations upon redox change, clearly suggesting that hydrogen bond and nonbonded contacts of Tyr residues with neighboring amino acids are not affected upon reduction.

Conformational Changes upon DNA Binding

Upon binding of SoxR to DNA, the DNA-binding domain undergoes an outward rotation of ~9°, and the Fe–S cluster-binding domain receives an outward rotation of ≈6°, resulting in widening of the distance between the α2 and α2′ helices. The α5 helix connecting both domains exhibits an inner helical twist, leading to a change in the relative positions of dimerization helices[17]. UVRR results disclose that Trp residues undergo small environmental changes upon DNA binding, consistent with the X-ray crystal structure showing that the hydrogen bond of Trp91 and nonbonded contacts of Trp91 and Trp98 are not affected. This finding suggests that the individual domains of DNA-free and -bound SoxR do not present significant structural differences. An analogous set of interactions has been reported for the MerR family of drug-bound BmrR–DNA complexes[24]. Upon DNA binding, BmrR undergoes conformational changes in terms of remodeling of the coiled-coil α5 helix and significant inward movement of the wing. However, the individual DNA-binding and drug-binding domains of DNA-free and DNA-bound BmrR are structurally similar.

Following DNA binding, UVRR spectra of the protein exhibited significant changes in terms of Tyr, but not Trp bands. Parts A and B of Figure 4 depict magnified images of the environment of Tyr residues in the DNA-free and bound forms, respectively. Tyr31 in the DNA recognition helix (α2) and Tyr49 in the loop between helices α2 and α3 are absolutely conserved among not only SoxR proteins but also other members of the MerR family, including MerR, CueR, ZntR, Mta, and BmrR. Tyr56 in the α3 helix is not conserved and exposed to solvent. In the DNA-free form, OH of Tyr31 forms a hydrogen bond with nitrogen of Gln64. Upon DNA binding, rotation of Tyr31 is accompanied by rearrangement of the hydrogen bond from Gln64 to the phosphate backbone of

DNA. On the other hand, Tyr49 forms hydrogen bonds with Arg47 and Glu32 in the DNA-free protein. Upon DNA binding, Tyr49 is surrounded by hydrophobic residues, concomitant with cleavage of the hydrogen bond. Instead, Arg47 donates a hydrogen bond to the phosphate backbone DNA and may be functionally important in stabilizing the activated DNA conformation[17]. Similar conformational changes have been reported for other proteins of the MerR family, including BmrR[24], MtaN[25], and MerR[26]. UVRR results revealed decreased intensities of the Y9a, Y8b, and Y8a bands. Model compound studies have clarified that the intensity and frequency of Tyr bands are influenced by the strength of the hydrogen bond[27]. Therefore, it is reasonable to assume that the changes in hydrogen bonding of Tyr49 trigger spectral changes upon DNA binding.

Conformational Changes of Trp and Tyr Residues upon Reduction of DNA-Bound SoxR

UVRR spectral data indicate that the conformational changes upon reduction of DNA-bound SoxR are not significantly different from those of the DNA-free form. This result has important implications for the function of SoxR. Reduction of the [2Fe–2S] cluster triggers significant changes in the environment around Trp91 and Trp98, which may induce interdomain reorganization required for DNA distortion. However, this process does not affect the environment around Tyr31, Tyr49, and Tyr56. Notably, the hydrogen bond interaction between Tyr31 in the α2 helix and the phosphate backbone of DNA remains unaltered in the reduced form, suggesting that this bond is not important for redox-dependent regulation of structural transition in the activated DNA conformation.

Electrochemical studies have shown that the reduction potential of SoxR bound to the promoter DNA is positively shifted dramatically from −290[28] to 200 mV[29]. The shift (490 mV) is possibly derived from the conformational distortion induced by binding of reduced SoxR to DNA. The coordinate and electronic structures of the [2Fe–2S] cluster of SoxR are altered upon DNA binding but do not directly reflect changes in the Trp environment.

Propagation of Structural Changes from the [2Fe–2S] Cluster to DNA Distortion

Structural alterations of the [2Fe–2S] cluster of SoxR induced by redox changes are communicated to the DNA-binding domain, leading to target promoter DNA distortion. The redox-dependent structural fluctuation of [2Fe–2S] cluster proteins has been studied in oxidized and reduced ferredoxin and putidaredoxin structures with high-resolution X-ray crystallography[30]. In both proteins, the [2Fe–2S] cluster is shielded from the solvent by surrounding residues. The bridging and cysteinyl sulfur atoms are hydrogen-bonded to the backbone amide. Reduction of the prosthetic group significantly affects this hydrogen bond. The additional negative charge on the sulfur atoms attracts the amides of the main chain and increases charge repulsion with the oxygen atom. This is consistent with theoretical calculations, where most of the added charge in the reduced [2Fe–2S] cluster is evenly distributed between the bridging and cysteinyl sulfur atoms and compensated by the

NH--S hydrogen bond[31] In the [2Fe–2S] cluster of SoxR, the lower sulfur atom (S1) is hydrogen-bonded to the amide of Gly123 and displays van der Waals interactions with amides of Cys124 and Leu125, whereas the other side of S2 is fully exposed to solvent. Upon reduction, an additional negative charge on the S1 atom may attract main-chain amides. The conformational changes affect the [2Fe–2S] cluster binding loop of Gly123, which, in turn, would pull up Arg55′ in the α3′ helix, thereby altering the structure of the DNA-binding domain. The above sequential events may induce considerable changes in the Raman spectra of Trp91. An analogous set of events in drug-bound BmR–DNA complex appears crucial for transcription activation. These interactions may thus be common to all MerR family regulators[32].

4.5 Conclusion

UVRR analysis of the oxidized and reduced forms of the [2Fe–2S] transcription factor, SoxR, has facilitated new insights into the structural basis of the general mechanism of transcriptional activation by the MerR family. These results support significant environmental changes for Trp91 and Trp98 in the long dimerization region upon reduction. In contrast, the environment around Tyr in the DNA-binding domain is barely altered. These findings confirm the importance of interactions between Trp91 and the [2Fe–2S] cluster binding loop.

References

(1) (a) K. R. Rodgers, *Curr. Opin. Chem. Biol.*, **1999,** *3,* 158-167. (b) M. A. Gilles-Gonzalez, G. Gonzalez, *J. Inorg. Biochem*., **2005,** *99,* 1-22.

(2) (a) T. V. O'Halloran, *Science*, **1993,** *261,* 715-725. (b) N. L. Brown, J. V. Stoyanov, S. P. Kidd, J. L. Hobman, *FEBS Microbiol. Rev.*, **2003,** *27,* 145-163. (c) T. V. O'Halloran, B. Frantz, M. K. Shin, D. M. Ralston, J. G. Wright, *Cell*, **1989**, *56*, 119-129.

(3) A. Changela, K. Chen, Y. Xue, J. Holschen, C. E. Outten, T. V. O'Halloran, A. Mondragón, *Science*, **2003**, *301*, 1383-1387.

(4) E. E. Heldwein, R. G. Brennan, *Nature*, **2001**, *409*, 378-382.

(5) K. J. Newberry, J. L. Huffman, M. C. Miller, N. Vazquez-Laslop, A. A. Neyfakh, R. G. Brennan, *J. Biol. Chem*., **2008**, *283*, 26795-26804.

(6) I. Harada, H. Takeuchi, *Raman and ultraviolet resonance raman spectra of proteins and related compounds in Spectroscopy and Biological Systems,* **1986,** pp113-175, John Wiley, New York.

(7) (a) S. F. El-Mashtoly, H. Takahashi, T. Shimizu, T. Kitagawa, *J. Am. Chem. Soc.,* **2007**, *129*, 3556-3563. (b) A. Sato, Y. Gao, T. Kitagawa, Y. Mizutani, *Proc. Natl. Acad. Sci. USA*., **2007,** *104*, 9627-9632. (c) M. Mizuno, M. Shibata, J. Yamada, H. Kandori, Y. Mizutani, *J. Phys. Chem. B,* **2009,** *113*, 12121-12128.

(8) S. Watanabe, A. Kita, K. Kobayashi, Y. Takahashi, K. Miki, *Acta Crystallogr. Sct. F: Struct. Biol. Cryst. Commun.*, **2006,** *62*, 1275-1277.

(9) D. E. Schlamadinger, J. E. Gable, J. E. Kim, *J. Phys. Chem. B*, **2009,** *113*, 14769-14778.

(10) S. Hashimoto, K. Obata, H. Takeuchi, R. Needleman, J. K. Lanyi, *Biochemistry*, **1997**, *36*, 11583-11590.

(11) H. Takeuchi, *Biopolymers*, **2003**, *72*, 305-317.

(12) I. Harada, T. Miura, H. Takeuchi, *Spectruchim. Acta, Part A*, **1986,** *42*, 307-312.

(13) T. Miura, H. Takeuchi, I. Harada, *J. Raman Spectrosc*., **1989**, *20*, 667-671.

(14) T. Miura, H. Takeuchi, I. Harada, *Biochemistry*, **1988**, *27*, 88-94.

(15) L. J. Juszczak, R. Z. B. Desamero, *Biochemistry*, **2009**, *48*, 2777-2787.

(16) N. Haruta, T. Kitagawa, *Biochemistry*, **2001,** *41*, 6595-6604.

(17) S. Watanabe, A. Kita, K. Kobayashi, K. Miki, *Proc. Natl. Acad. Sci. USA.*, **2008**, *105*, 4121-4126.

(18) (a) S. P. Fodor, R. P. Rava, T. R. Hays, T. G. Spiro, *J. Am. Chem. Soc.*, **1985**, *107*, 1520-1529. (b) J. P. Perno, C. A. Grygon, T. G. Spiro, *J. Phys. Chem*., **1989,** *92*, 5672-5678. (c) I. Mukerji, A. P. Williams, *Biochemistry*, **2002**, *41*, 69-77.

(19) J. Chen, S. L. Bender, J. M. Keough, B. A. Barry, *J. Phys. Chem. B*, **2009,** *113*, 11367-11370.

(20) (a) M. Matsuno, H. Takeuchi, *Bull. Chem. Soc. Jpn,*. **1998,** *71*, 851-857. (b) T. Fujisawa, M. Terajima, Y. Kimura, *J. Chem. Phys.*, **2006**, *124*, 184503-184509. (c) L. C. T. Schoute, R. Heburn, A. M. Kelley, *J. Phys. Chem. A*, **2007**, *111*, 1251-1258.

(21) Y. Xue, A. V. Davis, G. Balakrishnan, J. P. Stasser, B. M. Staehlin, P. Focia, T. G. Spiro, *Nat. Chem. Biol*., **2008**, *4*, 107-109.

(22) Z. Q. Wen, G. J. Jr. Thomas, *Biochemistry*, **2000**, *39*, 146-152.

(23) A. Okada, T. Miura, H. Takeuchi, *Biochemistry*, **2001**, *40*, 6053-6060.

(24) M. Kumaraswami, K. J. Newberry, R. G. Brennan, *J. Mol. Biol*., **2010**, *398*, 264-275.

(25) K. J. Newberry, R. G. Brennan, *J. Biol. Chem*., **2004**, *279*, 20356-20362.

(26) L. Song, Q. Teng, R. S. Phillips, J. M. Brewer, A. O. Summers, *J. Mol. Biol*., **2007**, *371*, 79-92.

(27) (a) K. R. Rodgers, C. Su, S. Subramaniam, T. G. Spiro, *J. Am. Chem. Soc*., **1992,** *114*, 3697-3709. (b) H. Takeuchi, M. Watanabe, Y. Satoh, I. Harada, *J. Raman Spectrosc*., **1989**, *20*, 233-237.

(28) P. Gaudu, B. Weiss, *Proc. Natl. Acad. Sci. USA.*, **1996**, *93*, 10094-10098.

(29) A. A. Gorodetsky, L. E. P. Dietrich, P. E. Lee, B. Demple, D. K. Newman, J. K. Barton, *Proc. Natl. Acad. Sci. USA*., **2008**, *105*, 3684-3689.

(30) (a) R. Morales, M. H. Charon, G. Hudry-Clergeon, Y. Petillot, S. Norager, M. Medina, M. Frey, *Biochemistry*, **1999**, *38*, 15764-15773. (b) I. F. Sevrikoukova, *J. Mol. Biol*., **2005**, *347*, 607-621.

(31) L. Noodleman, C. Y. Peng, D. A. Case, J. M. Mouesca, *Coord. Chem. Rev.*, **1995**, *144*,

199-244.

(32) K. J. Newberry, J. L. Huffman, M. C. Miller, N. Vazquez-Laslop, A. A. Neyfakh, R. G. Brennan, *J. Biol. Chem.*, **2008**, *283*, 26795-26804.

Chapter 5
Binding of Promoter DNA to SoxR Protein Decreases the Reduction Potential of the [2Fe-2S] Cluster

5.1 Introduction

Since the transcriptional activity of SoxR is regulated by an alteration of the cellular redox balance, it is important to know the reduction potential of this protein. The reduction potential of SoxR without bound DNA from *E. coli*[1, 2] and *Pseudomonas aeruginosa*[3] was determined to be approximately −290 mV, a value close the intracellular reduction potential of *E. coli* (−260 to −280 mV) [4]. On the other hand, electrochemistry measurements on DNA-modified electrodes have shown that the reduction potential of SoxR bound to DNA is +200 mV. This potential value corresponds to a dramatic shift of +490 mV versus the values found in the absence of DNA[5]. However, the reduction potential is beyond the range ever previously observed for [2Fe–2S] proteins, which vary from −150 to −460 mV[6, 7]. In addition, a very significant difficulty in comparing these values to assess the effect of DNA is that these DNA-bound and DNA-free experiments were carried out under completely different conditions. Understanding the effect of the binding of DNA on the redox properties of SoxR requires the same conditions to be used.

NADPH–cytochrome P-450 (CRP) contains one FAD and one FMN per molecule of the enzyme. The FAD accepts the reducing equivalents of two electrons from NADPH to the one-electron acceptor cytochrome P-450 via the FMN domain[8]. The reduction potentials of the individual one-electron couples of FAD and FMN of CRP are −109 mV($FMN/FMNH^{\bullet}$), −270 mV($FMNH^{\bullet}/FMNH_2$), −290 mV ($FAD/FADH^{\bullet}$), and −365 mV($FADH^{\bullet}/FADH_2$), respectively[9]. This raises the possibility that SoxR may accept an electron from both flavins. It is possible to measure the reduction potential from equilibrium data coupled with NADPH and CRP in the presence of electron-transfer mediators. It is reported in this chapter the determination of the reduction potential of SoxR in the absence and presence of DNA. It was shown, in contrast to the previous report[5], that the reduction potential in the SoxR is a comparatively small negative shift upon DNA binding.

5.2 Experimental

Expression and Purification

SoxR was prepared in the same manner as described in CHAPTER 1. SoxR–DNA complexes were prepared according to the method previously used for its crystallization[10]. The palindromic oligonucleotide (5′-GCCTCAAGTTAACTTGAGGC-3′, where the *soxS* promoter sequence is in

bold), purchased from Sigma Genosis Biotech Co., Ltd. (Japan), formed double-stranded DNA. The oligonucleotide was dissolved in aqueous solution containing 20 mM Tris-HCl (pH 7.6), 50 mM KCl, and 10 mM potassium/sodium tartrate, heated to 94 °C, and gradually cooled to room temperature. For preparation of SoxR–DNA complexes, 40–50 μM SoxR (in a solution also containing 20 mM MOPS, pH 7.6, 300 mM KCl, and 10 mM potassium/sodium tartrate) and the oligonucleotide solution were mixed at molar ratios of 2 : 1.05-1.1 and incubated for more than 4 h at 4 °C[10]. Below 0.3 M KCl, the complex formation was confirmed by native polyacrylamide gel[10].

The expression plasmids pCWori$^+$ for porcine CRP were transformed into *E. coli* BL21 as described previously[11]. CRP was purified essentially as described previously[12]. All other chemicals were of the highest grade available from commercial suppliers.

Assay of SoxR Reduction by NADPH/CRP

The reduction of SoxR was measured in a 3 mL cuvette using optical absorption spectroscopy. The samples contained 100–220 μM NADPH, 40–100 μM SoxR, and 0.3 M KCl. Indigodisulfonic acid ($E_0' = -116$ mV)[13] and phenosafranine ($E_0' = -289$ mV)[14] were used for as the electron-transfer mediators. The samples were deoxygenated in sealed optical cells by repeated evacuation and flushing with argon. The reactions were started by adding NADPH. The spectra of the SoxR solution were monitored until no further changes were observed, indicating that the solutions had reached equilibrium. The reduction of SoxR was monitored using Δ(absorbance coefficient) (mM^{-1} cm^{-1}) of 5.8 (417 nm) and 7.8 (462 nm) between the oxidized and reduced forms. No absorbance of indigodisulfate and phenosafranine was detected in visible region due to the reduced states of these mediators during the reactions. The concentration NADPH was calculated using extinction coefficient of 6.22 mM^{-1} cm^{-1} at 340 nm.Optical absorption spectra were measured with a Hitachi U-2900 spectrometer.

5.3 Results

The addition of 137 μM NADPH and 0.4 μM CRP to a solution of SoxR under anaerobic conditions resulted in a decrease in absorption of [2Fe–2S] clusters of SoxR from 400 to 600 nm (inset of Figure 5-1), concomitant with the decrease of NADPH at 340 nm (Figure 5-1). When the sample was aerated, the original spectrum was completely restored within 5 min, which indicates that the absorbance changes in Figure 5-1 correspond to reversible reduction of the [2Fe–2S] cluster of SoxR, and not by irreversible destruction of the iron–sulfur cluster. Approximately 10–20% of SoxR was reduced during the first hour and further absorption changes were not observed under the conditions. Upon addition of NADPH generating systems (glucose 6-phosphate and glucose

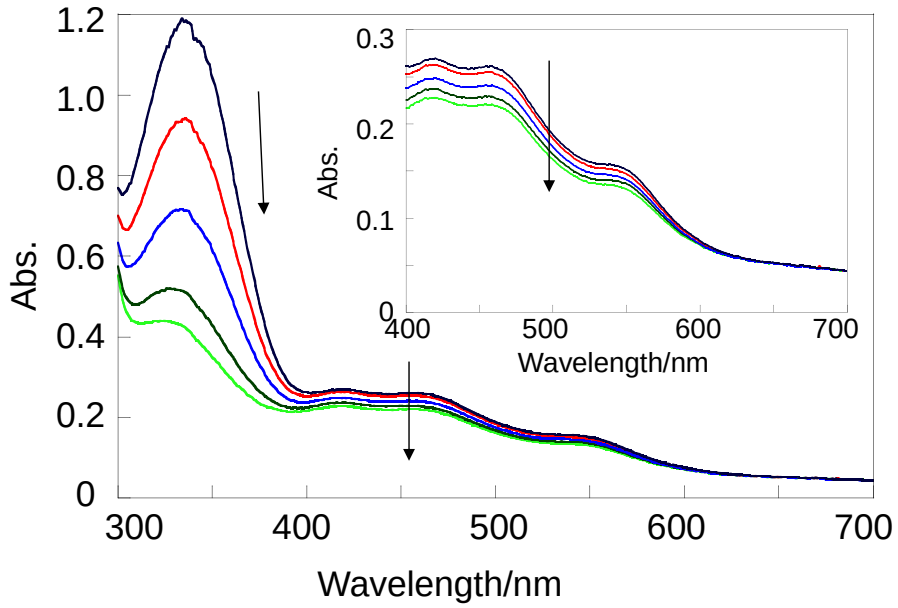

Figure 5-1. Spectral changes of SoxR upon anaerobic addition of NADPH and CRP. The sample contained 137 μM NADPH, 25 μM SoxR, 0.42 μM CRP, 0.3 M KCl and 20 mM MOPS/KOH (pH 7.6) in 2 mL final volume. The spectra were taken at 0 (black), 14 (red), 25 (blue), 44 (dark green) and 60 min (light green) after addition of NADPH. The inset shows an expanded scale of absorbance changes of SoxR.

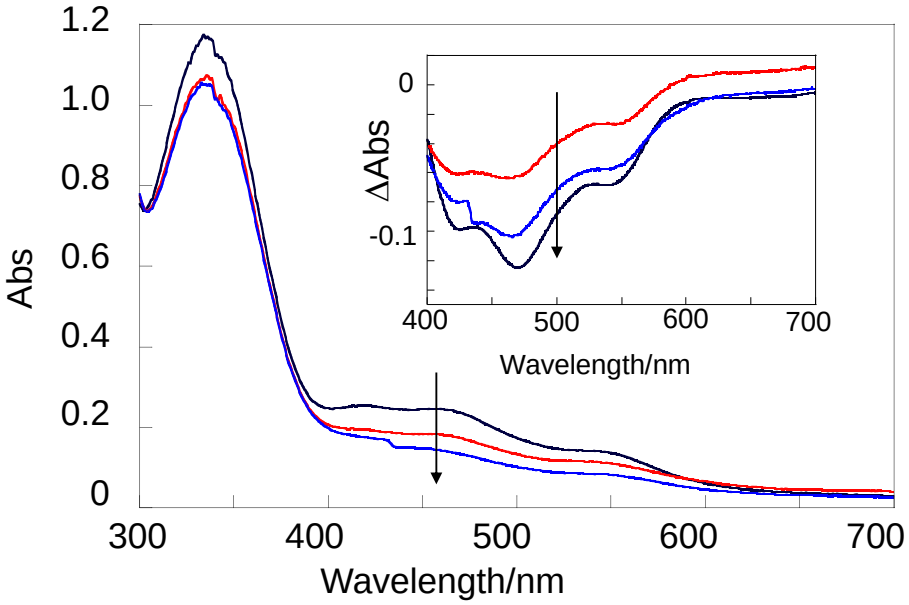

Figure 5-2. Spectral chenges of SoxR upon anaerobic addition of CRP and NADPH along with an NADPH-generating system. The sample contained 137 μM NADPH, 25 μM SoxR, 0.42 μM CRP and 20 mM MOPS/KOH (pH 7.6), in 2 mL final volume. The spectra were taken at 0 (black), 7 (red) and 25 min (blue) after addition of NADPH. The inset shows difference spectra before and after the reaction at 7 (red) and 25 min (blue) and oxidized minus reduced SoxR (black).

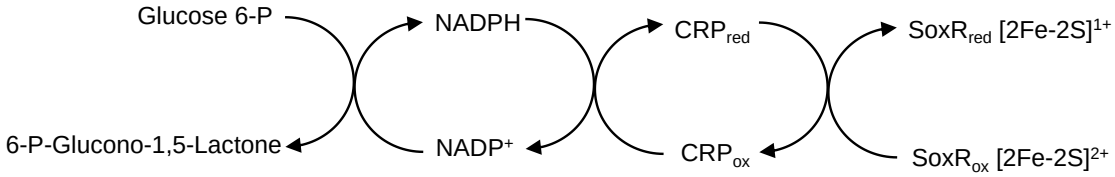

Figure 5-3. Coupling reactions of NADPH consumption with CRP by SoxR.

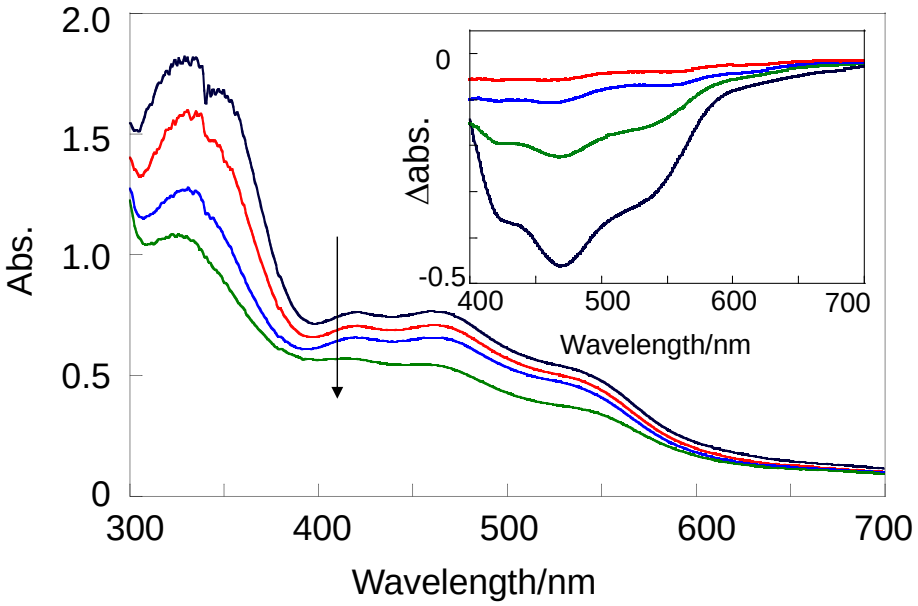

Figure 5-4. Spectral changes of SoxR upon anaerobic addition of NADPH and CRP in the presence of indigosulfate and phenosafranine. The sample contained 161 μM NADPH, 75 μM SoxR, 0.42 μM CRP, 1 μM indigosulfate, 1 μM phenosafranine, 0.3 M KCl and 20 mM MOPS/KOH (pH 7.6), in 2 mL final volume. The spectra were taken at 0 (black), 5 (red), 10 (blue) and 15 min (green) after addition of NADPH. The inset shows difference spectra before and after the reaction at 5 (red), 10 (blue) and 15 min (green) and oxidized minus reduced SoxR (black).

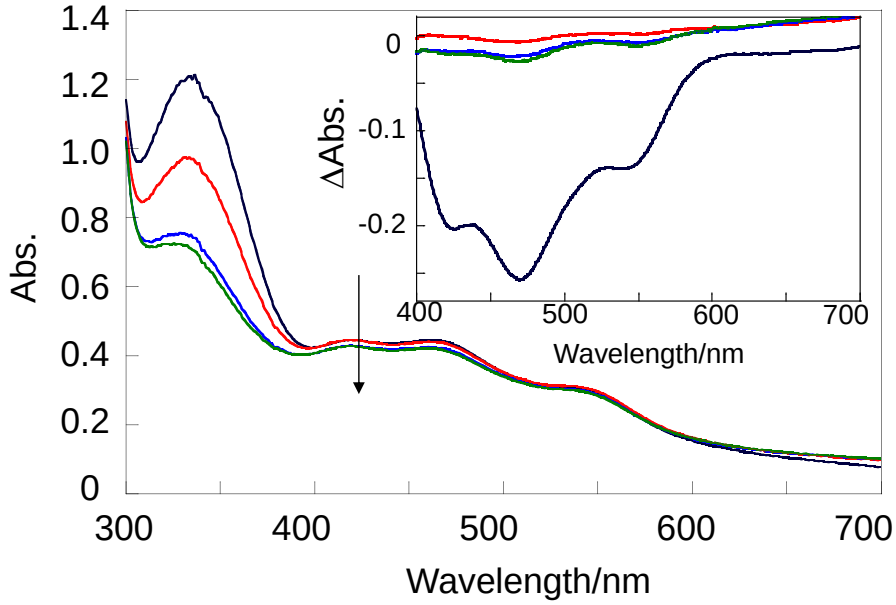

Figure 5-5. Spectral changes of SoxR-DNA upon anaerobic addition of NADPH and CRP in the presence of indigosulfate and phenosafranine. The sample contained 161 μM NADPH, 40 μM SoxR, 0.42 μM CRP, 1 μM indigosulfate, 1 μM phenosafranine, 0.3 M KCl and 20 mM MOPS/KOH (pH 7.6), in 2 mL final volume. The spectra were taken at 0 (black), 5 (red), 10 (blue) and 30 min (green) after addition of NADPH. The inset shows difference spectra before and after the reaction at 5 (red), 10 (blue) and 30 min (green) and oxidized minus reduced SoxR (black).

Table 5-1. Calculation of the oxidation-reduction potentials of SoxR from the equilibrated reactions with NADPH/CRP[α]

Composite	NADPH/μM	$NADP^+$/μM	$[SoxR]_{ox}$/μM	$[SoxR]_{red}$/μM	E_0'/mV
SoxR	7.2	146.6	29.6	44.4	-293
	7.3	79.3	29.5	3.2	-313
SoxR-DNA	8.2	128.8	29.3	3.4	-319
	24.3	132.6	29.0	2.7	-301

[α] All experiments were carried out in 20 mM MOPS- KOH buffer (pH 7.6) and 0.3 M KCl at 25 ˚C under an argon atmosphere: CRP 0.42 μM, indigosulfate 1 μM and phenosafranine 1 μM. The reduction was measured from the decreases of NADPH and $SoxR_{ox}$ in absorbance at 340 and 460 nm, respectively. A value of -340 mV in E_0' ($NADPH/ NADP^+$) was used for calculation.

6-dehydrogenase) to the solution, SoxR was nearly completely reduced (Figure 5-2). Inset of Figure 5-2 shows difference spectra obtained after the reaction, where the difference spectrum obtained at 25 min was nearly identical to the $SoxR_{red}$ minus $SoxR_{ox}$ spectrum. Based on these results, CRP can serve as an NADPH- dependent electron carrier for SoxR through protein–protein electron transfer (Figure 5-3).

Since equilibrium of oxidation–reduction of SoxR and NADPH/CRP was difficult to reach, reduction was carried out in the presence of a small amount of electron-transfer mediators (indigodisulfate and phenosafranine) [9], [13], [14], [15].

$$\mathrm{NADPH} + 2[\mathrm{2Fe\text{-}2S}]^{2+} \overset{K_{eq}}{\rightleftharpoons} \mathrm{NADP^+} + 2[\mathrm{2Fe\text{-}2S}]^{+} \qquad (5\text{-}1)$$

The mediators are required for electron transfer between protein molecules. Equilibrium constants for the oxidation–reduction of SoxR and NADPH/CRP (Reaction 5-1) could be measured, for instance, from the result shown in Figure 5-4. Approximately 50% of SoxR was reduced during the first 10 min under these conditions. The equilibrium mixture contained components (NADPH, $NADP^+$, indigodisulfate, phenosafranine, CRP, $SoxR_{ox}$, and $SoxR_{red}$). Since no absorbance other than SoxR was detected in the visible region during the measurements (inset of Figure 5-4), the concentrations of $SoxR_{ox}$ and $SoxR_{red}$ were estimated. The absorbance correction due to the oxidation of NADPH was subtracted from absorbance changes of SoxR at 340 nm using extinction coefficients ($mM^{-1}\ cm^{-1}$) of $\varepsilon_{ox340} = 20.7$ and $\varepsilon_{red} = 11.0$. Their concentrations were estimated on the basis of the absorbance data listed in Table 1. On the assumption that $E_0'(\mathrm{NADPH/NADP^+}) = -340$ mV[16], the data yielded, for instance, $E_0'(SoxR_{red}/SoxR_{ox}) = -293$ mV from the Nernst equation (eq 2), where R and F are the gas constant and the Faraday constant, respectively. The value is comparable to that reported previously (−285 mV) [1], [2].

$$\begin{aligned} &E_0' (\mathrm{NADPH/NADP^+}) + (RT \ln([\mathrm{NADP^+}]/[\mathrm{NADPH}])/2F \\ &= E_0' (SoxR_{red}/SoxR_{ox}) + (RT \ln([SoxR_{ox}]/[SoxR_{red}])/F \end{aligned} \qquad (5\text{-}2)$$

Experiments under similar anaerobic conditions were carried out with the DNA–SoxR complex. Figure 5-5 shows the absorbance changes of SoxR–DNA complex after addition of NADPH. Noted that less than 10% of the [2Fe–2S] was reduced during the first 10 min (inset of Figure 5-5), and further changes were not observed under these conditions. This suggests that the reduction potential of the DNA–SoxR is more negative than that of DNA-free form. The equilibrium data are shown in Table 5-1. A value of −310 to −330 mV was calculated for $E_0'(SoxR_{red}\text{–DNA}/SoxR_{ox}\text{–DNA})$. In a control experiment, a similar experiment was performed in the presence of nonsence DNA, but more than 50% of SoxR was reduced under these conditions, as the case of the presence of DNA.

5.4 Discussion

Based on the present results, the equilibria presented in Scheme 5-1 were assumed to occur, where K_{dox} is the dissociation constants of $SoxR_{ox}$ and the DNA and K_{dred} is that between $SoxR_{red}$ and the promoter DNA. It is apparent from the results shown in Figures 5-4 and 5-5 that the redox equilibrium between $SoxR_{ox}$ and $SoxR_{red}$ is somewhat shifted to the oxidized form in the presence of DNA. That is, the reduction potential of SoxR–DNA is more negative than that of DNA-free form. From the equilibrium data coupled with NADPH/CRP, we have determined that the reduction potential of DNA–SoxR complex is −320 mV versus NHE. This −320 mV reduction potential for DNA–SoxR obtained from our experiment differs markedly from that of the electrochemistry measurement (+200 mV) [5] but is more consistent with several experimental observations. First, we did not observe a reduction of the $[2Fe–2S]^{2+}$ of the DNA-bound form of SoxR by O_2^-(CHAPTER 1). O_2^- (with an $E_0'(O_2^-/O_2)$ = −160 mV(32, 33)) cannot act as a reductant for $[2Fe–2S]^{2+}$ of SoxR (with an $E_0'(SoxR_{red}–DNA)/(SoxR_{ox}–DNA)$ = −320 mV). Had the previously reported value of +200 mV been applied here, the reduction would have been observed. Second, the reported reduction potentials of [2Fe–2S] proteins are in the range of −150 to −460 mV, except for Rieske proteins[6, 7]. Many Rieske proteins have positive potentials (+100 to +400 mV), where histidine ligation causes upshifts of the reduction potential. Third, the dissociation constant of the $SoxR_{red}$ with the DNA (K_{dred}) can be evaluated from that of $SoxR_{ox}$(K_{dox}) and the reduction potentials of DNA–SoxR and SoxR using eq 3.

$$E_0' (SoxR_{red}\text{-DNA}/SoxR_{ox}\text{-DNA}) = E_0' (SoxR_{red}/SoxR_{ox}) + RT/[F \ln(K_{dox}/K_{dred})] \quad (5\text{-}3)$$

Using a gel mobility shift assay, Hidalgo and Demple previously determined the dissociation constant of $SoxR_{ox}$ to DNA (K_{dox}) to be 4.5×10^{-10} M[17]. From the data, K_{dred} is estimated to be 1.1×10^{-10} M, suggesting that the binding affinity of $SoxR_{red}$ with the DNA is approximately 4-fold lower than that of $SoxR_{ox}$. This is consistent with a report by Gaudu and Weiss[1] that $SoxR_{ox}$ is about twice as effective as $SoxR_{red}$ in protecting the *soxS* operator from endonucleolytic cleavage. In contrast, the electrochemistry-determined ~490 mV shift in potential would correspond to an increase in DNA binding affinity of more than 3 orders of magnitude between $SoxR_{red}$ and $SoxR_{ox}$.
The [4Fe–4S] clusters in proteins exhibit a broad range of reduction potentials (−700 to +400 mV) [6, 18]. The differences are generally attributed to hydrogen bonding and electrostatic effects from the surrounding proteins and solvent[19]. Each hydrogen-bonding interaction with the cluster can cause a potential shift of 80 mV. The substantial shift in SoxR potential upon DNA binding may reflect the structural difference between the free and DNA-bound complex. However, crystal structures of DNA-free and DNA-bound SoxR do not show large differences (Figure 5-6). The small shift in the

Scheme 5-1. Thermodynamic relationship of the DNA binding to $SoxR_{ox}$ and $SoxR_{red}$[a]

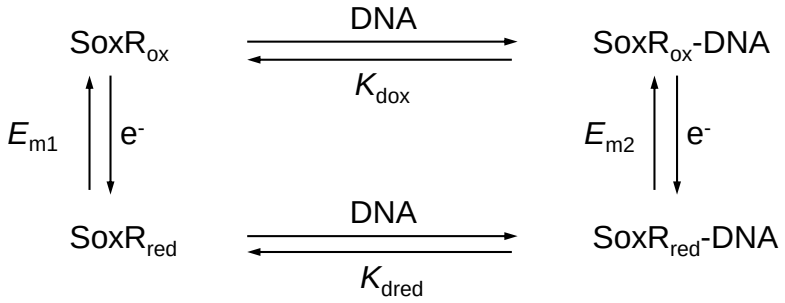

[a] E_{m1} and E_{m2} are reduction potentials of [2Fe-2S] cluster of SoxR with DNA-free and DNA-bound forms, respectively.

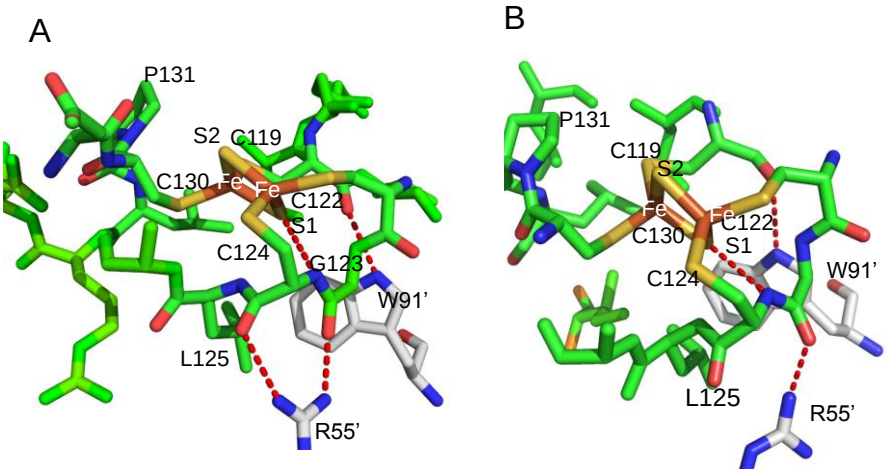

Figure 5-6. Structure of the [2Fe-2S] cluster of SoxR in the (A) DNA-bound and (B) DNA-free states. These structures were produced with PyMol using a structure form the Protein Data Bank (PDB: 2ZHG and 2ZHH).

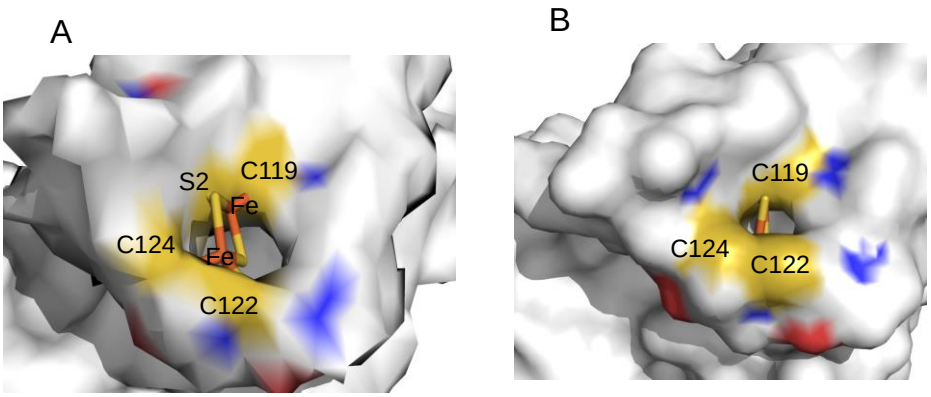

Figure 5-7. Surface representation of the Fe-S cluster –binding domain of (A) DNA-bound and (B) DNA-free forms. Iron and sulfur atoms of the [2Fe-2S] cluster and cysteine residues are colored.

SoxR reduction potential upon DNA binding appears to be consistent with the relatively small differences between the crystal structures of DNA-free and DNA-bound SoxR (Figure 5-6). For example, the hydrogen bond of the lower sulfur (S_1) of the [2Fe–2S] cluster with the amide of Gly123 is not affected upon the binding of DNA. There are some differences in the environments of the clusters between the crystal structures, for example, the [2Fe–2S] cluster is more buried in a hydrophobic core in the DNA-free form than in the DNA-bound form (Figure 5-7), but such differences cannot lead to the dramatic +490 mV shift indicated previously by electrochemistry.

Gorodetsky et al[5]. showed that DNA binding positively shifts the reduction potential of SoxR to 200 mV, and the shifts suggested that the DNA-bound form is primarily in the reduced form in the reducing intracellular environment. In such a case, the oxidation of SoxR may be a regulatory step and oxidative stress serves to promote oxidation of SoxR. However, the present data show that the reduction potential of DNA-bound SoxR (−320 mV) is slightly more negative than that of the cytoplasm (−260 to −280 mV). This suggests that SoxR would be primarily in an oxidized form in the absence of the reduction system, even without imposing oxidative stress. Under conditions of normal aerobic growth, a reductive pathway involving a NADPH-dependent specific enzyme appears to maintain SoxR in a reduced inactive form (Figure 5-8). Several studies suggested that the *SoxRS* regulon is responsive to intracellular NADPH/$NADP^+$ [20]. Recently, the analysis of fluorescence-activated cell sorting revealed that the transcription in SoxR is linked to the level of NADPH[21]. NADPH-dependent SoxR reduction is enzyme-mediated, allowing for a rapid adjustment to changes in cellular conditions[22]. The identity of SoxR reductase has not been characterized, and there still remain reducing systems other than these systems.

5.5 Conclusion

The reduction potentials of DNA-bound and DNA-free forms of SoxR were -320 and -293 mV versus NHE, respectively. These results indicate that DNA binding causes a moderate shift in the reduction potential of SoxR.

References

(1) P. Gaudu, B. Weiss, *Proc. Natl. Acad. Sci. USA.*, **1996,** *93*, 10094-10098.

(2) H. DDing, E. Hidalgo, B. Demple, *J. Biol. Chem.*, **1996**, *271*, 33173-33175.

(3) K. Kobayashi, S. Tagawa, *J. Biochem.*, **2004,** *136*, 607-615.

(4) C. Hwang, A. J. Sinskey, H. F. Lodish, *Science*, **1992,** *257*, 1496-1502.

(5) A. A. Gorodetsky, L. E. Dietrich, P. E. Lee, B. Demple, D. K. Newman, J. K. Barton, *Proc. Natl. Acad. Sci. USA.*, **2008,** *105*, 3684-3689.

(6) R. Cammack, *Adv. Inorg. Chem.*, **1992,** *38*, 281-322.

(7) J. Meyer, *J. Biol. Inorg. Chem.*, **2008,** *13*, 157-170.

(8) T. Iyanagi, H. S. Mason, *Biochemistry,* **1973**, *12,* 2297-2308.

(9) T. Iyanagi, N. Makino, H. S. Mason, *Biochemistry*, **1974**, *13*, 1701-1710.

(10) S. Watanabe, A. Kita, K. Kobayashi, Y. Takahashi, K. Miki, *Acta Crystallogr.*, **2006**, *F62*, 1275-1277.

(11) S. Kimura, T. Iyanagi, *J. Biochem*., **2003,** *134*, 403-413.

(12) K. Yamamoto, S. Kimura, Y. Shiro, T. Iyanagi, *Arch. Biochem. Ciophys.* **2005,** *440,* 65-78.

(13) P. W. Preisler, E. S. Hill, R. G. Loeffel, P. A. Shaffer, *J. Am. Chem. Soc*., **1959,** *81,* 1991-1995.

(14) R. D. Stieliler, T. T. Chen, W. M. Clark, *J. Am. Chem. Soc.*, **1933,** *55,* 891-907.

(15) T. Iyanagi, S. Watanabe, K. F. Anan, *Biochemistry*, **1984,** *23*, 1418-1425.

(16) M. Zheng, G. Storz, *Biochem. Pharmacol.*, **2000**, *59,* 1-6.

(17) E. Hidalgo, B. Demple, *EMBO J.*, **1994**, *13,* 138-146.

(18) H. Beinert, *J. Biol. Inorg. Chem.*, **2000,** *5*, 2-15.

(19) (a) H. A. Heering, Y. B. M. Mulsink, W. R. Hagen, T. E. Meyer, *Biochemistry*, **1995,** *34*, 14675-14686. (b) A. Dey, F. E. Jr. Jenny, M. W. W. Adams, E. Babini, Y. Takahashi, K. Fukuyama, K. O. Hodgson, B. Hedman, E. I. Solomon, *Science*, **2007**, *318*, 1464-1468. (c) S. Niu, T. Ichise, *J. Am. Chem. Soc*., **2009**, *131,* 5724-5725. (d) P. Zheng, S. J. Takayama, A. G. Mauk, H. Li, *J. Am. Chem. Soc.*, **2012**, *134*, 4124-4131.

(20) (a) S. I. Liochev, I. Fridovich, *Proc. Natl. Acad. Sci. USA.*, **1992,** *89*, 5892-5896. (b) A. R. Krapp, R. E. Rodriguez, H. O. Poli, D. H. Paladini, J. F. Palatnik, N. Carrillo, *J. Bacteriol.*, **2002**, *184*, 1474-1480. (c) A. R. Krapp, M. V. Humbert, N. Carrillo, *Microbiology*, **2011**, *157*, 957-965. (d) S. Siedler, S. Bringer, T. polen, M. Bott, *Biotechnol. Bioeng.*, **2014,** *111*, 2067-2075.

(21) S. Sieldler, G. Schendzielorz, S. Binder, L. Eggeling, S. Bringer, M. Bott, *ACS Synth. Biol*., **2013**, *3,* 41-47.

(22) (a) K. Kobayashi, S. Tagawa, *FEBS Lett.*, **1999,** *451,* 227-230. (b) M. S. Koo, J. H. Lee, S. Y. Rah, W. S. Yeo, K. L. lee, Y. S. Koh, S. O. Kang, J. H. Roe, *EMBO J.* **2003**, *22,* 2614-2622.

Conclusion

In this dissertation, the mechanism by which the [2Fe-2S] transcription factor, SoxR, responds to oxidative stress, was investigated. SoxR senses oxidative stress using the redox states of the [2Fe-2S] cluster and regulates the transcription by structural changes between the oxidized and reduced forms. NO also activates SoxR by direct nitrosylation of the [2Fe-2S] cluster.

In CHAPTER 1, the reaction of O_2^- with *E. coli* SoxR was investigated by pulse radiolysis method. $SoxR_{red}$ react with O_2^- to form $SoxR_{ox}$ with a rate constant as much as SOD (1.5×10^8 $M^{-1}s^{-1}$). This result indicates that O_2^- functions as a signal molecule of SoxR in *E. coli* cell. On the other hands, the rate constant of *P. aeruginosa* SoxR was 10-fold lower than *E. coli* SoxR. This difference reflects on the physiological function of SoxR mediated gene regulation. *P. aeruginosa* SoxR is activated by the endogenous redox-cycling antibiotic compound pyocyanin, which is the physiological signal for up-regulating quorum sensing-controlled gene expression and serves as an electron acceptor to balance the intracellular redox state.

In CHAPTER 2, the reaction of NO with SoxR was investigated by pulse radiolysis method. Spectrophotometric analyses revealed the transient formation of 1 and 2 equivalents of nitrosylation products in the [2Fe-2S] cluster of SoxR. In contrast, the second process was not observed with Fd, The difference between SoxR and Fd may reflect on the unusual CX_2CXCX_5C motif for SoxR. This suggest that the reaction of the second equivalent of NO may be important for the disassembly of a variety of iron–sulfur proteins.

In CHAPTER 3, the redox-dependent structural change of promoter DNA bound to SoxR by fluorescence probed was investigated. It became clear that the activation of SoxR is controlled by the large structural change in central part of promoter DNA.

In CHAPTER 4, the structural change of SoxR by UV resonance Raman spectroscopy was investigated. The results support significant environmental changes for Trp91 and Trp98 in the long dimerization region upon reduction. In contrast, the environment around Tyr in the DNA-binding domain is barely altered. These findings confirm the importance of interactions between the sensing domain and the DNA binding domain of the opposite promoter.

In CHAPTER 5, the reduction potential for SoxR in the absence and presence of DNA was determined from equilibrium data coupled with NADPH and NADPH-cytochrome CRP. The reduction potentials of DNA-bound and DNA-free states of SoxR were -320 and -293 mV versus NHE, respectively. These results indicated that DNA binding causes a moderate shift in the reduction potential of SoxR.

In this thesis, the mechanistic and structural studies in the function of SoxR protein has been shown. SoxR is a unique protein that [2Fe-2S] cluster function as a sensor for oxidative stress in SoxR, while most iron-sulfur cluster proteins work as redox center in electron carrier. The transcriptional

activity of SoxR is controlled by environment signals, this work will give an important knowledge for sensor mechanisms found widely in cells. The author demonstrated how minor changes in the primary event can lead to the diversity of the SoxR protein with broad range sensing capasities. In *P. aeruginosa*, especially SoxR affects drug resistance by the regulate of an efflux pump, a transporter, and a putative monooxygenase. Further advance will continue to be made to elucidate the mechanisms in drug resistance or supporting data for drug development leading to medical contributions. This work has a possibility to develop a new therapeutic medication for *P. aeruginosa* that cause to hospital infection.

List of Publications

The content of this thesis is composed of the following papers;

1. Protein Conformational Changes of the Oxidative Stress Sensor, SoxR, upon Redox Changes of the [2Fe-2S] Cluster Probed with Ultraviolet Resonance Raman Spectroscopy
   Kazuo Kobayashi, Misao Mizuno, Mayu Fujikawa and Yasuhisa Mizutani
   Biochemistry, **2011**, *50*, 9468-9474 (CHAPTER 4)

2. Direct Oxidation of the [2Fe-2S] Cluster in SoxR Protein by Superoxide: DISTINCT DIFFERENTIAL SENSITIVITY TO SUPEROXIDE-MEDIATED SIGNAL TRANSDUCTION
   Mayu Fujikawa, Kazuo Kobayashi and Takahiro Kozawa
   The Journal of Biological Chemistry, **2012**, *287*, 35702-35708 (CHAPTER 1)

3. Mechanistic Studies on Formation of the Dinitrosyl Iron Complex of the [2Fe-2S] Cluster of SoxR Protein
   Mayu Fujikawa, Kazuo Kobayashi and Takahiro Kozawa
   The Journal of Biochemistry, **2014**, *156*, 163-172 (CHAPTER2)

4. Oxidative Stress Sensing by the Iron-sulfur Cluster in the Transcription Factor, SoxR
   Kazuo Kobayashi, Mayu Fujikawa and Takahiro Kozawa
   Journal of Inorganic Biochemistry, **2014**, *133*, 87-91 (CHAPTER 1 – 5)

5. Redox-Dependent DNA Distortion in a SoxR Protein-Promoter Complex Studied Using Fluorescent Probes
   Mayu Fujikawa, Kazuo Kobayashi and Takahiro Kozawa
   The Journal of Biochemistry, in press (CHAPTER 3)

6. Binding of Promoter DNA to SoxR Protein Decreases the Reduction Potential of the [2Fe-2S] Cluster
   Kazuo Kobayashi, Mayu Fujikawa and Takahiro Kozawa
   Biochemistry, **2015**, *54*, 334-339 (CHAPTER 5)

The other supplement paper

Mammalian serum albumins as a chiral mediator library for bio-supramolecular photochirogenesis: Optimizing enantiodifferentiating photocyclodimerization of 2-anthracenecarboxylate

Masaki Nishijima, Masato Goto, Mayu Fujikawa, Chen Yang, Tadashi Mori, Takehiko Wada and Yoshihisa Inoue

Chemical Comunications, **2014,** *50*, 14082-14085.

Acknowledgments

The author would like to express her sincerest gratitude to Professor Dr Takahiro Kozawa, in Institute of Scientific and Industrial Research, Osaka University for his many valuable suggestions, fruitful discussions and continuous encouragement.

The author would like to express deeply thanks to Professor Dr. Takashi Hayashi and Professor Dr. Tsuyoshi Inoue, Department of Applied Chemistry, Graduate School of Engineering, Osaka University for reviewing this thesis and helpful comments.

The author would like to express her appreciation and gratitude to Dr. Kazuo Kobayashi, in Institute of Scientific and Industrial Research, Osaka University for his continuous guideline throughout this work, many helpful comments and hearty encouragement.

The author would like to express her special thanks to Dr. Yusa Muroya, in Institute of Scientific and Industrial Research, Osaka University for his many helpful advices and hearty encouragement.

The author would like to express her great thanks to Dr. Hiroki Yamamoto, in the Institute of Scientific and Industrial Research, Osaka University for his helpful suggestions and hearty encouragement.

The author would like to thank to Professor Yasuhisa Mizutani and Dr. Misao Mizuno, Department of Chemistry, Graduate School of Science, Osaka University for measurement of UVRR spectroscopy.

Acknowledgement is also made to all members of Professor Dr. Takahiro Kozawa's group for their hearty supports, encouragement and friendship.

Finally, the author would like to express her special gratitude to her parents and family for their constant support, hearty encouragement and understanding on this work.

Mayu Fujikawa